Jül-4317

Institute for Energy Research (IEF)
Safety Research and Reactor Technology (IEF-6)

TINTE – Nuclear Calculation Theory Description Report

H. Gerwin, W. Scherer, A. Lauer, I. Clifford

JÜLICH
FORSCHUNGSZENTRUM

TINTE – Nuclear Calculation Theory Description Report

*H. Gerwin, W. Scherer, A. Lauer, I. Clifford**

*Pebble Bed Modular Reactor (Pty) Ltd, South Africa

Berichte des Forschungszentrums Jülich; 4317
ISSN 0944-2952
Institute for Energy Research (IEF)
Safety Research and Reactor Technology (IEF-6) Jül-4317

Forschungszentrum Jülich GmbH · Zentralbibliothek, Verlag
D-52425 Jülich · Bundesrepublik Deutschland
☎ 02461 61-5220 · Telefax: 02461 61-6103 · e-mail: zb-publikation@fz-juelich.de

ABSTRACT

The Time Dependent Neutronics and Temperatures (TINTE) code system deals with the nuclear and the thermal transient behaviour of the primary circuit of the High-temperature Gas-cooled Reactor (HTGR), taking into consideration the mutual feedback effects in two-dimensional axisymmetric geometry. This document contains a complete description of the theoretical basis of the TINTE nuclear calculation, including the equations solved, solution methods and the nuclear data used in the solution. This document was prepared in compliance with the layout and review requirements of [1] and [2], and forms part of the verification and validation of TINTE.

CONTENTS

FIGURES

TABLES

ABBREVIATIONS

This list contains the abbreviations used in this document.

Abbreviation or Acronym	Definition
1D	one-dimensional
ANL	Argonne National Laboratory
Bq	Becquerel
DIN	Deutsches Institut für Normung e. V. (German Institute of Standards)
DMACD	Data Methods and Code Development
ECP	Engineering Change Proposal
ENDF	Evaluated Nuclear Data File
HTGR	High Temperature Gas-cooled Reactor
HTR	High Temperature Reactor
LEU	Low-enriched Uranium
n/a	not applicable
NEA	Nuclear Engineering Analysis
OTTO	Once-Through-Then-Out
PBMR	Pebble Bed Modular Reactor
TINTE	Time Dependent Neutronics and Temperatures
V&V	Verification and Validation
VSOP	“Very Superior Old Program” (Version 99)
w.r.t	with respect to

1. INTRODUCTION

The Time Dependent Neutronics and Temperatures (TINTE) code system deals with the nuclear and the thermal transient behaviour of the primary circuit of a High Temperature Gas-cooled Reactor (HTGR), taking into consideration the mutual feedback effects, in two-dimensional axisymmetric geometry.

The original TINTE documentation consists of three parts, the first of which **[3]** was published (in German) more than a decade ago. The mathematical basis for this document has been verified in **[5]**, which contains mathematical checks to the equation derivations of **[3]**. The third of these documents **[4]** contains additional detail on the calculation structure and certain data sources.

The TINTE documentation was found to lack important detail. Some of this detail was found hidden within the documentation itself (**[3]** and **[4]**) and within the referenced documents. Some could only be found by a detailed analysis of the TINTE source code. A process of matching the TINTE source code with its theoretical basis was therefore found necessary to 'fill in the blanks'.

This document describes a more complete theoretical basis for the TINTE nuclear calculations. In many cases, the equations of **[3]** remain unchanged. In other cases, additional information and/or equations are provided, giving a more complete picture of the TINTE calculation. Full derivations of the relevant equations are not always provided; in these cases, however, the full derivation is referenced.

This document is not intended as a replacement to either **[3]** or **[4]** but should be regarded as an updated compilation of information from a number of sources, providing a more complete picture of the theoretical basis of the TINTE nuclear calculation.

This document was prepared in compliance with the layout and review requirements of **[1]** and **[2]**, and forms part of the verification and validation of the software product TINTE.

1.1 NOMENCLATURE

A list of relevant symbols and their meanings is provided below.

$\mathbf{A}_f$ Face area vector [cm^2]

B Neutron diffusion equation buckling [cm^{-2}]

B_g Graphite burn-up due to oxidation [$atoms.cm^{-3}$]

C_l Delayed neutron precursor concentration [$neutrons.cm^{-3}$]

C_{N_2} Nitrogen concentration [$mol.m^{-3}$]

C_{H_2} Hydrogen concentration [$mol.m^{-3}$]

C_C Carbon concentration [$mol.m^{-3}$]

D Neutron diffusion coefficient [cm]

E Energy per interaction [J]

F Interaction rate [$interactions.s^{-1}$]

I Iodine concentration [$atoms.cm^{-3}$]

J Neutron current density magnitude [$neutron.cm^{-2}.s^{-1}$]

$\mathbf{J}$ Neutron current density vector [neutron.cm^{-2}.s^{-1}]

k Reactor multiplication factor

K General-purpose multiplication factor

L Neutron leakage per unit flux [cm^2]

N Atom number density [atoms.cm^{-3}]

Q Heat production [J]

r Radial coordinate [cm]

R Ratio of the interaction rate in a given isotope to the total interaction rate

S General-purpose source term, iteration mesh transformation factor

t Time [s]

T Temperature [K]

v Average neutron velocity [cm.s^{-1}]

V Volume [cm^3]

x Molar fraction

X Xenon concentration [atoms.cm^{-3}]

z Axial coordinate [cm]

α Heat flux resistance for the fuel coated particle overheating model [K.cm^3.W^{-1}]

β Delayed neutron fraction

χ Ratio of local to total heat production

Δ Time interval [s]

ε Fractional error. In the context of paragraph 3.2.6 this represents the solid material fraction.

ϕ Scalar neutron flux [neutrons.cm^{-2}.s^{-1}]

γ Convergence accelerating parameter or direct fission yield fraction

λ Decay constant [Bq]

λ_{extrap} Boundary extrapolated length [cm]

ν Net number of neutrons produced per fission

θ Azimuthal ordinate [radian]

σ Microscopic cross section [cm^2]

Σ Macroscopic cross section [cm^{-1}]

τ Time interval [s]

$\Omega(x)$ The volume-weighted average of variable x

ς General-purpose fractional multiplication factor ($0 \leq \varsigma \leq 1$)

General superscripts, subscripts and embellishments may include the following:

0	Initial condition
1	End-of-interval condition or w.r.t. the fast energy group
2	w.r.t thermal energy group
B	Graphite burn-up
C	Carbon
eq	Equilibrium
f	Fission. Fuel material in the context of paragraph 3.2.6.
H_2	Hydrogen
i	Discrete axial location index (iteration mesh) or other general index
$\hat{i}$	Discrete axial location index (material mesh)
ii	Discrete axial location index (fine iteration mesh)
j	Discrete radial location index (iteration mesh)
$\hat{j}$	Discrete radial location index (material mesh)
jj	Discrete radial location index (fine iteration mesh)
k	Discrete azimuthal location index (iteration mesh)
$\hat{k}$	Discrete azimuthal location index (material mesh)
kk	Discrete azimuthal location index (fine iteration mesh)
l	Delayed neutron precursor group
m	Moderator material
N_2	Nitrogen
r	w.r.t the radial direction
z	w.r.t the axial direction
ϕ	w.r.t the neutron flux
θ	w.r.t the azimuthal direction
$\widetilde{x}$	Located at the control volume edge
$\overline{x}$	Spatial or temporal average value
$\dot{x}$	Temporal derivative $\frac{dx}{dt}$
x'	Modified
x'''	Per unit volume
x^*	Effective value

Cross-section-related subscripts may include the following:

a	Absorption (including fission absorption)
f	Fission
r	Removal (scattering out of energy group)
s	Scattering out of the energy group
tr	Transport
$Gd7$	Absorption be ^{157}Gd
$Sm9$	Absorption by ^{149}Sm
$Sm1$	Absorption be ^{151}Sm
$Xe5$	Absorption by ^{135}Xe

Note that Σ_{r1} and Σ_{r2} are equivalent to $\Sigma_s^{1\to 2}$ and $\Sigma_s^{2\to 1}$ respectively in the context of TINTE.

Heat-production-related subscripts may include the following:

A	The remaining actinides, excluding ^{232}Th and ^{238}U
B	Breeding from the isotopes ^{232}Th and ^{238}U
Cs	^{134}Cs neutron capture reaction
d	Decay
E	Capture reactions other than ^{134}Cs and the actinides
mod	Neutron moderation
n	Fission neutron
n,γ	n,γ reaction
f	Fission
k	Time interval index
l	Local
p	Prompt
r	Fission fragment rebound
S	Fission product
β	β-particle
γ	γ-particle

2. MODELLING REQUIREMENTS

The TINTE code is required to calculate the time-dependent nuclear and thermal-hydraulic behaviour of a High Temperature Reactor (HTR). More specifically, the nuclear calculation shall model the time-dependent nuclear behaviour of a HTR in two-dimensional axisymmetric (r,z) geometry.

The following physical processes shall be modelled:

- The time-dependent neutron flux.
- The neutron cross sections.
- Short- and medium-term reactor dynamics – The influences of delayed neutrons and neutron poisons such as ^{135}Xe shall be modelled.
- The time-dependent heat source distribution – Prompt and decay heat shall be modelled. Non-local heat production due to gammas, neutron capture and moderation shall be modelled.

3. MODELLING DESCRIPTION

3.1 PHYSICAL PROCESSES

Of primary importance in modelling the operation of the nuclear reactor is the knowledge of the neutron distribution in the reactor core. For the purposes of TINTE, the neutron distribution as a function of space, time and energy is desired. The following physical processes are modelled:

- The time-dependent absorption, scattering and fission of neutrons.
- The prompt and delayed production of neutrons from fission.
- The production and decay of saturation fission products such as ^{135}I and ^{135}Xe.
- The heat production due to fission, both locally within the fuel and no-locally due to neutron moderation, absorption and gamma radiation.
- The influence of state variables (temperature, etc.) on material cross sections.

3.1.1 The Spatial Domain

The reactor is modelled in TINTE using a discrete spatial mesh. The accuracy of such a discrete approximation is dependent largely on the model that is used. A rectangular mesh is chosen as this allows certain optimizations to be made to the numerical solution of the neutron flux. Because TINTE is tailored towards the modelling of cylindrical reactors, a cylindrical coordinate system was chosen. It should be noted that, despite the fact that the equations derived in this document include the azimuthal coordinate, the final TINTE implementation neglects the azimuthal dependence.

This axisymmetric assumption has a number of consequences. Control rods and other discrete components, which have azimuthal dependence, are assumed to be homogenized in the azimuthal direction. This further complicates the generation of cross sections for calculations. The influence of, as an example, a single control rod cannot be accurately determined. True spatial oscillations cannot be modelled.

The definition of the spatial domain is discussed further in paragraph 3.2.1.

3.1.2 The Time-dependent Neutron Flux

The neutron flux is modelled using the diffusion approximation. The diffusion approximation is derived from the neutron transport equation under the following assumptions [7]:

a. Absorption is much less likely than scattering.
b. There is a linear spatial variation of the neutron distribution.
c. Scattering is isotropic.

Condition (a) is satisfied for most moderating and structural materials within the nuclear reactor (graphite, water, etc.), but not for fuel and control rod materials. Condition (b) is satisfied a few mean free paths away from the boundary of a large (relative to the mean free path) homogenous media with relatively uniform source distributions. Condition (c) is satisfied for the scattering from heavy atomic mass nuclei. It is clear at this point that the diffusion approximation cannot be used independently to obtain accurate predictions. In general, more accurate transport calculations would be used along with diffusion theory to predict the neutron flux distribution of a reactor. These transport calculations are generally used to prepare effective macroscopic cross sections, which may then be used in the diffusion calculation. The topic of macroscopic cross sections is discussed further in paragraph 3.1.3.

Additionally, the two-energy-group approximation was adopted, assuming a single fast and epithermal energy group and a single thermal energy group. This approximation, again, may be considered valid only if sufficient precalculation has been carried out to determine the neutron energy spectrum within the reactor. The neutron spectrum may then be used to reduce the continuous energy-dependent cross sections to two-group cross sections. This two-group approximation also assumes that a thermal reactor is being modelled.

The derivation of a solution method for the spatial- and time-dependent neutron flux is detailed in paragraph 3.2.3.

3.1.3 Neutron Cross Sections

In order to simplify the code, and improve computational time, it was decided that detailed transport calculations would be removed entirely from the TINTE nuclear calculation and would form part of the input data preparation procedure alone. The spatial two-group cross sections are therefore required as a user input to the code. Because of the many possible influencing parameters, these cross sections have to take into account numerous parameters:

- Long-term changes in cross sections due to fuel burn-up – The TINTE calculation assumes short- and medium-term dynamics and therefore long-term effects are ignored.
- Changes in reactor geometry – Constant reactor geometry is assumed. The influence of the addition of hydrogen and nitrogen in the coolant is considered, as well as the influence of graphite loss due to corrosion.
- Movement of fuel in the core due to continuous refuelling – Because short- and medium-term dynamics are assumed, the effect of fuel movement may be ignored.
- Medium-term changes in cross sections due to the build-up of neutron poisons such as Xe-135 and Sm-151.
- The leakage or buckling.
- Material temperatures – The temperature feedback is assumed to have a fuel temperature and moderator temperature component.

The common method of supplying groupwise cross-sectional data to codes is through multidimensional tables. It was decided that this method required too much memory to store the multidimensional tables and was computationally expensive to perform the multidimensional interpolating of data. Instead a polynomial representation of the cross sections was opted for. The method used for cross-section representation is detailed in paragraph 3.2.2.

3.1.4 Short-term Reactor Dynamics

The dynamics of a nuclear reactor is influenced by the delayed emission of neutrons from the decay of fission products. For pebble-bed-type HTRs, the influence of delayed neutrons is not dominant, however, it is still significant and should be accounted for. Although there are a relatively large number of fission products, each decaying via neutron emission, it is generally accepted that the observed composite emission characteristics can be well represented by defining six effective delayed neutron groups. Each group is characterized by a decay constant λ_i and relative fission yield β_i / β. The influence of the delayed neutrons is included in the time-dependent diffusion equation. The derivation of the equations to model the delayed neutron production is given in paragraph 3.2.3.3.

3.1.5 Medium-term Reactor Dynamics

All fission products influence the absorption of neutrons to some extent. Fission products that absorb neutrons are known as neutron poisons. Because absorption cross sections tend to decrease rapidly as a function of neutron energy, the influence of these poisons is greatest in thermal reactors.

The most important fission product poison is Xe-135. This is formed from the decay of Te-135 to I-135 and subsequent decay to Xe-135. The isotope is also formed directly by fission. This isotope has a significant influence on the medium-term operation of a reactor, specifically when power levels change and the neutron spectrum shifts.

The isotope Sm-149 is considered to be of less importance than Xe-135 but nonetheless its concentration influences the medium-term dynamic operation of the thermal reactor. In addition to Xe-135 and Sm-149, the isotopes Sm-151 and Gd-157 are considered important. Their fission yields are, however, smaller and their importance is therefore considered less.

The derivation of a set of discretized time-dependent equations for the neutron poison concentrations is given in paragraph 3.2.4.

3.1.6 Heat Production

The heat production is necessary to determine fuel and moderator temperatures within the reactor. Fission processes are responsible for most of the generated heat within a reactor. Fission energy is released via highly divergent processes, i.e. many different sources must be considered. Approximately 5% of the energy, calculated from the mass defect, is released as anti-neutrinos and is therefore unavailable for heat production in the reactor. The heat production is assumed to be divided into two parts, namely the prompt and decay heat. Decay heat is conservatively modelled using the DIN standard 25 485 [21]. The derivation of the modelling equations for heat production, as well as the assumptions made, is given in paragraph 3.2.5.

3.2 PHYSICAL MODELLING AND SOLUTION OF EQUATIONS

3.2.1 The Calculational Domain

The TINTE nuclear module is tailored towards modelling cylindrical reactors using an r-z-θ coordinate system. While the underlying theory of TINTE has been derived in three dimensions, the code itself is currently limited to two-dimensional axisymmetric calculations. Therefore, for many of the derivations given in this document the third (θ) ordinate is accounted for but is not enabled in the code.

A structured rectangular mesh is employed, shown in Figure 1. Multiple meshes are defined within the total computational domain. Since all meshes share common geometry, the concept of different meshes is not strictly correct, however, mapping of values from a given location in one mesh to its corresponding location in another is necessary and for this reason separate meshes are defined. The following meshes are defined (refer to Figure 1):

a. Nuclear material mesh - All nuclear properties and solutions are stored on this mesh. It corresponds exactly with the coarse grid definition of the total computational domain but is generally smaller in size, i.e. areas of the model that are far from the core and are considered neutronically insignificant are excluded.
b. Nuclear iteration mesh - The neutron flux calculation is carried out using this mesh. It is equivalent to the nuclear material mesh, however, material blocks may be lumped together in order to decrease solution time.
c. One-dimensional (1D) nuclear iteration mesh in the radial direction - This is equivalent to the nuclear iteration mesh, but with a fine sub-meshing applied in the radial direction. This mesh is used for the radial pass of the one-dimensional leakage iteration calculation described later in paragraph 3.2.3.6.
d. 1D nuclear iteration mesh in the axial direction - This is equivalent to (c) above for the axial direction.
e. 1D nuclear iteration mesh in the azimuthal direction - This is equivalent to (c) above for the azimuthal direction.

In addition to those above core, solid-material and gas-flow meshes are defined. These are used primarily for thermal-hydraulic calculations and therefore will not be discussed in detail.

A nuclear material is assigned to each nuclear material block. A material can be assigned to more than one block. Each material, in turn, has a unique set of cross-section polynomials (refer to paragraph 3.2.2) as well as history of operation and fission rate fractions for heat production calculations (refer to paragraph 3.2.5). The user supplies these material parameters.

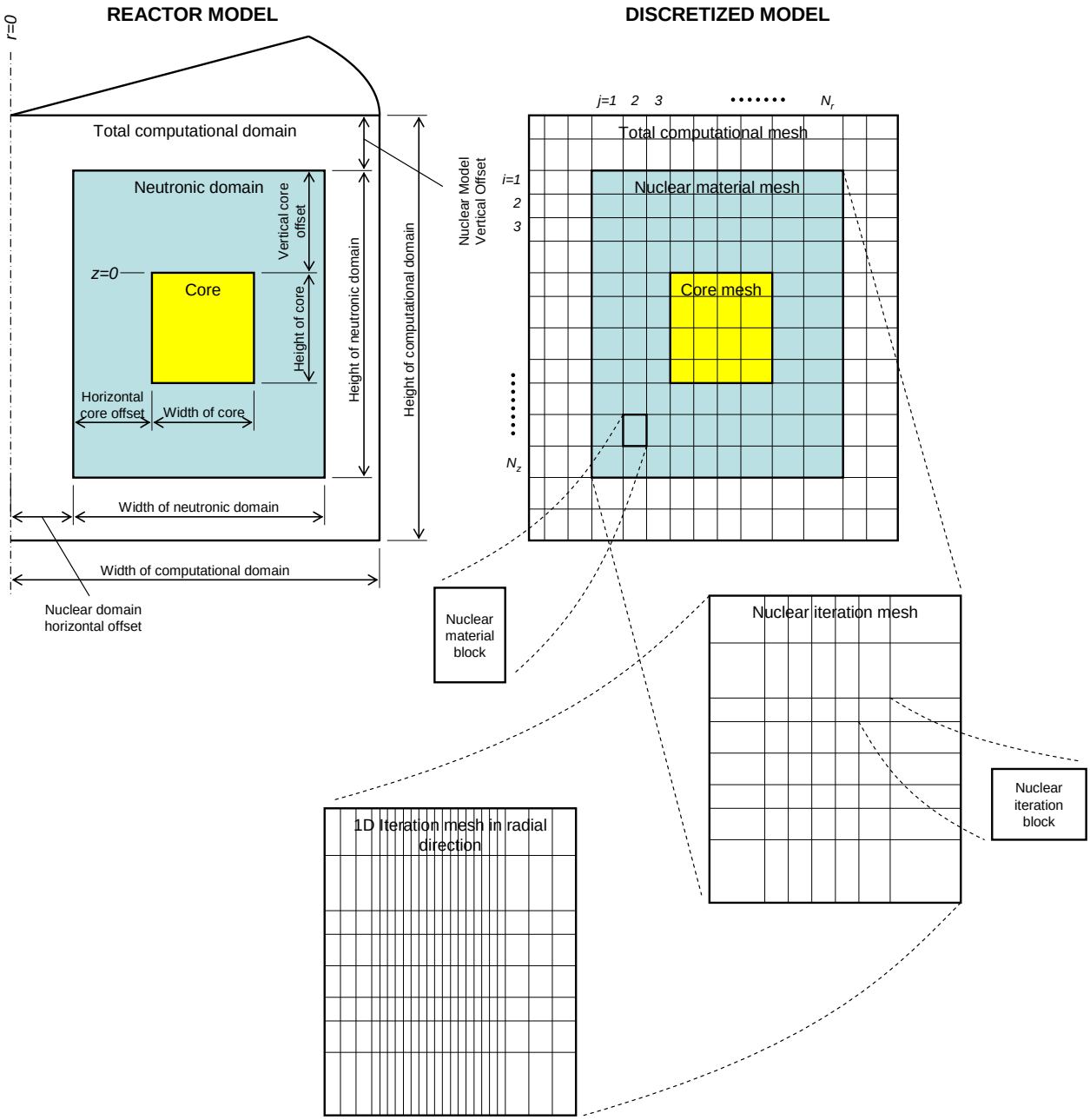

Figure 1: The TINTE Nuclear Calculational Domain

3.2.2 Cross Section Representation

Homogenized two-group material cross sections are generally a complex function of a number of parameters. In TINTE, the following parameters are accounted for:

- Fuel temperature, T_f, expressed in Kelvin [K]
- Moderator temperature, T_m, expressed in Kelvin [K]
- Leakage per unit volume per unit flux (buckling per unit volume), L''' [cm^{-1}]
- Xenon concentration, Xe [atoms.barn^{-1}.cm^{-1}]
- Concentration of nitrogen, C_N [mol.m^{-3}]
- Concentration of hydrogen, C_H [mol.m^{-3}]
- Graphite burn-up (oxidation), B_g [mol.m^{-3}]

In order to minimize computational time, it was decided that inline spectrum calculations and homogenization would not be carried out in TINTE, but rather that two-group homogenized cross sections would be generated externally. These cross sections are represented in TINTE by a series of Nth order polynomials of the form shown.

$$\begin{aligned}\Sigma\left(T_f, T_m, L''', Xe, C_{N_2}, C_{H_2O}, B_g\right) &= \Sigma_0 \\ &+ \left[A_1\left(T_f - T_{f0}\right) + A_2\left(T_f - T_{f0}\right)^2 + \ldots + A_m\left(T_f - T_{f0}\right)^m\right] \\ &+ \left[B_1\left(T_m - T_{m0}\right) + B_2\left(T_m - T_{m0}\right)^2 + \ldots + B_n\left(T_m - T_{m0}\right)^n\right] + \ldots\end{aligned} \quad (\mathbf{3}.1)$$

This representation was chosen, as opposed to multidimensional lookup tables, because it allows very rapid calculation of cross sections as a function of multiple parameters. Note that no serial expansions with mixed parameters are implemented, i.e. each polynomial term is a function of a single parameter only.

All coefficients are defined on a per material basis. The reference point Σ_0 is chosen as the macroscopic cross section of the material for the reference operating conditions (T_{f0}, T_{m0}, etc.) within the relevant region of the reactor. The coefficients A_i, B_i, etc. are defined thereafter to correct for changes in the operating conditions of the reactor. In practice, the polynomial coefficients are pre-calculated based either on VSOP 99 [19] steady-state results or on the results of previous TINTE calculations for an assumed range of operating conditions. Using this method, the cross sections are accurately calculated near the reference operating conditions but become less accurate as one moves away from the reference operating conditions. In TINTE, the precalculation of macroscopic cross sections for given operating conditions is performed using the TISPEC spectrum code.

Each nuclear material mesh is assigned to a nuclear material and, therefore, a unique cross-section set is calculated using the temperatures, buckling, etc. within the nuclear material mesh at the start of each nuclear time-interval. For steady-state calculations, the temperatures, buckling, etc. are carried over from the previous iteration. The following cross sections/nuclear parameters are calculated:

- Fast and thermal macroscopic transport cross sections; Σ_{tr1} and Σ_{tr2}.
- Fast and thermal macroscopic absorption cross section (including fission); Σ_{a1} and Σ_{a2}.
- Fast and thermal macroscopic nu-fission cross section; $\nu\Sigma_{f1}$ and $\nu\Sigma_{f2}$.

- Fast and thermal macroscopic fission cross section; Σ_{f1} and Σ_{f2}.
- Fast and thermal macroscopic removal cross section; Σ_{r1} and Σ_{r2} (alternatively $\Sigma_s^{1\to 2}$ and $\Sigma_s^{2\to 1}$).
- Fast and thermal group reciprocal mean neutron velocity; $1/v_1$ and $1/v_2$.
- ^{135}Xe, ^{149}Sm, ^{151}Sm and ^{157}Gd thermal group microscopic cross sections; σ_{Xe5}, σ_{Sm9}, σ_{Sm1} and σ_{Gd7}.

3.2.2.1 Diffusion constants

The diffusion constants are calculated from the transport cross sections as:

$$D = \frac{1}{3\Sigma_{tr}} \tag{3.2}$$

A special treatment may be necessary for cavity regions and pebble-bed-type cores, as neutron streaming can take place. This is accounted for by assuming different diffusion constants in the radial, axial and azimuthal directions [8]. Directional diffusion coefficients are defined using correction factors in the radial, axial and azimuthal directions. If we define $D^r = K_r D$, where D^r is the radial diffusion coefficient and K_r is assumed constant throughout the calculation for any given material, the directional macroscopic transport cross section may be written as:

$$\begin{aligned}
\Sigma_{tr}^r &= \frac{\Sigma_{tr}}{K_r} \\
&= \frac{\Sigma_{tr,0}}{K_r} \\
&\quad + \left[\frac{A_1}{K_r}\left(T_f - T_{f0}\right) + \frac{A_2}{K_r}\left(T_f - T_{f0}\right)^2 + \ldots + \frac{A_m}{K_r}\left(T_f - T_{f0}\right)^m \right] \\
&\quad + \left[\frac{B_1}{K_r}\left(T_m - T_{m0}\right) + \frac{B_2}{K_r}\left(T_m - T_{m0}\right)^2 + \ldots + \frac{B_n}{K_r}\left(T_m - T_{m0}\right)^n \right] + \ldots \\
&= \Sigma_{tr,0}^r \\
&\quad + \left[A_1^r\left(T_f - T_{f0}\right) + A_2^r\left(T_f - T_{f0}\right)^2 + \ldots + A_m^r\left(T_f - T_{f0}\right)^m \right] \\
&\quad + \left[B_1^r\left(T_m - T_{m0}\right) + B_2^r\left(T_m - T_{m0}\right)^2 + \ldots + B_n^r\left(T_m - T_{m0}\right)^n \right] + \ldots
\end{aligned}$$

New polynomial coefficients $A_i^r = \frac{A_i}{K_r}$, $B_i^r = \frac{B_i}{K_r}$, etc. for the nuclear material may therefore be defined. Similarly, for the axial and azimuthal directions, directional polynomial coefficients

$$A_i^z = \frac{A_i}{K_z},\ B_i^z = \frac{B_i}{K_z},\ A_i^\theta = \frac{A_i}{K_\theta}, \text{ etc.} \tag{3.3}$$

may be defined.

3.2.2.2 Overlaid cross-section sets

The ability to dynamically alter material compositions within the reactor model is particularly useful for a number of different cases, e.g. to simulate the addition of neutron poisons and/or additional moderator material to the reactor. In TINTE, this is achieved by means of overlaid cross sections. For each nuclear material, more than one cross-section set may be defined. The final cross section values, as calculated for the nuclear material mesh and used in the diffusion calculation, are calculated by fractionally overlaying the cross sections calculated using the polynomial expansions of Equation 3.1. An example is given:

$$\Sigma = (1 - \varsigma_B - \varsigma_C - \ldots)\Sigma_A + \varsigma_B \Sigma_B + \varsigma_C \Sigma_C + \ldots \qquad (\mathbf{3}.4)$$

The fractions ς_B, ς_C, etc. are either user-specified or are set by the TINTE control modules. Note that $\sum \varsigma_i \leq 1$.

3.2.2.3 Modelling of control rods

With the exception of a central control rod, axial control rods cannot be represented directly in two-dimensional axisymmetric geometry. A number of models are commonly used to overcome this limitation. The 'grey' curtain model is adopted in TINTE [9]. This allows continuous control rod movements to be simulated by adjusting the neutron poison concentration in a given material. A major disadvantage to this method or representation is that it is often difficult to derive the neutron poison concentration and, therefore, the rod efficiency from the geometry and composition of the control rods. If rod efficiency is known beforehand, however, this model is easily implemented by means of overlaid cross-section sets. Typically, a cross-section set is defined for the control rod fully inserted and one for the control rod withdrawn from a given material mesh as shown in Figure 2. This method requires that each material mesh containing control rods must be assigned a unique material with overlaid cross-section sets.

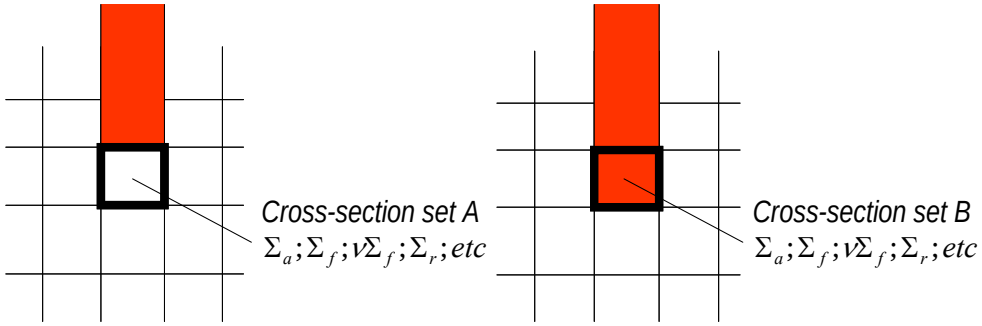

Figure 2: Defining Cross-section Sets for the Simulation of Control Rod Movement

A typical overlaid cross section is calculated, in the case of Figure 2, as $\Sigma = (1 - \varsigma)\Sigma_A + \varsigma \Sigma_B$. The correct choice of the parameter ς $(0 \leq \varsigma \leq 1)$ is essential for modelling small control rod movements because the parameter is not linearly dependent on control rod position. This topic is covered in greater detail in the TINTE control module descriptions.

It should be noted that TINTE contains no equations to directly calculate the control rod worth. The user is expected to supply the overlaid cross-section sets.

3.2.3 The Neutron Flux Solution

3.2.3.1 The time-dependent diffusion equations

The two-group time-dependent diffusion equation is given below, including delayed neutron precursors [7].

In the fast energy group:

$$\frac{1}{v_1}\frac{\partial \phi_1}{\partial t} = \nabla D_1 \nabla \phi_1 - \left(\Sigma_{a1} + \Sigma_s^{1\to 2}\right)\phi_1 + \Sigma_s^{2\to 1}\phi_2 + (1-\beta)P + \sum_{l=1}^{6}\lambda_l C_l + S_\phi \qquad (\mathbf{3}.5)$$

In the thermal energy group:

$$\frac{1}{v_2}\frac{\partial \phi_2}{\partial t} = \nabla D_2 \nabla \phi_2 - \left(\Sigma_{a2} + \Sigma_s^{2\to 1}\right)\phi_2 + \Sigma_s^{1\to 2}\phi_1 \qquad (\mathbf{3}.6)$$

It should be noted that upward scattering is allowed for and the selected group structure (energy division) is left open.

All fission neutrons are assumed created in the fast energy group. Neutron production is described by:

$$P = \frac{1}{k}\left(\nu\Sigma_{f1}\phi_1 + \nu\Sigma_{f2}\phi_2\right) \qquad (\mathbf{3}.7)$$

where k is the effective reactor multiplication constant. In general, k is calculated for the equilibrium case and remains unchanged during time-dependent calculations. In TINTE, however, there are special cases (fixed power transients) where k is updated during the time-dependent calculation. This is discussed further in paragraph 3.2.3.10.

3.2.3.2 Spatial discretization

A three-dimensional r-z-θ coordinate system is used with a rectangular structured mesh. The laplacian operator in this case, for the case of anisotropic diffusion constant, becomes:

$$\nabla D \nabla \phi = \frac{1}{r}\frac{\partial}{\partial r} r D^r \frac{\partial \phi}{\partial r} + \frac{1}{r}\frac{\partial}{\partial \theta}\frac{1}{r} D^\theta \frac{\partial \phi}{\partial \theta} + \frac{\partial}{\partial z} D^z \frac{\partial \phi}{\partial z}$$

When considering each component separately:

$$\left(\nabla D \nabla \phi\right)^r = \frac{1}{r}\frac{\partial}{\partial r} r D^r \frac{\partial \phi}{\partial r}$$

$$\left(\nabla D \nabla \phi\right)^z = \frac{\partial}{\partial z} D^z \frac{\partial \phi}{\partial z}$$

$$\left(\nabla D \nabla \phi\right)^\theta = \frac{1}{r}\frac{\partial}{\partial \theta}\frac{1}{r} D^\theta \frac{\partial \phi}{\partial \theta}$$

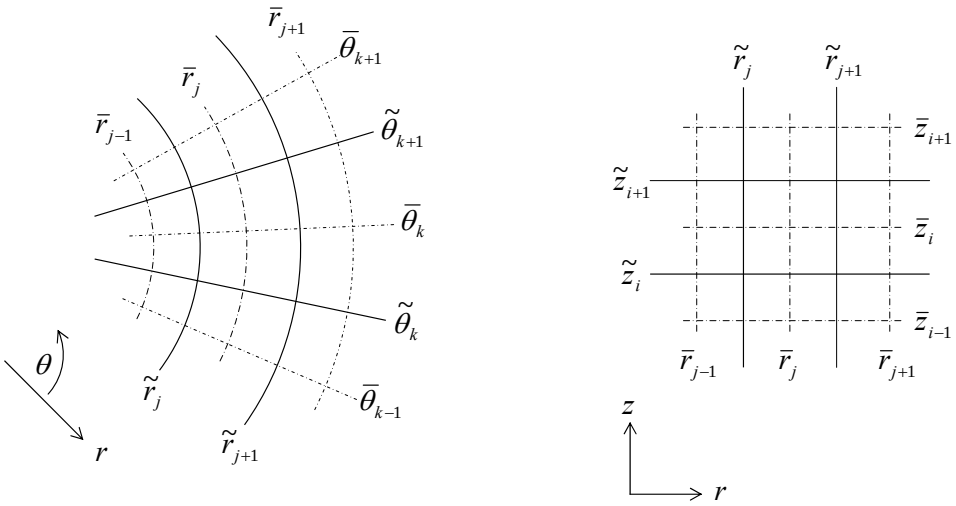

Figure 3: Spatial Discretization Layout

Consider the spatial coordinates of Figure 3. The current at the radial mesh interface $\tilde{r}_j$ may be written as:

$$J_j^r = -D^r \left.\frac{\partial \phi}{\partial r}\right|_j$$

It is, however, necessary to determine an effective diffusion constant at the interface as adjacent meshes may contain different materials. We equate the neutron flow densities on both sides of the interface, applying a finite-difference approximation.

$$-\bar{D}_{j-1}^r \frac{\tilde{\phi}_j - \bar{\phi}_{j-1}}{\tilde{r}_j - \bar{r}_{j-1}} = -\bar{D}_j^r \frac{\bar{\phi}_j - \tilde{\phi}_j}{\bar{r}_j - \tilde{r}_j}$$

$$\frac{\bar{D}_{j-1}^r}{\tilde{r}_j - \bar{r}_{j-1}} \tilde{\phi}_j - \frac{\bar{D}_{j-1}^r}{\tilde{r}_j - \bar{r}_{j-1}} \bar{\phi}_{j-1} = \frac{\bar{D}_j^r}{\bar{r}_j - \tilde{r}_j} \bar{\phi}_j - \frac{\bar{D}_j^r}{\bar{r}_j - \tilde{r}_j} \tilde{\phi}_j$$

$$\tilde{\phi}_j = \frac{\dfrac{\bar{D}_j^r}{\bar{r}_j - \tilde{r}_j} \bar{\phi}_j + \dfrac{\bar{D}_{j-1}^r}{\tilde{r}_j - \bar{r}_{j-1}} \bar{\phi}_{j-1}}{\dfrac{\bar{D}_j^r}{\bar{r}_j - \tilde{r}_j} + \dfrac{\bar{D}_{j-1}^r}{\tilde{r}_j - \bar{r}_{j-1}}}$$

The current at the j[th] radial mesh interface, dependent on only the mesh-centred fluxes, can now be calculated.

$$\tilde{J}_j^r = -\tilde{D}_j^r \frac{\bar{\phi}_j - \bar{\phi}_{j-1}}{\bar{r}_j - \bar{r}_{j-1}} = -\bar{D}_j^r \frac{\bar{\phi}_j - \tilde{\phi}_j}{\bar{r}_j - \tilde{r}_j}$$

$$= \bar{D}_j^r \frac{\bar{\phi}_j - \dfrac{\dfrac{\bar{D}_j^r}{\bar{r}_j - \tilde{r}_j} \bar{\phi}_j + \dfrac{\bar{D}_{j-1}^r}{\tilde{r}_j - \bar{r}_{j-1}} \bar{\phi}_{j-1}}{\dfrac{\bar{D}_j^r}{\bar{r}_j - \tilde{r}_j} + \dfrac{\bar{D}_{j-1}^r}{\tilde{r}_j - \bar{r}_{j-1}}}}{\bar{r}_j - \tilde{r}_j}$$

$$\therefore \tilde{J}_j^r = \frac{-1}{\frac{\bar{r}_j - \tilde{r}_j}{\bar{D}_{r,j}} + \frac{\tilde{r}_j - \bar{r}_{j-1}}{\bar{D}_{r,j-1}}} \left(\bar{\phi}_j - \bar{\phi}_{j-1}\right) \tag{3.8}$$

The equivalent relationship for the j+1th mesh may be written and similarly relationships for the axial and azimuthal currents may be derived.

We now consider the two-group diffusion equations and integrate over a given volume V.

$$\int_V \frac{1}{v_1}\frac{\partial \phi_1}{\partial t} dV = \int_V \nabla D_1 \nabla \phi_1 \, dV - \int_V \left(\Sigma_{a1} + \Sigma_s^{1\to 2}\right)\phi_1 \, dV + \int_V \Sigma_s^{2\to 1}\phi_2 \, dV + \int_V (1-\beta) P \, dV$$
$$+ \int_V \sum_{l=1}^{6} \lambda_l C_l \, dV + \int_V S_\phi dV$$

$$\int_V \frac{1}{v_2}\frac{\partial \phi_2}{\partial t} dV = \int_V \nabla D_2 \nabla \phi_2 \, dV - \int_V \left(\Sigma_{a2} + \Sigma_s^{2\to 1}\right)\phi_2 \, dV + \int_V \Sigma_s^{1\to 2}\phi_1 \, dV$$

Application of Gauss' Theorem to the laplacian terms allows the volume integral to be transformed to a surface integral.

$$\int_V \frac{1}{v_1}\frac{\partial \phi_1}{\partial t} dV = \int_{\partial V} \left(D_1 \nabla \phi_1\right) \bullet d\mathbf{S} - \int_V \left(\Sigma_{a1} + \Sigma_s^{1\to 2}\right)\phi_1 \, dV + \int_V \Sigma_s^{2\to 1}\phi_2 \, dV + \int_V (1-\beta) P \, dV$$
$$+ \int_V \sum_{l=1}^{6} \lambda_l C_l \, dV + \int_V S_\phi dV$$

$$\int_V \frac{1}{v_2}\frac{\partial \phi_2}{\partial t} dV = \int_{\partial V} \left(D_2 \nabla \phi_2\right) \bullet d\mathbf{S} - \int_V \left(\Sigma_{a2} + \Sigma_s^{2\to 1}\right)\phi_2 \, dV + \int_V \Sigma_s^{1\to 2}\phi_1 \, dV$$

The surface integrals may be decomposed into a sum over the bounding faces of the mesh.

$$\int_V \frac{1}{v_1}\frac{\partial \phi_1}{\partial t} dV = \sum_f \int_f \left(D_1 \nabla \phi_1\right) \bullet d\mathbf{S} - \int_V \left(\Sigma_{a1} + \Sigma_s^{1\to 2}\right)\phi_1 \, dV + \int_V \Sigma_s^{2\to 1}\phi_2 \, dV + \int_V (1-\beta) P \, dV$$
$$+ \int_V \sum_{l=1}^{6} \lambda_l C_l \, dV + \int_V S_\phi dV$$

$$\int_V \frac{1}{v_2}\frac{\partial \phi_2}{\partial t} dV = \sum_f \int_f \left(D_2 \nabla \phi_2\right) \bullet d\mathbf{S} - \int_V \left(\Sigma_{a2} + \Sigma_s^{2\to 1}\right)\phi_2 \, dV + \int_V \Sigma_s^{1\to 2}\phi_1 \, dV$$

For continuous functions under the integrals, the integration midpoint rule can be applied to all integrals.

$$\left(\frac{1}{v_1}\frac{\partial \phi_1}{\partial t}\right) V = \sum_f \left(D_1 \nabla \phi_1\right)_f \bullet \mathbf{A}_f - \left(\Sigma_{a1} V + \Sigma_s^{1\to 2} V\right)\phi_1 + \Sigma_s^{2\to 1} V \phi_2 + (1-\beta) P V$$
$$+ \left(\sum_{l=1}^{6} \lambda_l C_l\right) V + S_\phi V$$

$$\left(\frac{1}{v_2}\frac{\partial \phi_2}{\partial t}\right) V = \sum_f \left(D_2 \nabla \phi_2\right)_f \bullet \mathbf{A}_f - \left(\Sigma_{a2} V + \Sigma_s^{2\to 1} V\right)\phi_2 + \Sigma_s^{1\to 2} V \phi_1$$

Given the definition of $\mathbf{J} = -D\nabla\phi$, further defining the neutron leakage from each mesh surface as $L_f\phi = \mathbf{J}_f \bullet \mathbf{A}_f = -(D\nabla\phi)_f \bullet \mathbf{A}_f$ and considering the structured mesh definition, the equations may be written as:

$$\left(\frac{1}{v_1}\frac{\partial\phi_1}{\partial t}\right)V = \left(\tilde{L}^r_{1,j} - \tilde{L}^r_{1,j+1} + \tilde{L}^z_{1,i} - \tilde{L}^z_{1,i+1} + \tilde{L}^\theta_{1,k} - \tilde{L}^\theta_{1,k+1}\right)\phi_1 - \left(\Sigma_{a1}V + \Sigma_s^{1\to2}V\right)\phi_1 + \Sigma_s^{2\to1}V\phi_2 + (1-\beta)PV + \left(\sum_{l=1}^{6}\lambda_l C_l\right)V + S_\phi V \quad (\mathbf{3}.9)$$

$$\left(\frac{1}{v_2}\frac{\partial\phi_2}{\partial t}\right)V = \left(\tilde{L}^r_{2,j} - \tilde{L}^r_{2,j+1} + \tilde{L}^z_{2,i} - \tilde{L}^z_{2,i+1} + \tilde{L}^\theta_{2,k} - \tilde{L}^\theta_{2,k+1}\right)\phi_2 - \left(\Sigma_{a2}V + \Sigma_s^{2\to1}V\right)\phi_2 + \Sigma_s^{1\to2}V\phi_1 \quad (\mathbf{3}.10)$$

where the face leakage values, using Equation (**3**.8) are calculated as:

$$\tilde{L}^r_j\phi_j = \frac{-\tilde{r}_j(\tilde{z}_{i+1} - \tilde{z}_i)(\tilde{\theta}_{k+1} - \tilde{\theta}_k)}{\frac{\bar{r}_j - \tilde{r}_j}{\bar{D}^r_j} + \frac{\tilde{r}_j - \bar{r}_{j-1}}{\bar{D}^r_{j-1}}}(\phi_j - \phi_{j-1}) \quad (\mathbf{3}.11)$$

The equivalent equation for the axial direction is:

$$\tilde{L}^z_i\phi_i = \frac{-\frac{1}{2}(\tilde{r}_{j+1}{}^2 - \tilde{r}_j{}^2)(\tilde{\theta}_{k+1} - \tilde{\theta}_k)}{\frac{\bar{z}_i - \tilde{z}_i}{\bar{D}^z_i} + \frac{\tilde{z}_i - \bar{z}_{i-1}}{\bar{D}^z_{i-1}}}(\phi_i - \phi_{i-1}) \quad (\mathbf{3}.12)$$

The equivalent equation for the azimuthal direction is:

$$\tilde{L}^\theta_k\phi_k = -\frac{1}{\bar{r}_j}\frac{(\tilde{r}_{j+1} - \tilde{r}_j)(\tilde{z}_{i+1} - \tilde{z}_i)}{\frac{\tilde{\theta}_k - \tilde{\theta}_k}{\bar{D}^\theta_k} + \frac{\tilde{\theta}_k - \bar{\theta}_{k-1}}{\bar{D}^\theta_{k-1}}}(\phi_k - \phi_{k-1}) \quad (\mathbf{3}.13)$$

3.2.3.2.1 Boundary conditions

The vacuum boundary condition is obtained by assuming the flux is zero at a given distance from the boundary, known as the extrapolated length λ_{extrap}. Neutron transport theory calculations have given rise to the common definition [7] of the extrapolated distance of:

$$\lambda_{extrap} = 0.71\Sigma_{tr}^{-1} = 0.71\times3D \quad (\mathbf{3}.14)$$

Consider a vacuum boundary located at $\tilde{\bar{z}}_1$. The flux at a distance λ_{extrap} from the boundary is zero as shown in Figure 4.

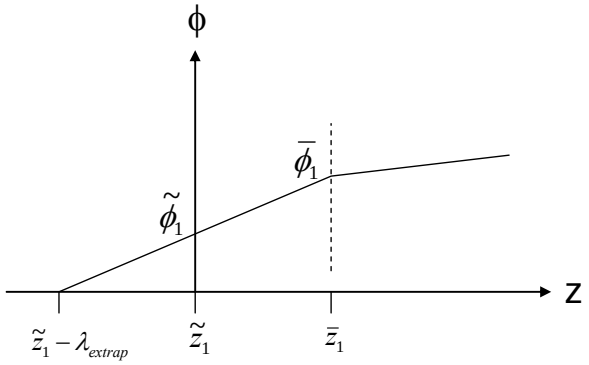

Figure 4: The Extrapolated Length Boundary Condition

Assuming a linear flux profile, the flux at the boundary may be found.

$$\frac{\tilde{\bar{\phi}}_1}{\lambda_{extrap}} = \frac{\bar{\phi}_1 - \tilde{\bar{\phi}}_1}{\bar{z}_1 - \tilde{\bar{z}}_1}$$

$$\tilde{\bar{\phi}}_1 = \frac{\lambda_{extrap}}{\lambda_{extrap} + \bar{z}_1 - \tilde{\bar{z}}_1}\bar{\phi}_1$$

Using this, the leakage per unit surface area at the boundary is given by:

$$\tilde{J}_1^{\,z} = \tilde{L}_1^{z\,\prime\prime}\,\phi_1 = -D^z \left.\frac{\partial \phi}{\partial z}\right|_{boundary}$$

$$= -\tilde{\bar{z}}_1 \bar{D}_1^{\,z} \frac{\bar{\phi}_1 - \tilde{\bar{\phi}}_1}{\bar{z}_1 - \tilde{\bar{z}}_1}$$

$$= -\bar{D}_1^{\,z} \frac{1 - \dfrac{\lambda_{extrap}}{\lambda_{extrap} + \bar{z}_1 - \tilde{\bar{z}}_1}}{\bar{z}_1 - \tilde{\bar{z}}_1}\bar{\phi}_1$$

$$= \frac{-\bar{D}_1^{\,z}}{\lambda_{extrap} + \bar{z}_1 - \tilde{\bar{z}}_1}\bar{\phi}_1$$

$$= \frac{-1}{\dfrac{\bar{z}_1 - \tilde{\bar{z}}_1}{\bar{D}_1^{\,z}} + \dfrac{\lambda_{extrap}}{\bar{D}_1^{\,z}}}\bar{\phi}_1$$

Therefore, with reference to Equation (3.11), a first-mesh vacuum boundary condition may be represented by replacing the term $\frac{\tilde{\bar{z}}_i - \bar{z}_{i-1}}{\bar{D}_{i-1}^{\,z}}$ with $\frac{\lambda_{extrap}}{\bar{D}_i^{\,z}}$. Similarly, for a final-mesh vacuum boundary, the term $\frac{\bar{z}_i - \tilde{\bar{z}}_i}{\bar{D}_i^{\,z}}$ may be replaced by $\frac{\lambda_{extrap}}{\bar{D}_{i-1}^{\,z}}$. This replacement is applicable to all directions, namely axial, radial and azimuthal.

For the special case of a reflecting boundary, the zero gradient boundary condition is approximated using a very large extrapolated length to diffusion coefficient ratio.

$$\lim_{\frac{\lambda_{extrap}}{D^z}\to\infty} D^z \left.\frac{\partial\phi}{\partial z}\right|_{boundary} = \lim_{\frac{\lambda_{extrap}}{D^z}\to\infty} D^z \frac{\bar{\phi}_1 - \tilde{\phi}_1}{\lambda_{extrap}} = 0$$

The value $\frac{\lambda_{extrap}}{\overline{D}_i^z}$ is chosen to be 10^{50}. For typical diffusion lengths (in the order of centimetres to metres), the error introduced by this approximation is in the order of 10^{-40}, which is considered negligible.

3.2.3.3 Delayed neutron production

Although there are a relatively large number of fission products, which subsequently decay via neutron emission, the observed composite emission characteristics of delayed neutrons may be well represented by defining six effective delayed neutron groups. Each group is characterized by a decay constant, λ_l, and a relative yield fraction, β_l / β. The decay constants λ_l for the delayed neutron groups are given in Table 1 for ^{235}U fuel. In the TINTE implementation, this group structure is used for all fissionable isotopes. The source and derivation of the delayed neutron data are discussed in Appendix B and Appendix C.

Table 1: Decay Constants for the Six Delayed Neutron Precursor Groups, ^{235}U [12]

Delayed Neutron Group	Group Decay Constant λ_l [s^{-1}]
1	3.87
2	1.4
3	0.311
4	0.116
5	0.03174
6	0.01272

A fraction β_l of delayed neutrons is produced per fission in the l^{th} precursor group. The total fraction of delayed neutrons is therefore $\beta = \sum_{l=1}^{6} \beta_l$. The values β_l are dependent on the nucleus split by fission and are therefore material-dependent. The effective fraction, $\beta_{l,i}$, for a material is determined by its component fissionable isotopes.

$$\beta_{l,i} = \left[\left(\frac{\beta_l}{\beta}\right)_{U5} \beta_{U5} F_{U5,i} + \left(\frac{\beta_l}{\beta}\right)_{Th2} \beta_{Th2} F_{Th2,i} + \ldots + \left(\frac{\beta_l}{\beta}\right)_{Pu2} \beta_{Pu2} F_{Pu2,i} \right] \frac{1}{F_{U5,i} + F_{Th2,i} + \ldots + F_{Pu2,i}} \quad (\mathbf{3}.15)$$

The ratios $\frac{F_{U5,i}}{F_{U5,i} + F_{Th2,i} + \ldots + F_{Pu2,i}} \equiv R_{U5,i}$, etc., representing the fraction of fissions in a fissionable isotope, for each nuclear material, are assumed to be user-supplied parameters. The relative group yield fractions β_l / β and total yield fractions β for each fissionable isotope are given in Table 2 and Table 3. The source and derivation of these values are discussed in Appendix B and Appendix C.

It should be noted that all β values given are physical [13] values, i.e. no compensation for the differences in energy spectra of the prompt and delayed neutrons has been made.

Table 2: Fractional Fission Yield (β) of Delayed Neutrons for Fissionable Isotopes*

Fractional Fission Yield (β) of Delayed Neutrons [%]									
^{235}U	^{232}Th	^{233}U	^{234}U	^{236}U	^{238}U	^{239}Pu	^{240}Pu	^{241}Pu	^{242}Pu
0.6904	2.3981	0.2962	0.4342	1.1693	1.751	0.2245	0.285	0.5354	1.0524

Table 3: Fraction of Delayed Neutrons (β_l / β) for Fissionable Isotopes and the Six Delayed Neutron Precursor Groups†

Group	Fractional Fission Yield (β_l / β) for Delayed Neutron Precursor Group [%]									
	^{235}U	^{232}Th	^{233}U	^{234}U	^{236}U	^{238}U	^{239}Pu	^{240}Pu	^{241}Pu	^{242}Pu
1	2.6	2.8	0.6	2.6	2.6	4	1.2	2.2	0.3	1
2	12.8	18	11.9	12.8	12.8	30.5	14.1	15.3	24.7	23.7
3	40.7	45.6	26	40.7	40.7	37.7	31	32.8	32.1	39.1
4	18.8	16	27	18.8	18.8	13	26.3	24.1	22.1	18.9
5	21.3	14.1	25.8	21.3	21.3	13.6	18.6	18.1	15.2	12.9
6	3.8	3.5	8.7	3.8	3.8	1.2	8.8	7.6	5.6	4.5

3.2.3.3.1 Transient case

The time-dependent precursor concentration may be described by the following differential Equation [7].

$$\frac{\partial C_l}{\partial t} = \beta_l P - \lambda_l C_l \tag{**3**.16}$$

If the production P is assumed linear over the time interval Δ, the integration of Equation (**3**.16) may be carried out. The concentration at the end of the time interval is found to be:

$$\lambda_l C_{l1} = \beta_l P_1 + \left(\lambda_l C_{l0} - \beta_l P_0\right) e^{-\lambda_l \Delta} - \beta_l \frac{P_1 - P_0}{\lambda_l \Delta}\left(1 - e^{-\lambda_l \Delta}\right) \tag{**3**.17}$$

The mean concentration for the interval is found to be:

$$\lambda_l \overline{C}_l = \lambda_l C_{l0} \frac{1 - e^{-\lambda_l \Delta}}{\lambda_l \Delta} + \beta_l P_0 \left(\frac{1}{2} + \frac{e^{-\lambda_l \Delta} - \dfrac{1 - e^{-\lambda_l \Delta}}{\lambda_l \Delta}}{\lambda_l \Delta} \right) + \beta_l P_1 \left(\frac{1}{2} - \frac{1 - \dfrac{1 - e^{-\lambda_l \Delta}}{\lambda_l \Delta}}{\lambda_l \Delta} \right) \tag{**3**.18}$$

The derivations of Equations (**3**.17) and (**3**.18) are given in [5].

---

* Refer to Appendix B.

† Refer to Appendix C.

3.2.3.3.2 Steady-state case

For the steady-state delayed neutron precursor concentration, the time-derivative in (**3**.16) disappears, resulting in the following relation:

$$\lambda_l C_l = \beta_l P \tag{**3**.19}$$

3.2.3.4 Time Discretization

The time discretized diffusion equations are given below. The derivation using Equations (**3**.5), (**3**.6) and (**3**.18) is given in [5].

$$\left(\frac{1}{v_1\Delta} - \nabla D_1 \nabla + \Sigma_{a1} + \Sigma_s^{1\to 2}\right)\phi_1^1 - \Sigma_s^{2\to 1}\phi_2^1 - P_1\left(1 - 2\sum_l \beta_l \frac{1 - \frac{1-e^{-\lambda_l\Delta}}{\lambda_l\Delta}}{\lambda_l\Delta}\right)$$
$$= \frac{1}{v_1\Delta}\phi_1^0 + P_0\left(\beta + 2\sum_l \beta_l \frac{e^{-\lambda_l\Delta} - \frac{1-e^{-\lambda_l\Delta}}{\lambda_l\Delta}}{\lambda_l\Delta}\right) - \sum_l \lambda_l C_{l0}\left(1 - 2\frac{1-e^{-\lambda_l\Delta}}{\lambda_l\Delta}\right) + S_\phi \tag{**3**.20}$$

$$\left(\frac{1}{v_2\Delta} - \nabla D_2 \nabla + \Sigma_{a2} + \Sigma_s^{2\to 1}\right)\phi_2^1 - \Sigma_s^{1\to 2}\phi_1^1 = \frac{1}{v_2\Delta}\phi_2^0 \tag{**3**.21}$$

If a one-dimensional calculation with leakages from adjacent cells is assumed and the spatial discretization of paragraph 3.2.3.2 is applied to Equations (**3**.20) and (**3**.21).

$$\left(\frac{1}{v_1\Delta}V - \left(\tilde{L}_{1,j}^r - \tilde{L}_{1,j+1}^r + \tilde{L}_{1,i}^z - \tilde{L}_{1,i+1}^z + \tilde{L}_{1,k}^\theta - \tilde{L}_{1,k+1}^\theta\right) + \Sigma_{a1}V + \Sigma_s^{1\to 2}V\right)\phi_1^1 - \Sigma_s^{2\to 1}\phi_2^1 V$$
$$- P_1 V\left(1 - 2\sum_l \beta_l \frac{1 - \frac{1-e^{-\lambda_l\Delta}}{\lambda_l\Delta}}{\lambda_l\Delta}\right)$$
$$= \frac{1}{v_1\Delta}V\phi_1^0 + P_0 V\left(\beta + 2\sum_l \beta_l \frac{e^{-\lambda_l\Delta} - \frac{1-e^{-\lambda_l\Delta}}{\lambda_l\Delta}}{\lambda_l\Delta}\right) - \sum_l \lambda_l C_{l0}\left(1 - 2\frac{1-e^{-\lambda_l\Delta}}{\lambda_l\Delta}\right)V + S_\phi V \tag{**3**.22}$$

$$\left(\frac{1}{v_2\Delta}V - \left(\tilde{L}_{2,j}^r - \tilde{L}_{2,j+1}^r + \tilde{L}_{2,i}^z - \tilde{L}_{2,i+1}^z + \tilde{L}_{2,k}^\theta - \tilde{L}_{2,k+1}^\theta\right) + \Sigma_{a2}V + \Sigma_s^{2\to 1}V\right)\phi_2^1 - \Sigma_s^{1\to 2}V\phi_1^1$$
$$= \frac{1}{v_2\Delta}V\phi_2^0 \tag{**3**.23}$$

3.2.3.5 The Steady-state Calculation

In order to ensure that the steady-state solution is also the stationary state of the time-dependent equations, a quasi-transient solution method is adopted. An artificial time interval is chosen, which is applied to the $\frac{1}{v}$ terms in Equations (**3**.22) and (**3**.23).

For the delayed neutron production terms, however, it is assumed that the time interval tends towards infinity (steady-state condition). The exponential terms in Equation (**3**.22) drop away and the equation is reduced to:

$$\left(\frac{1}{v_1\Delta}V-\left(\tilde{L}^r_{1,j}-\tilde{L}^r_{1,j+1}+\tilde{L}^z_{1,i}-\tilde{L}^z_{1,i+1}+\tilde{L}^\theta_{1,k}-\tilde{L}^\theta_{1,k+1}\right)+\Sigma_{a1}V+\Sigma_s^{1\to2}V\right)\phi_1^1-\Sigma_s^{2\to1}\phi_2^1V-P_1V$$
$$=\frac{1}{v_1\Delta}V\phi_1^0+\beta P_0 V-\sum_l \lambda_l C_{l0}V+S_\phi V$$

Using Equation (**3**.19), the delayed neutron terms drop away completely; resulting in the steady state discretized fast group diffusion equation.

$$\left(\frac{1}{v_1\Delta}V-\left(\tilde{L}^r_{1,j}-\tilde{L}^r_{1,j+1}+\tilde{L}^z_{1,i}-\tilde{L}^z_{1,i+1}+\tilde{L}^\theta_{1,k}-\tilde{L}^\theta_{1,k+1}\right)+\Sigma_{a1}V+\Sigma_s^{1\to2}V\right)\phi_1^1-\Sigma_s^{2\to1}\phi_2^1V-P_1V$$
$$=\frac{1}{v_1\Delta}V\phi_1^0+S_\phi V \qquad \text{(3.24)}$$

Equations (**3**.24) and (**3**.23) are transformed into an eigenvalue problem by adjusting the neutron poison level. For this, the production terms are replaced by P/k, where k is the eigenvalue. In the eigenvalue problem, the flux level is unknown and is determined by specifying the thermal power of the reactor. Therefore, the neutron fluxes are calculated assuming an eigenvalue. The neutron fluxes are normalized to the user-specified reactor power. The eigenvalue is then updated according to the calculated flux. This process is repeated until the neutron fluxes and eigenvalue converge. This represents the intermediate flux iteration loop.

3.2.3.5.1 The start-up feedback term

When the calculation is started, the neutron flux is not known. For the first neutron flux calculation, the 'old-time' fluxes (ϕ^0) are assumed zero. As a result, the right-hand sides of Equations (**3**.23) and (**3**.24) become zero and $S_\phi V$ respectively. The methodology used for the initial neutron flux calculation is discussed in paragraph 3.2.3.8.2.

3.2.3.6 The leakage iteration method

An iterative method is employed for solving the discretized two-group diffusion equation (Equations (**3**.22) and (**3**.23)) in a coupled manner. This method is derived from the method used by Naito et al [10] and Monterosso and Vincenti [11].

The reactor is divided into a number of layers along the z-axis and a number of channels in the rθ-plane, as shown in Figure 5. A block is formed at the intersection of each layer with each channel. The blocks correspond to the nuclear iteration meshes described in Chapter 2. This method, therefore, yields neutron flux values within the nuclear iteration mesh.

The iterative method of solving the two-group diffusion equations using this method is described. The leakage from adjacent (radial and azimuthal) directions is initially assumed. A

one-dimensional calculation is carried out in the axial direction to obtain updated fluxes and axial leakages. The updated axial leakages are used for the one-dimensional calculation in the radial direction, yielding updated fluxes and radial leakages. The updated radial and axial leakages are then used for the one-dimensional calculation in the azimuthal direction, yielding updated fluxes and azimuthal leakages. The one-dimensional calculations are iterated until consistency is obtained.

In calculating accurately the flux within each block, it is necessary to obtain accurate leakage values. For this purpose, each block is further subdivided in the direction of the channel, into a number of fine meshes (sublayers) to improve on the finite-difference approximation that would normally be applied to each block. This fine meshing of the channels is implemented through the 1D leakage iteration meshes described in Chapter 2. In this way, for each channel (as defined by the iteration mesh) a single 1D calculation is carried out using a fine mesh discretization in the 1D direction for N channels and N dimensions. The total number of 1D calculations carried out can therefore be written for the three-dimensional case as:

$$N_{1D} = N_i \left(N_{cy} N_{cz} + N_{cx} N_{cz} + N_{cx} N_{cy} \right)$$

Where

N_{1D} is the number of required one-dimensional calculations for convergence.

N_i is the number of iterations required to achieve convergence of the azimuthal leakages.

N_{cx}, N_{cy}, N_{cz} are the number of coarse iteration mesh divisions defined in the x, y and z directions respectively.

The leakage iteration method has the following characteristics:

a. A fine-mesh difference technique is applied to only the channels and layers. It is therefore not necessary to store the flux at all fine-mesh points. This reduces computational time and memory usage.
b. Because the leakage at each surface of a block is calculated using a fine-mesh difference approximation, the discretization error is reduced.
c. When only one fine mesh point is located within each block, this method becomes equivalent to the finite-difference method.

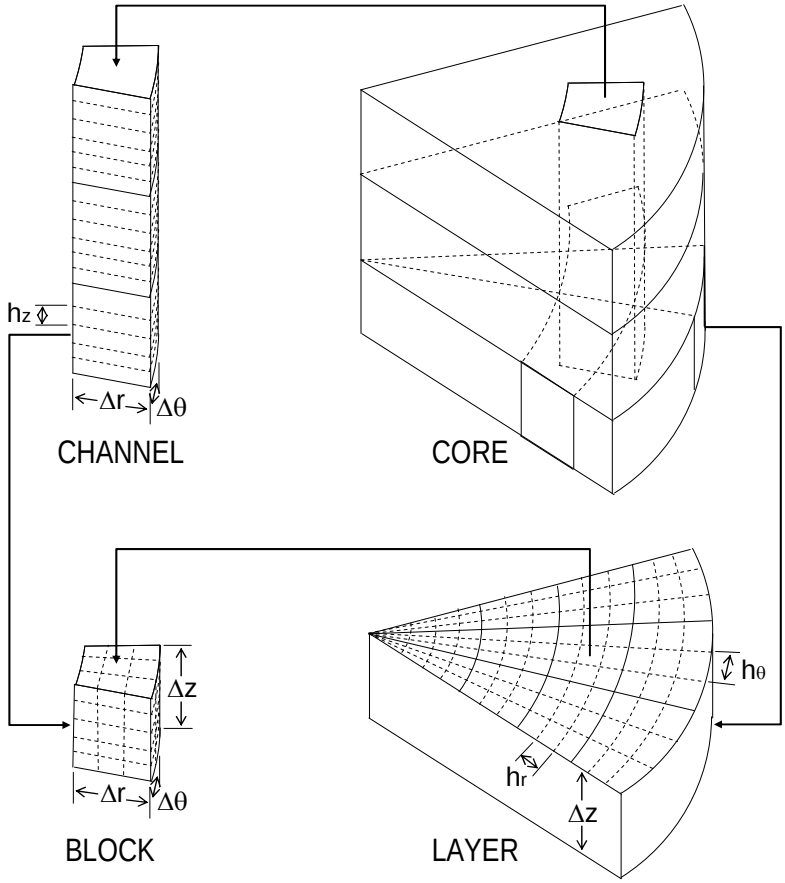

Figure 5: Configuration of Channels, Layers and Blocks

The one-dimensional discretized diffusion equation in the axial direction is obtained for the fast group by substituting Equation (**3**.12) in (**3**.22).

$$\left(\frac{1}{v_1\Delta}V-\left(\tilde{L}^{r}_{1,j}-\tilde{L}^{r}_{1,j+1}+\tilde{L}^{\theta}_{1,k}-\tilde{L}^{\theta}_{1,k+1}\right)+\Sigma_{a1}V+\Sigma_s^{1\to 2}V\right)\phi^1_{1,i}$$
$$+\frac{\left(\tilde{r}_{j+1}{}^2-\tilde{r}_j{}^2\right)\left(\tilde{\theta}_{k+1}-\tilde{\theta}_k\right)}{\frac{\bar{z}_i-\tilde{z}_i}{\bar{D}^z_{1,i}}+\frac{\tilde{z}_i-\bar{z}_{i-1}}{\bar{D}^z_{1,i-1}}}\left(\phi^1_{1,i}-\phi^1_{1,i-1}\right)-\frac{\left(\tilde{r}_{j+1}{}^2-\tilde{r}_j{}^2\right)\left(\tilde{\theta}_{k+1}-\tilde{\theta}_k\right)}{\frac{\bar{z}_{i+1}-\tilde{z}_{i+1}}{\bar{D}^z_{1,i+1}}+\frac{\tilde{z}_{i+1}-\bar{z}_i}{\bar{D}^z_{1,i}}}\left(\phi^1_{1,i-1}-\phi^1_{1,i}\right)$$
$$-\Sigma_s^{2\to 1}V\phi^1_{2,i}-P^1_iV\left(1-2\sum_l\beta_l\frac{1-\frac{1-e^{-\lambda_l\Delta}}{\lambda_l\Delta}}{\lambda_l\Delta}\right)$$
$$=\frac{1}{v_1\Delta}V\phi^0_{1,i}+P^0_iV\left(\beta+2\sum_l\beta_l\frac{e^{-\lambda_l\Delta}-\frac{1-e^{-\lambda_l\Delta}}{\lambda_l\Delta}}{\lambda_l\Delta}\right)-\sum_l\lambda_lC_{l0,i}\left(1-2\frac{1-e^{-\lambda_l\Delta}}{\lambda_l\Delta}\right)V+S_\phi V$$

Note that P^0_i and P^1_i refer to the production in mesh I at times t_0 and t_1 respectively.

Similarly, substitution of Equation (**3**.12) in (**3**.23) yields the discretized one-dimensional diffusion equation in the axial direction, for the thermal group.

$$\left(\frac{1}{v_2\Delta}V-\left(\tilde{L}^r_{2,j}-\tilde{L}^r_{2,j+1}+\tilde{L}^\theta_{2,k}-\tilde{L}^\theta_{2,k+1}\right)+\Sigma_{a2}V+\Sigma_s^{2\to1}V\right)\phi^1_{2,i}$$
$$+\frac{\left(\tilde{r}_{j+1}{}^2-\tilde{r}_j{}^2\right)\left(\tilde{\theta}_{k+1}-\tilde{\theta}_k\right)}{\frac{\bar{z}_i-\tilde{z}_i}{\bar{D}^z_{2,i}}+\frac{\tilde{z}_i-\bar{z}_{i-1}}{\bar{D}^z_{2,i-1}}}\left(\phi^1_{2,i}-\phi^1_{2,i-1}\right)-\frac{\left(\tilde{r}_{j+1}{}^2-\tilde{r}_j{}^2\right)\left(\tilde{\theta}_{k+1}-\tilde{\theta}_k\right)}{\frac{\bar{z}_{i+1}-\tilde{z}_{i+1}}{\bar{D}^z_{2,i+1}}+\frac{\tilde{z}_{i+1}-\bar{z}_i}{\bar{D}^z_{2,i}}}\left(\phi^1_{2,i+1}-\phi^1_{2,i}\right)$$
$$-\Sigma_s^{1\to2}V\phi^1_{1,i}=\frac{1}{v_2\Delta}V\phi^0_{2,i}$$

This system of equations may be written generically as:

$$p_{1,i}\phi^1_{1,i}-r_{1,i}\phi^1_{1,i-1}-r_{1,i+1}\phi^1_{1,i+1}-s_i\phi^1_{2,i}=q_{1,i}\qquad(i=1,\ldots L)\tag{3.25}$$

$$p_{2,i}\phi^1_{2,i}-r_{2,i}\phi^1_{2,i-1}-r_{2,i+1}\phi^1_{2,i+1}-m_i\phi^1_{1,i}=q_{2,i}\qquad(i=1,\ldots L)\tag{3.26}$$

These equations may be written in matrix form for each channel.

$$\mathbf{A\Phi}=\begin{bmatrix}\begin{bmatrix}p_{11}&-s_1\\-m_1&p_{21}\end{bmatrix}&\begin{bmatrix}-r_{12}&0\\0&-r_{22}\end{bmatrix}&&&\\\begin{bmatrix}-r_{12}&0\\0&-r_{22}\end{bmatrix}&\begin{bmatrix}p_{12}&-s_2\\-m_2&p_{22}\end{bmatrix}&\ddots&&\\&\ddots&\ddots&\begin{bmatrix}-r_{13}&0\\0&-r_{23}\end{bmatrix}&\\&&\begin{bmatrix}-r_{1,L}&0\\0&-r_{2,L}\end{bmatrix}&\begin{bmatrix}p_{1,L}&-s_L\\-m_L&p_{2,L}\end{bmatrix}\end{bmatrix}\begin{bmatrix}\begin{bmatrix}\phi^1_{11}\\\phi^1_{21}\end{bmatrix}\\\begin{bmatrix}\phi^1_{12}\\\phi^1_{22}\end{bmatrix}\\\vdots\\\begin{bmatrix}\phi^1_{1,L}\\\phi^1_{2,L}\end{bmatrix}\end{bmatrix}=\begin{bmatrix}\begin{bmatrix}q_{11}\\q_{21}\end{bmatrix}\\\begin{bmatrix}q_{12}\\q_{22}\end{bmatrix}\\\vdots\\\begin{bmatrix}q_{1,L}\\q_{2,L}\end{bmatrix}\end{bmatrix}\tag{3.27}$$

where, for the transient case in the axial direction, the coefficients are defined as:

$$p_{1,i}=\frac{1}{v_1\Delta}V-\left(\tilde{L}^r_{1,j}-\tilde{L}^r_{1,j+1}+\tilde{L}^\theta_{1,k}-\tilde{L}^\theta_{1,k+1}\right)+\Sigma_{a1}V+\Sigma_s^{1\to2}V$$
$$-\frac{1}{k}\nu\Sigma_{f1}V\left(1-2\sum_l\beta_l\frac{1-\frac{1-e^{-\lambda_l\Delta}}{\lambda_l\Delta}}{\lambda_l\Delta}\right)+\frac{\left(\tilde{r}_{j+1}{}^2-\tilde{r}_j{}^2\right)\left(\tilde{\theta}_{k+1}-\tilde{\theta}_k\right)}{\frac{\bar{z}_i-\tilde{z}_i}{\bar{D}_{z,i}}+\frac{\tilde{z}_i-\bar{z}_{i-1}}{\bar{D}_{z,i-1}}}+\frac{\left(\tilde{r}_{j+1}{}^2-\tilde{r}_j{}^2\right)\left(\tilde{\theta}_{k+1}-\tilde{\theta}_k\right)}{\frac{\bar{z}_{i+1}-\tilde{z}_{i+1}}{\bar{D}_{z,i+1}}+\frac{\tilde{z}_{i+1}-\bar{z}_i}{\bar{D}_{z,i}}}\tag{3.28}$$

$$p_{2,i}=\frac{1}{v_2\Delta}V-\left(\tilde{L}^r_{2,j}-\tilde{L}^r_{2,j+1}+\tilde{L}^\theta_{2,k}-\tilde{L}^\theta_{2,k+1}\right)+\Sigma_{a2}V+\Sigma_s^{2\to1}V$$
$$+\frac{\left(\tilde{r}_{j+1}{}^2-\tilde{r}_j{}^2\right)\left(\tilde{\theta}_{k+1}-\tilde{\theta}_k\right)}{\frac{\bar{z}_i-\tilde{z}_i}{\bar{D}^z_{2,i}}+\frac{\tilde{z}_i-\bar{z}_{i-1}}{\bar{D}^z_{2,i-1}}}+\frac{\left(\tilde{r}_{j+1}{}^2-\tilde{r}_j{}^2\right)\left(\tilde{\theta}_{k+1}-\tilde{\theta}_k\right)}{\frac{\bar{z}_{i+1}-\tilde{z}_{i+1}}{\bar{D}^z_{2,i+1}}+\frac{\tilde{z}_{i+1}-\bar{z}_i}{\bar{D}^z_{2,i}}}\tag{3.29}$$

$$r_{1,i}=\frac{\left(\tilde{r}_{j+1}{}^2-\tilde{r}_j{}^2\right)\left(\tilde{\theta}_{k+1}-\tilde{\theta}_k\right)}{\frac{\bar{z}_i-\tilde{z}_i}{\bar{D}^z_{1,i}}+\frac{\tilde{z}_i-\bar{z}_{i-1}}{\bar{D}^z_{1,i-1}}}\tag{3.30}$$

$$r_{2,i}=\frac{\left(\tilde{r}_{j+1}{}^2-\tilde{r}_j{}^2\right)\left(\tilde{\theta}_{k+1}-\tilde{\theta}_k\right)}{\frac{\bar{z}_i-\tilde{z}_i}{\bar{D}^z_{2,i}}+\frac{\tilde{z}_i-\bar{z}_{i-1}}{\bar{D}^z_{2,i-1}}}\tag{3.31}$$

$$s_i = \Sigma_s^{2\to 1} V + \frac{1}{k} \nu \Sigma_{f2} V \left(1 - 2 \sum_l \beta_l \frac{1 - \frac{1 - e^{-\lambda_l \Delta}}{\lambda_l \Delta}}{\lambda_l \Delta} \right) \tag{3.32}$$

$$m_i = \Sigma_s^{1\to 2} V \tag{3.33}$$

$$q_{1,i} = \frac{1}{v_1 \Delta} V \phi_{1,i}^0 + P_i^0 V \left(\beta + 2 \sum_l \beta_l \frac{e^{-\lambda_l \Delta} - \frac{1 - e^{-\lambda_l \Delta}}{\lambda_l \Delta}}{\lambda_l \Delta} \right) - \sum_l \lambda_l C_{l0,i} \left(1 - 2 \frac{1 - e^{-\lambda_l \Delta}}{\lambda_l \Delta} \right) V + S_\phi V \tag{3.34}$$

$$q_{2,i} = \frac{1}{v_2 \Delta} V \phi_{2,i}^0 \tag{3.35}$$

For the steady-state calculation, $P_{1,i}$, s_i and $q_{1,i}$ differ from the transient case (refer to paragraph 3.2.3.5). They are given below.

$$\begin{aligned} p_{1,i} = {} & \frac{1}{v_1 \Delta} V - \left(\tilde{L}_{1,j}^r - \tilde{L}_{1,j+1}^r + \tilde{L}_{1,k}^\theta - \tilde{L}_{1,k+1}^\theta \right) + \Sigma_{a1} V + \Sigma_s^{1\to 2} V \\ & - \frac{1}{k} \nu \Sigma_{f1} V + \frac{\left(\tilde{r}_{j+1}^{\,2} - \tilde{r}_j^{\,2} \right) \left(\tilde{\theta}_{k+1} - \tilde{\theta}_k \right)}{\frac{\bar{z}_i - \tilde{z}_i}{\overline{D}_{z,i}} + \frac{\tilde{z}_i - \bar{z}_{i-1}}{\overline{D}_{z,i-1}}} + \frac{\left(\tilde{r}_{j+1}^{\,2} - \tilde{r}_j^{\,2} \right) \left(\tilde{\theta}_{k+1} - \tilde{\theta}_k \right)}{\frac{\bar{z}_{i+1} - \tilde{z}_{i+1}}{\overline{D}_{z,i+1}} + \frac{\tilde{z}_{i+1} - \bar{z}_i}{\overline{D}_{z,i}}} \end{aligned} \tag{3.36}$$

$$s_i = \Sigma_s^{2\to 1} V + \frac{1}{k} \nu \Sigma_{f2} V \tag{3.37}$$

$$q_{1,i} = \frac{1}{v_1 \Delta} V \phi_{1,i}^0 + S_\phi V \tag{3.38}$$

The matrix $\mathbf{A}$, consisting of 2 x 2 sub-matrices, may be considered to be a tridiagonal matrix and therefore a direct solution may be found.

The recursion formulae [11] are given as:

$$\mathbf{\Phi}_i = \begin{bmatrix} \varphi_{1,i}^1 \\ \varphi_{2,i}^1 \end{bmatrix} = \mathbf{a}_i \bullet \mathbf{\Phi}_{i+1} + \mathbf{b}_i \tag{3.39}$$

where the matrix $\mathbf{a}_i$ is:

$$\mathbf{a}_i = \left(\mathbf{P}_i - \mathbf{R}_i \bullet \mathbf{a}_{i-1} \right)^{-1} \mathbf{R}_{i+1} = \left(\begin{bmatrix} p_{1,i} & -s_i \\ -m_i & p_{2,i} \end{bmatrix} - \begin{bmatrix} -r_{1,i} & 0 \\ 0 & -r_{2,i} \end{bmatrix} \bullet \mathbf{a}_{i-1} \right)^{-1} \bullet \begin{bmatrix} -r_{1,i+1} & 0 \\ 0 & -r_{2,i+1} \end{bmatrix} \tag{3.40}$$

and the vector $\mathbf{b}_i$ is:

$$\begin{aligned}\mathbf{b}_i &= \left(\mathbf{P}_i - \mathbf{R}_i \bullet \mathbf{a}_{i-1}\right)^{-1} \bullet \left(\mathbf{Q}_i + \mathbf{R}_i \bullet \mathbf{b}_{i-1}\right) \\ &= \left(\begin{bmatrix} p_{1,i} & -s_i \\ -m_i & p_{2,i} \end{bmatrix} - \begin{bmatrix} -r_{1,i} & 0 \\ 0 & -r_{2,i} \end{bmatrix} \bullet \mathbf{a}_{i-1}\right)^{-1} \bullet \left(\begin{bmatrix} q_{1,i} \\ q_{2,i} \end{bmatrix} + \begin{bmatrix} -r_{1,i} & 0 \\ 0 & -r_{2,i} \end{bmatrix} \bullet \mathbf{b}_{i-1}\right)\end{aligned} \quad (\mathbf{3}.41)$$

The boundary conditions are:

$$\mathbf{\Phi}_0 = \mathbf{\Phi}_{L+1} = \begin{bmatrix} 0 \\ 0 \end{bmatrix}$$

Therefore $\mathbf{a}_0 = 0$ and $\mathbf{b}_0 = 0$.

Starting with the known $\mathbf{a}_0$ and $\mathbf{b}_0$, all values of $\mathbf{a}_i$ and $\mathbf{b}_i$ are calculated forwards using Equations (**3**.40) and (**3**.41). These values are then substituted into the recursion formulae (**3**.39) to obtain the updated neutron flux.

The inversion of the 2 x 2 matrices $\left(\mathbf{P}_i - \mathbf{R}_i \bullet \mathbf{a}_{i-1}\right)$ is carried out directly using the equation:

$$\mathbf{W}^{-1} = \frac{1}{|\mathbf{W}|}\left(\text{cof } \mathbf{W}\right)^T \quad (\mathbf{3}.42)$$

where the determinant is easily obtained as:

$$|\mathbf{W}| = \det\begin{bmatrix} w_{11} & w_{12} \\ w_{21} & w_{22} \end{bmatrix} = w_{11}w_{22} - w_{12}w_{21} \quad (\mathbf{3}.43)$$

and the transposed cofactor matrix is given by:

$$\left(\text{cof } \mathbf{W}\right)^T = \begin{bmatrix} w_{22} & -w_{12} \\ -w_{21} & w_{11} \end{bmatrix} \quad (\mathbf{3}.44)$$

Updated leakages at the block boundaries are obtained using one of Equations (**3**.11), (**3**.12) or (**3**.13), depending on the chosen coordinate. The leakage values at boundaries are calculated using modified forms of Equations (**3**.11), (**3**.12) and (**3**.13) as described in paragraph 3.2.3.2.1.

3.2.3.7 Mapping properties to/from the iteration mesh

3.2.3.7.1 Calculating the material mesh based neutron flux

In order to derive a method of mapping properties to/from the iteration mesh, a simple one-dimensional case is considered. Consider the iteration block, shown in Figure 6, consisting of three material blocks and nine fine iteration blocks. Note that the hat ($\hat{1}$, $\hat{2}$, etc.), in the context of this paragraph, refers to material block indices.

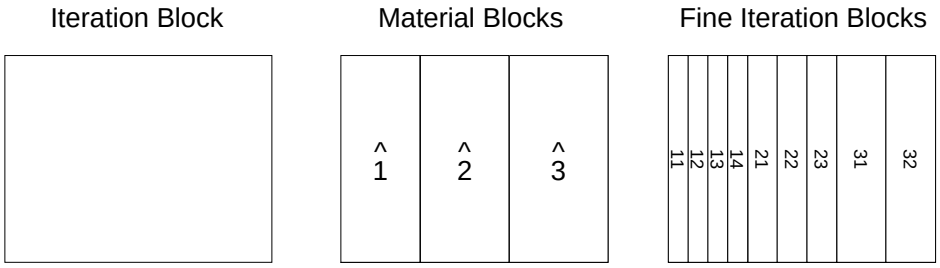

Figure 6: Calculating the Material Mesh Based Neutron Flux, 1D Case

We consider the volume integrated neutron flux within material block 1.

$$\int_{\hat{1}} \phi \, dV = \phi_{\hat{1}} V_{\hat{1}} = \phi_{11} V_{11} + \phi_{12} V_{12} + \phi_{13} V_{13} + \phi_{14} V_{14}$$

$$\therefore \phi_{\hat{1}} V = \sum_{ii \in \hat{1}} \phi_{ii} V_{ii}$$

Within each material block, the subdivisions have equal volume, therefore:

$$\phi_{\hat{1}} V_{\hat{1}} = V_{11} \sum_{ii \in \hat{1}} \phi_{ii}$$

$$\therefore \phi_{\hat{1}} = \frac{1}{n_{\hat{1}}} \sum_{ii \in \hat{1}} \phi_{ii} \qquad (\mathbf{3}.45)$$

Where $n_{\hat{i}}$ is the number of fine iteration blocks in the i[th] material block. This is simply the arithmetic mean of the fine block neutron fluxes.

Starting with the obvious relationship $\phi_{\hat{1}} = \phi_{\hat{1}}$, and introducing Equation (**3**.45):

$$\phi_{\hat{1}} = \left(\frac{\phi_{\hat{1}}}{\phi} \right) \phi = \frac{\sum_{ii \in \hat{1}} \phi_{ii}}{\phi} \frac{\phi}{n_{\hat{1}}}$$

$$\therefore \phi_{\hat{1}} = \frac{S_{\hat{1}}}{n_{\hat{1}}} \phi$$

Here $S_{\hat{1}} = \dfrac{\sum_{ii \in \hat{1}} \phi_{ii}}{\phi}$ is the one-dimensional mesh transformation factor.

This approach may be extended to two dimensions. If one considers that the flux solutions have been obtained in the radial and axial directions using separate meshes, separate transformation factors $S_{r\hat{i}}$ and $S_{z\hat{j}}$ are defined for each direction. These may be used to define partially mapped radial and axial fluxes $\phi_{z\hat{1}}$, $\phi_{z\hat{2}}$, $\phi_{r\hat{1}}$, etc. as shown in Figure 7.

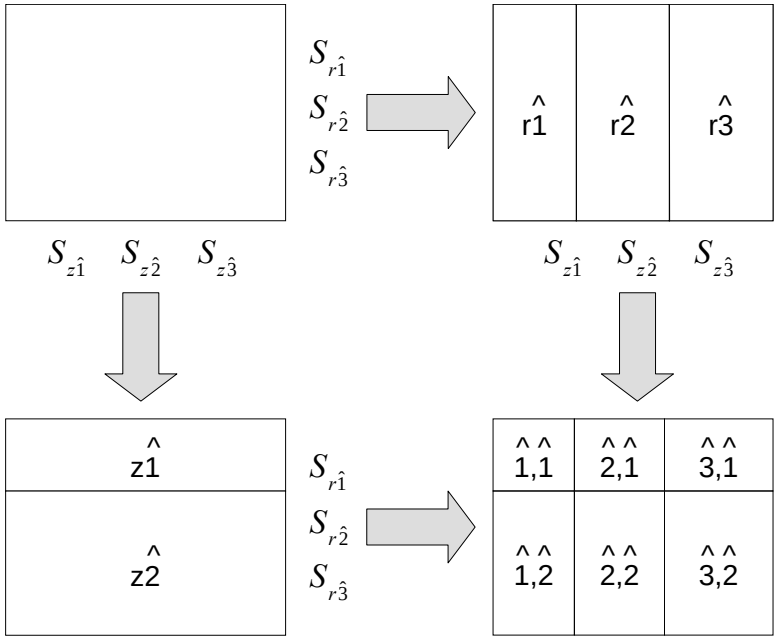

Figure 7: Calculating the Material Mesh Based Neutron Flux, 2D Case

The same mapping approach may then be followed using the partially mapped fluxes to obtain fully mapped fluxes in the material blocks. The fully mapped fluxes in two dimensions may therefore be obtained using the relationship:

$$\phi_{\hat{i},\hat{j}} = \frac{S_{r\hat{i}}}{n_{r\hat{i}}} \frac{S_{z\hat{j}}}{n_{z\hat{j}}} \phi \tag{**3**.46}$$

This may again be extended to the full three-dimensional case as follows:

$$\phi_{\hat{i},\hat{j},\hat{k}} = \frac{S_{z\hat{i}} S_{r\hat{j}} S_{\theta\hat{k}}}{n_{r\hat{i}} n_{z\hat{j}} n_{\theta\hat{k}}} \phi \tag{**3**.47}$$

where

$$S_{z\hat{i}} = \frac{\sum_{ii \in \hat{i}} \phi_{zz,ii}}{\phi^z} \tag{**3**.48}$$

$$S_{rj} = \frac{\sum_{jj \in \hat{j}} \phi_{rr,jj}}{\phi^r} \tag{**3**.49}$$

$$S_{\theta k} = \frac{\sum_{kk \in \hat{k}} \phi_{\theta\theta,kk}}{\phi^\theta} \tag{**3**.50}$$

and $n_{r\hat{i}}$, $n_{z\hat{j}}$ and $n_{\theta\hat{k}}$ is the total number of fine blocks per material mesh for the radial, axial and azimuthal iteration meshes respectively.

In the absence of flux data, the flux is assumed constant, yielding the following:

$$S_{z\hat{i}} = \sum_{ii \in \hat{i}} 1 \tag{**3**.51}$$

$$S_{r\hat{j}} = \sum_{jj \in \hat{j}} 1 \tag{3.52}$$

$$S_{\theta\hat{k}} = \sum_{kk \in \hat{k}} 1 \tag{3.53}$$

This is equivalent to the number of fine mesh intervals in the material block, and is used as an initial guess for the transformation factors.

3.2.3.7.2 Calculating coarse iteration mesh based properties

By using the volume-integrated flux over the coarse iteration block, as in paragraph 3.2.3.7.1, the iteration block flux ϕ^z for the axial solution is calculated as the volume-weighted sum of the fine-block fluxes.

$$\phi^z = \frac{\sum_{ii} \phi_{zz,ii} V_{ii}}{\sum_{ii} V_{ii}} \tag{3.54}$$

where V_{ii} is the axial fine-block volume and $\phi_{zz,ii}$ the axial fine-block neutron flux. Similarly, for the radial and azimuthal directions:

$$\phi^r = \frac{\sum_{jj} \phi_{rr,jj} V_{jj}}{\sum_{jj} V_{jj}} \tag{3.55}$$

$$\phi^\theta = \frac{\sum_{kk} \phi_{\theta\theta,kk} V_{kk}}{\sum_{kk} V_{kk}} \tag{3.56}$$

For a well-converged solution, $\phi \approx \phi^r \approx \phi^z \approx \phi^\theta$, therefore, a simple arithmetic mean is sufficient to determined the combined flux. The combined iteration block flux is therefore calculated as the arithmetic mean of the three solutions.

$$\phi = \frac{1}{3}\left(\phi^r + \phi^z + \phi^\theta\right) \tag{3.57}$$

The adjacent leakage at the fine-block edges is calculated using volume weighting of the iteration block leakages.

$$\tilde{L}^z_{ii} = \tilde{L}^z \frac{V_{ii}}{\sum_{ii} V_{ii}} \tag{3.58}$$

$$\tilde{L}^r_{jj} = \tilde{L}^r \frac{V_{jj}}{\sum_{jj} V_{jj}} \tag{3.59}$$

$$\tilde{L}^\theta_{kk} = \tilde{L}^\theta \frac{V_{kk}}{\sum_{kk} V_{kk}} \tag{3.60}$$

3.2.3.7.3 Mapping properties from the material mesh to the coarse iteration meshes

Consider the two-dimensional fine iteration block shown in Figure 8. Note, in this case, the iteration block shown has a depth equal to a single fine interval, i.e. this is a view from above a channel.

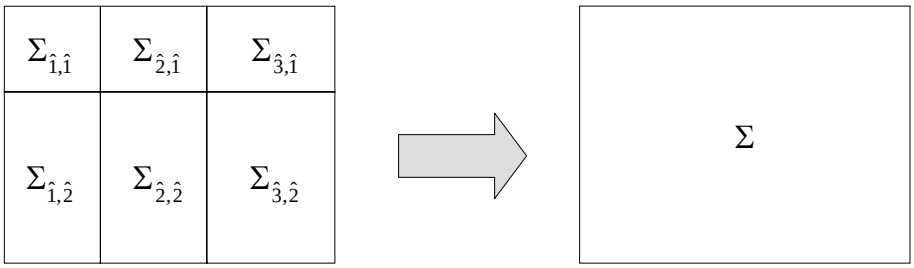

Figure 8: Mapping Cross Sections to the Coarse Iteration Mesh

By conservation of the reaction rate within both meshes, the following applies:

$$\Sigma\phi V = \Sigma_{\hat{1},\hat{1}}\phi_{\hat{1},\hat{1}}V_{\hat{1},\hat{1}} + \Sigma_{\hat{1},\hat{2}}\phi_{\hat{1},\hat{2}}V_{\hat{1},\hat{2}} + \Sigma_{\hat{1},\hat{3}}\phi_{\hat{1},\hat{3}}V_{\hat{1},\hat{3}} + \Sigma_{\hat{2},\hat{1}}\phi_{\hat{2},\hat{1}}V_{\hat{2},\hat{1}} + \Sigma_{\hat{2},\hat{2}}\phi_{\hat{2},\hat{2}}V_{\hat{2},\hat{2}} + \Sigma_{\hat{2},\hat{3}}\phi_{\hat{2},\hat{3}}V_{\hat{2},\hat{3}}$$

$$\therefore \Sigma V = \Sigma_{\hat{1},\hat{1}}\frac{\phi_{\hat{1},\hat{1}}}{\phi}V_{\hat{1},\hat{1}} + \Sigma_{\hat{1},\hat{2}}\frac{\phi_{\hat{1},\hat{2}}}{\phi}V_{\hat{1},\hat{2}} + \Sigma_{\hat{1},\hat{3}}\frac{\phi_{\hat{1},\hat{3}}}{\phi}V_{\hat{1},\hat{3}} + \Sigma_{\hat{2},\hat{1}}\frac{\phi_{\hat{2},\hat{1}}}{\phi}V_{\hat{2},\hat{1}} + \Sigma_{\hat{2},\hat{2}}\frac{\phi_{\hat{2},\hat{2}}}{\phi}V_{\hat{2},\hat{2}} + \Sigma_{\hat{2},\hat{3}}\frac{\phi_{\hat{2},\hat{3}}}{\phi}V_{\hat{2},\hat{3}}$$

$$\therefore \Sigma V = \sum_{\hat{i}=1}^{3}\sum_{\hat{j}=1}^{2}\Sigma_{\hat{i},\hat{j}}\frac{\phi_{\hat{i},\hat{j}}}{\phi}V_{\hat{i},\hat{j}}$$

Substituting Equation (**3**.46):

$$\Sigma V = \sum_{\hat{i}=1}^{3}\sum_{\hat{j}=1}^{2}S_{r\hat{i}}S_{z\hat{j}}\frac{V_{\hat{i},\hat{j}}}{n_{r\hat{i}}n_{z\hat{j}}}\Sigma_{\hat{i},\hat{j}}$$

Written in a more general notation for all three directions:

$$\left(\Sigma V\right)_{z,\hat{i}} = \sum_{\hat{j}\in j,\hat{k}\in k}S_{r\hat{j}}S_{\theta\hat{k}}\frac{V_{\hat{i},\hat{j},\hat{k}}}{n_{r\hat{j}}n_{\theta\hat{k}}}\Sigma_{\hat{i},\hat{j},\hat{k}} \quad (\mathbf{3}.61)$$

$$\left(\Sigma V\right)_{r,\hat{j}} = \sum_{\hat{i}\in i,\hat{k}\in k}S_{z\hat{i}}S_{\theta\hat{k}}\frac{V_{\hat{i},\hat{j},\hat{k}}}{n_{z\hat{i}}n_{\theta\hat{k}}}\Sigma_{\hat{i},\hat{j},\hat{k}} \quad (\mathbf{3}.62)$$

$$\left(\Sigma V\right)_{\theta,\hat{k}} = \sum_{\hat{i}\in i,\hat{j}\in j}S_{z\hat{i}}S_{r\hat{j}}\frac{V_{\hat{i},\hat{j},\hat{k}}}{n_{z\hat{i}}n_{r\hat{j}}}\Sigma_{\hat{i},\hat{j},\hat{k}} \quad (\mathbf{3}.63)$$

The above equations give the finite volume cross sections for a block of height equal to the material mesh height. This is because of the two-dimensional approach used in its' derivation. To obtain fine iteration block cross sections, the above expressions are divided by the number of fine blocks (of equal volume) per material mesh in the relevant direction.

$$\left(\Sigma V\right)_{zz,ii} = \sum_{\hat{j}\in j,\hat{k}\in k}S_{r\hat{j}}S_{\theta\hat{k}}\frac{V_{\hat{i},\hat{j},\hat{k}}}{n_{r\hat{j}}n_{z\hat{i}}n_{\theta\hat{k}}}\Sigma_{\hat{i},\hat{j},\hat{k}} \quad (\mathbf{3}.64)$$

$$\left(\Sigma V\right)_{rr,jj} = \sum_{\hat{i}\in i,\hat{k}\in k}S_{z\hat{i}}S_{\theta\hat{k}}\frac{V_{\hat{i},\hat{j},\hat{k}}}{n_{r\hat{j}}n_{z\hat{i}}n_{\theta\hat{k}}}\Sigma_{\hat{i},\hat{j},\hat{k}} \quad (\mathbf{3}.65)$$

$$(\Sigma V)_{\theta\theta,kk} = \sum_{\hat{i}\in i,\hat{j}\in j} S_{z\hat{i}} S_{r\hat{j}} \frac{V_{\hat{i},\hat{j},\hat{k}}}{n_{r\hat{j}} n_{z\hat{i}} n_{\theta\hat{k}}} \Sigma_{\hat{i},\hat{j},\hat{k}} \quad (\mathbf{3}.66)$$

This approach is applicable to all material properties, including cross sections $1/v$ terms and diffusion coefficients.

3.2.3.8 Convergence of the flux solution

By a repeated 'sweeping' of all three coordinates, the updated flux values from the radial, axial and azimuthal calculation converge. The convergence criteria used by TINTE are:

a. Flux convergence - The maximum error in the neutron flux is determined for the fluxes calculated for each one-dimensional calculation. For the radial, axial and azimuthal directions respectively, these are given below.

$$\varepsilon_{\phi,r} = \left| \frac{\phi_r - \frac{1}{2}[\phi_z + \phi_\theta]}{\frac{1}{3}[\phi_r + \phi_z + \phi_\theta]} \right| \quad (\mathbf{3}.67)$$

$$\varepsilon_{\phi,z} = \left| \frac{\phi_z - \frac{1}{2}[\phi_r + \phi_\theta]}{\frac{1}{3}[\phi_z + \phi_r + \phi_\theta]} \right| \quad (\mathbf{3}.68)$$

$$\varepsilon_{\phi,\theta} = \left| \frac{\phi_\theta - \frac{1}{2}[\phi_r + \phi_z]}{\frac{1}{3}[\phi_\theta + \phi_r + \phi_z]} \right| \quad (\mathbf{3}.69)$$

The effective maximum error in neutron flux for all directions is calculated as the arithmetic mean for the three directions, namely $\varepsilon_\phi = \frac{1}{3}[\varepsilon_{\phi,r} + \varepsilon_{\phi,z} + \varepsilon_{\phi,\theta}]$. For convergence, $\varepsilon_\phi < \varepsilon_{\phi,\min}$, where $\varepsilon_{\phi,\min}$ is a user-supplied parameter. This calculation uses coarse iteration block fluxes, as calculated using Equations (**3**.54) through (**3**.56).

b. Power convergence - The maximum error in the 'steady-state equivalent' heat production is determined for the fluxes calculated for each leakage iteration. Consider the error in fluxes calculated using channels in the radial direction:

$$\varepsilon_{Q,r} = \left| \frac{\dot{Q}_r - \frac{1}{2}[\dot{Q}_z + \dot{Q}_\theta]}{\frac{1}{3}[\dot{Q}_r + \dot{Q}_z + \dot{Q}_\theta]} \right| \quad (\mathbf{3}.70)$$

Similarly, the error in fluxes calculated for channels in the axial direction is:

$$\varepsilon_{Q,z} = \left| \frac{\dot{Q}_z - \frac{1}{2}[\dot{Q}_r + \dot{Q}_\theta]}{\frac{1}{3}[\dot{Q}_z + \dot{Q}_r + \dot{Q}_\theta]} \right| \quad (\mathbf{3}.71)$$

Similarly, the error in fluxes calculated for channels in the azimuthal direction is:

$$\varepsilon_{Q,\theta} = \left| \frac{\dot{Q}_\theta - \frac{1}{2}[\dot{Q}_r + \dot{Q}_z]}{\frac{1}{3}[\dot{Q}_\theta + \dot{Q}_r + \dot{Q}_z]} \right| \quad (\mathbf{3}.72)$$

where the 'steady-state equivalent' heat production is defined as $\dot{Q}_{r/z/\theta} = E_f \Sigma_{f1} \phi_1 + E_f \Sigma_{f2} \phi_2$ and is calculated using neutron flux values from the radial, axial or azimuthal directions respectively. The effective maximum error in the 'steady-state equivalent' heat production for all directions is calculated as the arithmetic mean for

the three directions, namely $\varepsilon_Q = \frac{1}{3}\left[\varepsilon_{Q,r} + \varepsilon_{Q,z} + \varepsilon_{Q,\theta}\right]$. This parameter is calculated by TINTE, however, it is not compared with any reference value and is therefore for information only. As for (a), coarse iteration block heat production is used for this calculation.

c. For steady-state calculations, the change in effective reactor multiplication constant with subsequent iterations is taken into account to determine if convergence has been achieved. The k-effective error is calculated as shown.

$$\varepsilon_k = \left|\frac{k^0 - k^1}{k^1}\right| \qquad (\mathbf{3}.73)$$

where k^1 and k^0 are the updated and old effective reactor multiplication constants respectively, calculated for subsequent iterations. For convergence, $\varepsilon_k < \varepsilon_{k,\min}$.

d. Number of iterations – In order to trap non-converging solutions, it is necessary to limit the number of iterations. In TINTE, the number of inner flux iterations (refer to paragraph 4.1.2) is limited to 9.

3.2.3.8.1 Source iteration

The Scarborough criteria state that convergence of a system of linear equations is guaranteed if the matrix $\mathbf{A}$ (Equation (**3**.27)) is diagonally dominant; i.e. the sum of the magnitudes of all non-diagonal terms in a row is less than or equal to, for all rows, and equal to, for at least one row, the magnitude of the diagonal term. The stability of the solution is therefore largely dependent on the magnitude of the diagonal terms $p_{1,i}$ and $p_{2,i}$. Apart from the Scarborough criteria, another important criterion is that all coefficients have the same sign. All non-diagonal terms will always be positive; it is therefore necessary to ensure that the main diagonal terms are never negative. This is ensured by including the 'new' production, as well as all negative leakages (leakage into the mesh), in the source term. Large source terms, however, result in very slow convergence. The following source iteration scheme is therefore introduced.

The 'new' production P_1 is divided into two fractions, γP_1 and $(1-\gamma)P_1$. The fraction γP_1 remains in the main diagonal of the matrix $\mathbf{A}$, while the remaining fraction is transferred to the source term. A value $\gamma = 1$ leads to the fastest convergence but may also lead to instability. By contrast, $\gamma = 0$ ensures stability but will slow down convergence. In a similar manner, for any negative transverse leakage terms, a fraction $\gamma\tilde{L}\phi$ remains in the main diagonal and the remaining fraction $(1-\gamma)\tilde{L}\phi$ is transferred to the source term.

A further improvement is made with regard to the transverse leakages. The leakage term $\tilde{L}\phi$ at the surface between adjacent channels may be defined using either the current channel as a reference or the adjacent channel. If the adjacent channel fluxes have already been solved for, it is advantageous to represent the leakage as a function of the adjacent channel fluxes because they may then be regarded as fixed sources when included in the source term. It is therefore clear that the choice of channels should be ordered specifically to take advantage of this 'passing of information' between adjacent channels.

A simple example is considered; an iterative solution is to be found for a one-dimensional purely absorbing channel with a source at one end. If the equation is linearized to the form of Equations (**3**.25) or (**3**.26), the updated flux in a mesh is dependent only on the mesh and its neighbouring meshes.

Each one-dimensional flux calculation transfers information (updated transverse leakages) to its neighbouring channels. The most efficient convergence is obtained by first calculating for the channel that is most likely to transfer the most information to its neighbours. The neighbouring channel calculations will thereafter transfer this information to their neighbours and so forth. In practical circumstances, the optimal starting channel would generally coincide with the location of the largest source of neutrons. This concept is illustrated in Figure 9. In this particular example, channel 16 contains a source and optimal convergence is obtained by starting the iterative scheme at channel 16 and working towards channel 1. In TINTE, this starting channel is chosen to be the channel with the smallest negative leakage. The calculation of fluxes proceeds outwards from this channel to the edges of the mesh. For the initial calculation, where leakage values are unknown, the centre of the reactor is chosen as a starting point for the calculation. Using this sequence for the one-dimensional calculations, the number of iterations required is approximately halved.

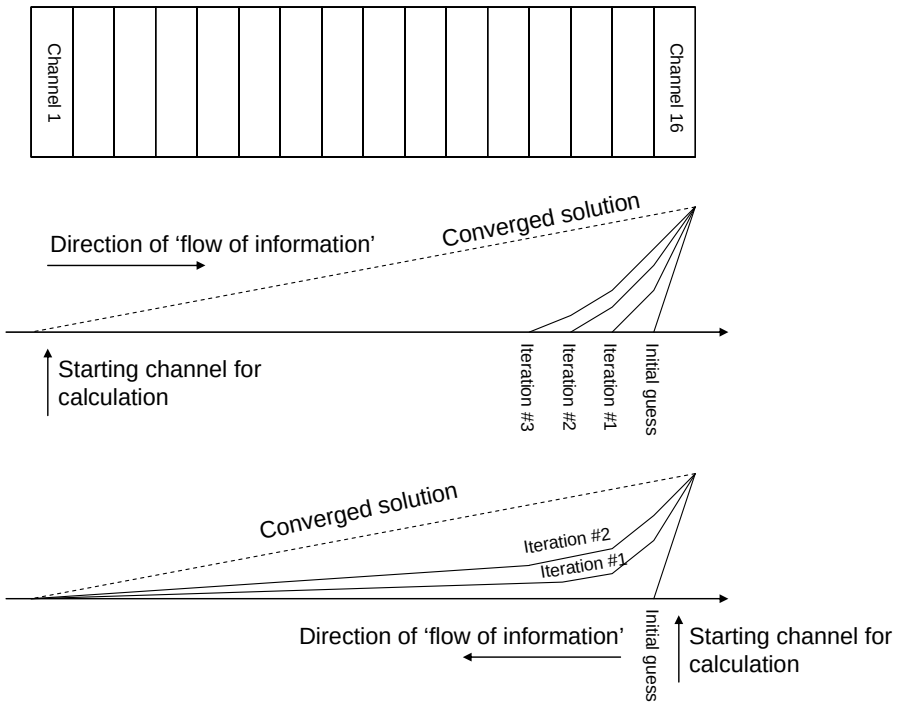

Figure 9: Choosing the Optimal Starting Channel to Improve Convergence of the Leakage Iteration Method

3.2.3.8.2 Obtaining an initial guess for the steady-state neutron flux and transverse leakage

In order to obtain an initial guess to the neutron flux, one-dimensional diffusion calculations are carried out for a single channel in the radial direction, followed by a single channel in the axial direction. For the radial calculation, the transverse leakages are assumed zero. The neutron fluxes and leakages obtained for this radial channel are then copied to all radial channels. These values therefore 'feed into' the axial calculation. The neutron fluxes and leakages obtained for this axial channel are then copied to all axial channels. The initial neutron flux guess is obtained by multiplying the radial and axial flux profiles together. The resulting profile is then normalized to the user-specified reactor power. Note that the azimuthal neutron flux is initially assumed constant and the azimuthal leakages are assumed zero, i.e. no azimuthal calculation is carried out.

The choice of a channel to use in each direction is arbitrary, as long as the channel contains some fissionable material, however, the best neutron flux estimate would be obtained for channels that pass through the location of maximum neutron production or power.

In the absence of flux or power data an estimate is obtained by considering the nu-fission cross section ($\nu\Sigma_f V$). Typically, the volumetric centre of the core would be adequate, but there are exceptions to this rule. Consider Figure 10, which shows a typical flux profile and nu-fission profile together. Note the low nu-fission cross section between C and D, which could, for example, represent a breeder blanket. Basic intuition would suggest that this region be ignored when locating the centre of the core, therefore the following method is used in TINTE to locate a more representative centre of the core. While sweeping through the nuclear domain in the positive r, z and θ direction, the nu-fission cross section is compared with a reference value, which is initially set to zero. If $\nu\Sigma_f V$ is at least 10 times the reference value, the reference value is updated. This would correspond to point A in the figure; it represents the start of a region of high neutron production. Sweeping continues until $\nu\Sigma_f V$ drops to 0.5 times the reference value. This would correspond to point C in the figure. The representative centre of the core is then assumed to lie halfway between A and C, namely at B. The factors 10 and 0.5, used to locate the boundaries, are arbitrarily chosen.

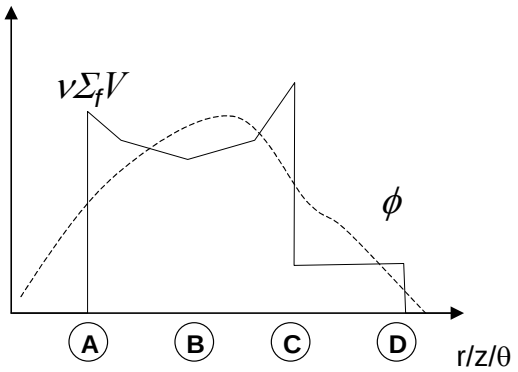

Figure 10: A Typical Flux Profile Shown against the Nu-fission Cross Section

3.2.3.9 Buckling feedback in the material mesh

The leakage in each direction is determined from separated one-dimensional calculations, and the values must then be mapped to the relevant material blocks when calculating the total leakage from the material blocks. This is necessary for the buckling feedback in the calculation of updated material cross sections (refer to paragraph 3.2.2). The mapping process may introduce sufficient numerical error such that the group neutron balances (Equations (**3**.22) and (**3**.23)) are not satisfied for the material blocks. For this reason, the material block leakages are calculated directly from Equations (**3**.22) and (**3**.23) for the calculated material block fluxes.

Equations (**3**.22) and (**3**.23) are rearranged to solve for the total leakage as shown.

$$L_1''' = -\frac{\left(\tilde{L}^r_{1,j} - \tilde{L}^r_{1,j+1} + \tilde{L}^z_{1,i} - \tilde{L}^z_{1,i+1} + \tilde{L}^\theta_{1,k} - \tilde{L}^\theta_{1,k+1}\right)}{V}$$

$$= \frac{1}{\phi_1^1}\left[\begin{array}{l} -\left(\frac{1}{v_1\Delta} + \Sigma_{a1} + \Sigma_s^{1\to 2}\right)\phi_1^1 + \Sigma_s^{2\to 1}\phi_2^1 + P_1\left(1 - 2\sum_l \beta_l \frac{1 - \frac{1-e^{-\lambda_l\Delta}}{\lambda_l\Delta}}{\lambda_l\Delta}\right) \\ + \frac{1}{v_1\Delta}\phi_1^0 + P_0\left(\beta + 2\sum_l \beta_l \frac{e^{-\lambda_l\Delta} - \frac{1-e^{-\lambda_l\Delta}}{\lambda_l\Delta}}{\lambda_l\Delta}\right) - \sum_l \lambda_l C_{l0}\left(1 - 2\frac{1-e^{-\lambda_l\Delta}}{\lambda_l\Delta}\right) + S_\phi \end{array}\right] \quad (3.74)$$

$$L_2''' = -\frac{\left(\tilde{L}^r_{2,j} - \tilde{L}^r_{2,j+1} + \tilde{L}^z_{2,i} - \tilde{L}^z_{2,i+1} + \tilde{L}^\theta_{2,k} - \tilde{L}^\theta_{2,k+1}\right)}{V}$$

$$= \frac{1}{\phi_2^1}\left[-\left(\frac{1}{v_2\Delta} + \Sigma_{a2} + \Sigma_s^{2\to 1}\right)\phi_2^1 + \Sigma_s^{1\to 2}\phi_1^1 + \frac{1}{v_2\Delta}\phi_2^0\right] \quad (3.75)$$

Here ϕ_1^1 and ϕ_2^1 are mapped from the fine-iteration blocks (refer to paragraph 3.2.3.7.1) and all cross sections, etc. are for the material block.

3.2.3.10 Global reactor parameters

The effective reactor multiplication constant (k-effective) is calculated as the ratio of production to loss of neutrons. This is implemented in TINTE as:

$$k = \frac{\int_{reactor} P_p dV}{\int_{reactor} R_{loss} dV - \int_{reactor} P_d dV} \quad (3.76)$$

where the discretized prompt neutron production rate term is given by:

$$P_p dV = \left(\nu\Sigma_{f1}\phi_1^1 + \nu\Sigma_{f2}\phi_2^1\right)\left(1 - 2\sum_l \beta_l \frac{1 - \frac{1-e^{-\lambda_l\Delta}}{\lambda_l\Delta}}{\lambda_l\Delta}\right)V \quad (3.77)$$

The discretized neutron loss term is given by:

$$R_{loss} dV = \left(\frac{1}{v_1\Delta}V - \left(\tilde{L}^r_{1,j} - \tilde{L}^r_{1,j+1} + \tilde{L}^z_{1,i} - \tilde{L}^z_{1,i+1} + \tilde{L}^\theta_{1,k} - \tilde{L}^\theta_{1,k+1}\right) + \Sigma_{a1}V\right)\phi_1^1 + \left(\frac{1}{v_2\Delta}V - \left(\tilde{L}^r_{2,j} - \tilde{L}^r_{2,j+1} + \tilde{L}^z_{2,i} - \tilde{L}^z_{2,i+1} + \tilde{L}^\theta_{2,k} - \tilde{L}^\theta_{2,k+1}\right) + \Sigma_{a2}V\right)\phi_2^1 \quad (3.78)$$

The discretized delayed neutron production term is given by:

$$P_d dV = \left[\frac{1}{v_1 \Delta}\phi_1^0 + \frac{1}{v_2 \Delta}\phi_2^0 + P_0 \left(\beta + 2\sum_l \beta_l \frac{e^{-\lambda_l \Delta} - \frac{1-e^{-\lambda_l \Delta}}{\lambda_l \Delta}}{\lambda_l \Delta} \right) - \sum_l \lambda_l C_{l0} \left(1 - 2\frac{1-e^{-\lambda_l \Delta}}{\lambda_l \Delta} \right) + Q \right] V \quad (\mathbf{3}.79)$$

Because, on the one hand, k is calculated during the steady-state solution and, on the other hand, the reactor is held critical during certain time-dependent calculations, it is convenient to define steady-state and transient components of the eigenvalue.

$$k = k_0 k' \quad (\mathbf{3}.80)$$

where k_0 is the eigenvalue calculated during the steady-state solution and k' the correction to k_0 for time-dependent calculations.

Using Equation (**3**.80), the prompt neutron production rate term during time-dependent solutions (refer to Equation (**3**.77)) becomes:

$$P_p' dV = \frac{1}{k_0}\left(\nu\Sigma_{f1}\phi_1^1 + \nu\Sigma_{f2}\phi_2^1\right)\left(1 - 2\sum_l \beta_l \frac{1 - \frac{1-e^{-\lambda_l \Delta}}{\lambda_l \Delta}}{\lambda_l \Delta} \right) V \quad (\mathbf{3}.81)$$

And thus k' may be calculated using the modified form of Equation (**3**.76).

$$k' = \frac{\int_{reactor} P_p' dV}{\int_{reactor} R_{loss} dV - \int_{reactor} P_d dV} \quad (\mathbf{3}.82)$$

The effective reactivity, assuming the critical reactor has $k = k_0$ ($k' = 1$), may be calculated for the time-dependent solution as follows:

$$\rho = \frac{k'-1}{k'} \equiv \frac{k - k_0}{k} \quad (\mathbf{3}.83)$$

The global inverse reactor period ω at any location in the reactor is defined such that the power density within the reactor changes according to the function:

$$\dot{Q}''' = \dot{Q}_0''' e^{\omega t}$$

$$\frac{\partial \dot{Q}'''}{\partial t} = \omega \dot{Q}_0''' e^{\omega t} = \omega \dot{Q}'''$$

$$\therefore \omega = \frac{1}{\dot{Q}'''} \frac{\partial \dot{Q}'''}{\partial t}$$

For a discrete time interval Δ, the derivative may be discretized to yield the inverse reactor period.

$$\omega = \frac{1}{\Delta} \frac{\dot{Q}_1''' - \dot{Q}_0'''}{\dot{Q}_0'''} \quad (\mathbf{3}.84)$$

For reactor control purposes, this is calculated at the location of maximum $\dot{Q}_1''' - \dot{Q}_0'''$ as this will, in most cases, correspond with the maximum ω.

3.2.4 Fission Product Poisoning

All fission products will act as neutron absorbers and their formation tends to reduce the global reactor multiplication constant (k-effective). Certain fission products are known as saturating fission products because their half-lives are sufficiently short that an equilibrium is reached between their production, decay and absorption during normal reactor operation. These isotopes will influence reactor operation in many cases such as reactor start-up, shutdown and power level changes and as such their influence must be taken into account. Of the saturating fission products, the isotopes ^{135}Xe and ^{149}Sm are generally considered the most important.

^{135}Xe has a very large thermal absorption cross section, 2.6×10^{6} barns. It is produced directly by fission and also by the decay of the isotope ^{135}I. This is in turn formed by the decay of the isotope ^{135}Te, which is a direct fission product.

^{149}Sm has a lower (approximately 60 times less) thermal absorption cross section than ^{135}Xe, 4×10^{4} barns. It is formed by the decay of the isotope ^{149}Pm, which in turn is formed by the decay of ^{149}Nd. ^{149}Nd is a direct fission product.

In both cases, the half-lives of the parent isotopes (^{135}Te and ^{149}Nd) are significantly shorter than that of their daughter isotopes (^{135}I and ^{149}Pm). The assumption is made, therefore, that these are formed directly by fission. The basic transmutation decay chain of Figure 11 may be used to represent a saturation fission product.

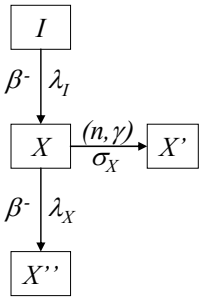

Figure 11: Transmutation Decay Chain for a Typical Saturation Fission Product

We consider the transmutation decay chain for a generic isotope pair ($I \rightarrow X$) of Figure 11. The differential equations describing the build-up and decay for each isotope are [7]:

$$\dot{I} = \gamma_I F - \lambda_I I \qquad (\mathbf{3}.85)$$

and

$$\dot{X} = \gamma_X F + \lambda_I I - \left(\lambda_X + \sigma_X \phi_2\right) X \qquad (\mathbf{3}.86)$$

where

I, X are the isotope concentrations of the parent and daughter isotopes respectively.

γ_I, γ_X are the fractional fission yields of the parent and daughter isotopes respectively.

F is the fission rate, defined as $\Sigma_f^1 \phi_1 + \Sigma_f^2 \phi_2$.

ϕ_2 is the thermal flux.

σ_X is the thermal microscopic absorption cross section of the isotope X.

Note that additional assumptions have been made regarding the formation of X and I. They may or may not be formed directly by fission, depending on the values of γ_I and γ_X.

Similarly, the value of λ_X determines whether the isotope is stable ($\lambda_X = 0$) or not ($\lambda_X > 0$). The concentrations of the generic isotopes X' and X'' are not required and are therefore not modelled.

Because the absorption cross sections of the saturation fission products is relatively low in the higher energy regions, absorption of neutrons by isotope X is assumed to take place in the thermal region only. In the case of ^{149}Sm, a large epithermal absorption resonance is present, however in a two-energy group model this effect cannot be modelled accurately. In order to take into account the spectrum change that such a resonance may have, neutron poison concentration dependence is included in the group cross-section calculation (refer to paragraph 3.2.2).

As stated above, the isotopes ^{135}Xe and ^{149}Sm are generally considered the most important saturation fission products. These are considered in the calculation, as well as the isotopes ^{151}Sm and ^{157}Gd, which are of lesser importance. Therefore, the following four isotope pairs are considered:

$$^{135}I \rightarrow ^{135}Xe$$

$$^{149}Pm \rightarrow ^{149}Sm$$

$$^{151}Pm \rightarrow ^{151}Sm$$

$$^{157}Eu \rightarrow ^{157}Gd$$

The decay constants (λ) for the transmutation decay chains, taken from ENDF/B 4 [12], are given in Table 4. The source for these values is discussed in more detail in Appendix D.

Table 4: Decay Constants for Neutron Poisons as used in TINTE

Isotope	Decay Constant (λ) [s^{-1}]
^{135}Xe	2.116E-5
^{135}I	2.883E-5
^{149}Sm	1E-30
^{149}Pm	3.626E-6
^{151}Sm	5.751E-9
^{151}Pm	6.876E-6
^{157}Gd	1E-30
^{157}Eu	1.260E-5

The production of strong absorber isotopes is assumed instantaneous and constantly proportional to the fission rate for each nuclear material. Values taken from ENDF/B 4 [12] for the fission yields of the relevant isotopes are given Table 5. The source of these values is discussed in more detail in Appendix D.

The effective fission yield for any material γ_i, consisting of a mixture of a number of fissionable isotopes, may be calculated as follows:

$$\gamma_i = \left[\gamma_{U5}F_{U5,i} + \gamma_{Th2}F_{Th2,i} + \ldots + \gamma_{Pu2}F_{Pu2,i}\right]\frac{1}{F_{U5,i} + F_{Th2,i} + \ldots + F_{Pu2,i}} \qquad (\mathbf{3}.87)$$

The ratios $\frac{F_{U5,i}}{F_{U5,i}+F_{Th2,i}+\ldots+F_{Pu2,i}} \equiv R_{U5,i}$, etc., which represent the fraction of fissions in each fissionable isotope, are assumed to be supplied by the user.

Table 5: Direct Fission Yield of Strong Absorbers for Fissionable Isotopes [12]

Isotope	Direct Fractional Fission Yield (γ) for Fissionable Isotope [%]									
	^{235}U	^{232}Th	^{233}U	^{234}U	^{236}U	^{238}U	^{239}Pu	^{240}Pu	^{241}Pu	^{242}Pu
^{135}Xe	0.25	1.33	1.34	0.25	0.25	0.015	1.15	1.15	0.23	0.23
^{135}I	6.35	3.52	4.86	6.35	6.35	6.55	6.3	6.3	6.95	6.95
^{149}Sm	0	0	0	0	0	0	0	0	0	0
^{149}Pm	1.084	1.084	1.084	1.084	1.084	1.084	1.084	1.084	1.084	1.084
^{151}Sm	0	0	0	0	0	0	0	0	0	0
^{151}Pm	0.4196	0.4196	0.4196	0.4196	0.4196	0.4196	0.4196	0.4196	0.4196	0.4196
^{157}Gd	0	0	0	0	0	0	0	0	0	0
^{157}Eu	0.00613	0.00613	0.00613	0.00613	0.00613	0.00613	0.00613	0.00613	0.00613	0.00613

3.2.4.1 Transient case

We consider the production decay chain for a generic isotope pair ($I \rightarrow X$). The differential equations describing the build-up and decay for each isotope are as given in Equations (**3**.85) and (**3**.86).

We assume a constant fission rate for the time interval $\Delta = t_1 - t_0$.

$$F(t) = \overline{F} = \frac{1}{2}(F_1 + F_0); \qquad t \in (t_{0,}, t_1)$$

Substitution of this into Equation (**3**.85) allows the time-dependent concentration of the parent isotope I to be solved for.

$$\frac{d}{dt} I(t) + \lambda_I I(t) = \gamma_I \overline{F}$$

This is an ordinary differential equation of the first kind $\dot{I} + p(t)I = q(t)$. The solution for $I(t)$ for time $t > t_0$ may be determined using integrating factors.

$$p(t) = \lambda_I$$
$$q(t) = \gamma_I \overline{F}$$

The integrating factor $\mu(t)$ is found as follows:

$$\mu = e^{\int_{t_0}^{t} p(t')dt'} = e^{\int_{t_0}^{t} \lambda_I dt'} = e^{\lambda_I (t - t_0)}$$

The solution for $I(t)$ becomes:

$$I(t) = \frac{\int_{t_0}^{t} \mu\, q(t) dt}{\mu} = \frac{\int_{t_0}^{t} e^{\lambda_I (t'-t_0)}\, \gamma_I \overline{F}\, dt' + I(t_0)}{e^{\lambda_I (t-t_0)}}$$

$$= e^{-\lambda_I (t-t_0)} \left\{ I(t_0) + \int_{t_0}^{t} dt' \gamma_I \overline{F}\, e^{\lambda_I (t'-t_0)} \right\}$$

$$= e^{-\lambda_I (t-t_0)} \left\{ I_0 + \gamma_I \overline{F} \int_{t_0}^{t} dt' e^{\lambda_I (t'-t_0)} \right\}$$

$$= e^{-\lambda_I (t-t_0)} \left[I_0 + \frac{\gamma_I}{\lambda_I} \overline{F} \left(e^{\lambda_I (t-t_0)} - 1 \right) \right]$$

$$I(t) = I_0 e^{-\lambda_I (t-t_0)} + \frac{\gamma_I}{\lambda_I} \overline{F} \left(1 - e^{-\lambda_I (t-t_0)} \right)$$

At the end of the time interval ($t = t_1$):

$$I_1 = I_0 e^{-\lambda_I \Delta} + \frac{\gamma_I}{\lambda_I} \overline{F} \left(1 - e^{-\lambda_I \Delta} \right) \qquad (\mathbf{3}.88)$$

A solution may now be found for the daughter isotope X, starting with Equation (**3**.86). We define $\lambda_2 = \lambda_X + \sigma_X \phi_2$. In this case we assume a constant flux over the time interval, i.e. $\phi_2(t) = \overline{\phi}_2 = \frac{1}{2}\left(\phi_2^{\,1} + \phi_2^{\,0} \right)$. Equation (**3**.86) now becomes:

$$\frac{d}{dt} X(t) + \lambda_2 X(t) = \gamma_X \overline{F} + \lambda_I I(t)$$

$$= \gamma_X \overline{F} + \lambda_I I_0 e^{-\lambda_I (t-t_0)} + \gamma_I \overline{F} \left(1 - e^{-\lambda_I (t-t_0)} \right)$$

$$= (\gamma_X + \gamma_I) \overline{F} + \left(\lambda_I I_0 - \gamma_I \overline{F} \right) e^{-\lambda_I (t-t_0)}$$

This is an ordinary differential equation of the first kind $\dot{X} + p(t) X = q(t)$. The solution for $X(t)$ for time $t > t_0$ may be determined using integrating factors.

$$p(t) = \lambda_2$$

$$q(t) = (\gamma_X + \gamma_I) \overline{F} + \left(\lambda_I I_0 - \gamma_I \overline{F} \right) e^{-\lambda_I (t-t_0)}$$

The integrating factor $\mu(t)$ is found as follows:

$$\mu = e^{\int_{t_0}^{t} p(t') dt'} = e^{\int_{t_0}^{t} \lambda_2 dt'} = e^{\lambda_2 (t-t_0)}$$

The solution for $X(t)$ becomes:

$$X(t) = \frac{\int_{t_0}^{t} \mu\, q(t) dt}{\mu} = \frac{\int_{t_0}^{t} e^{\lambda_2 (t'-t_0)} \left[(\gamma_X + \gamma_I)\overline{F} + (\lambda_I I_0 - \gamma_I \overline{F}) e^{-\lambda_I (t-t_0)} \right] dt' + X(t_0)}{e^{\lambda_2 (t-t_0)}}$$

$$= e^{-\lambda_2 (t-t_0)} \left\{ X(t_0) + \int_{t_0}^{t} e^{\lambda_2 (t-t_0)} \left[(\gamma_X + \gamma_I)\overline{F} + (\lambda_I I_0 - \gamma_I \overline{F}) e^{-\lambda_I (t'-t_0)} \right] dt' \right\}$$

$$= e^{-\lambda_2 (t-t_0)} \left\{ X(t_0) + \int_{t_0}^{t} (\gamma_X + \gamma_I)\overline{F} e^{\lambda_2 (t'-t_0)} dt' + \int_{t_0}^{t} (\lambda_I I_0 - \gamma_I \overline{F}) e^{(\lambda_2 - \lambda_I)(t'-t_0)} dt' \right\}$$

$$= e^{-\lambda_2 (t-t_0)} \left\{ X(t_0) + (\gamma_X + \gamma_I)\overline{F} \int_{t_0}^{t} e^{\lambda_2 (t'-t_0)} dt' + (\lambda_I I_0 - \gamma_I \overline{F}) \int_{t_0}^{t} e^{(\lambda_2 - \lambda_I)(t'-t_0)} dt' \right\}$$

The integrals may be evaluated and the equation simplified:

$$X(t) = e^{-\lambda_2 (t-t_0)} \left\{ X(t_0) + (\gamma_X + \gamma_I)\overline{F} \frac{1}{\lambda_2} \left(e^{\lambda_2 (t-t_0)} - 1 \right) + (\lambda_I I_0 - \gamma_I \overline{F}) \frac{1}{\lambda_2 - \lambda_I} \left(e^{(\lambda_2 - \lambda_I)(t-t_0)} - 1 \right) \right\}$$

$$= X(t_0) e^{-\lambda_2 (t-t_0)} + (\gamma_X + \gamma_I)\overline{F} \frac{1 - e^{-\lambda_2 (t-t_0)}}{\lambda_2} + (\lambda_I I_0 - \gamma_I \overline{F}) \frac{e^{-\lambda_I (t-t_0)} - e^{-\lambda_2 (t-t_0)}}{\lambda_2 - \lambda_I}$$

At the end of the time interval ($t = t_1$):

$$X_1 = X_0 e^{-\lambda_2 \Delta} + (\gamma_X + \gamma_I)\overline{F} \frac{1 - e^{-\lambda_2 \Delta}}{\lambda_2} + (\lambda_I I_0 - \gamma_I \overline{F}) \frac{e^{-\lambda_I \Delta} - e^{-\lambda_2 \Delta}}{\lambda_2 - \lambda_I} \qquad (\mathbf{3}.89)$$

It should be noted that Equation (**3**.89) differs slightly from the expression given in [3]. It is, however, consistent with the original German version of [3] and the TINTE source code.

3.2.4.2 Steady-state case

For the steady-state condition, the time-derivative of the fission product concentration is zero. Using Equations (**3**.85) and (**3**.86), the following equations therefore apply:

$$I_{eq} = \frac{\gamma_I}{\lambda_I} F \qquad (\mathbf{3}.90)$$

and

$$X_{eq} = \frac{\gamma_X + \gamma_I}{\lambda_2} F \qquad (\mathbf{3}.91)$$

No underrelaxation is applied to this solution. Therefore, the fission rate and thermal flux, as calculated by the two-group diffusion solution, are used directly for this calculation.

3.2.4.3 Approach-to-equilibrium case

For the case where a new equilibrium condition is to be established during a transient calculation, the steady-state equations are not used but rather a virtual time-stepping method is employed to maintain numerical stability, as a form of underrelaxation. In this case, the fission rate and thermal flux at the end of the time interval (as opposed to the mean as in the transient case) are used, in order to improve the convergence. Equation (**3**.88) may be rewritten as:

$$I = I_0 e^{-\lambda\tau_{virt}} + \frac{\gamma_I}{\lambda_I} F\left(1 - e^{-\lambda\tau_{virt}}\right) \quad (\mathbf{3}.92)$$

where $\lambda\tau_{virt}$ is a virtual time-stepping constant, chosen to ensure stability of the solution. In the case of the concentration of isotope X, the equilibrium concentration of isotope I is inserted into (**3**.87), yielding the differential equation:

$$\dot{X} = (\gamma_X + \gamma_I)F - (\lambda_X + \sigma_X\phi)X$$

The solution to this differential equation, assuming constant fission rate and flux over the time interval is:

$$X = X_0 e^{-\lambda\tau_{virt}} + \frac{\gamma_X + \gamma_I}{\lambda_2} F\left(1 - e^{-\lambda\tau_{virt}}\right) \quad (\mathbf{3}.93)$$

3.2.4.4 Calculation of neutron poison macroscopic cross sections

The microscopic absorption cross section ($\sigma_{a,X}$) for each isotope pair is calculated as described in paragraph 3.2.2. The total macroscopic absorption cross section for all strong absorber isotopes is given by:

$$\Sigma_{a,X} = \sum_{Xe135, Sm149, Sm151, Gd157} X_i \sigma_{a,i} \quad (\mathbf{3}.94)$$

This value is added to the thermal group absorption cross section.

3.2.5 Heat Production

Heat production in the reactor may be divided into a number of individual terms E_x, where the index x is:

r rebound energy of the fission fragments directly after fission

n kinetic energy of the prompt neutrons produced by fission

γp prompt gamma energy

γd delayed gamma energy

β beta decay energy

These energy contributions are combined into a prompt component:

$$E_p = E_r + E_n + E_{\gamma p} \quad (\mathbf{3}.95)$$

and as the decay heat:

$$E_d = E_{\gamma d} + E_\beta \quad (\mathbf{3}.96)$$

The total fission heat production is the sum of the prompt and decay contributions.

$$E_f = E_p + E_d \quad (\mathbf{3}.97)$$

Table 6: Fission Energy Release (MeV) for the Fissionable Isotopes [22]

Fissionable Isotope	^{235}U	^{232}Th	^{233}U	^{234}U	^{236}U	^{238}U	^{239}Pu	^{240}Pu	^{241}Pu	^{242}Pu
Total utilizable energy per fission, $E_{f,eq}$	193.7‡	185	191.1	189.6	191.9	194.8‡	199.9‡	197	202‡	199.1
Prompt energy per fission, E_p	180.8	168.7	180.8	179.4	179.9	178.2	189.5	187.4	189.2	187.9
Rebound energy of fission fragments, E_r	169.1	160.4	168.2	167.1	167.5	169.6	175.8	173.7	175.4	174
Average prompt fission neutron energy, E_{mod}	4.8	4.7	4.9	5.4	5.4	5.5	5.9	6.8	6	7
Beta decay energy per fission, E_β	6.5	8.1	5.2	6.1	7.4	8.3	5.3	6.4	6.6	7.7
Neutron capture energy§	8.7	8.7	8.7	8.7	8.7	10.9	11.5	8.7	11.9	8.7

‡ From supplement 1 of DIN 25 485 [21].

§ From DIN 25 485 [21]. Because the DIN standard does not specify values for the isotopes ^{232}Th, ^{233}U, ^{234}U, ^{236}U, ^{240}Pu and ^{242}Pu, these are assumed equal to the values for ^{235}U.

3.2.5.1 Prompt power

The prompt volumetric heat production may simply be calculated using the fission rate and prompt energy per fission.

$$\dot{Q}_p''' = \left(\Sigma_f^1 \phi_1 + \Sigma_f^2 \phi_2\right) E_p \qquad (\mathbf{3}.98)$$

The total prompt reactor power $\dot{Q}_p$ is therefore the volume integral $\int_V \dot{Q}_p''' dV$. This is written in a discretized form.

$$\dot{Q}_p = \sum_{ijk} \dot{Q}_p^{ijk} = \sum_{ijk} \left(\left(\Sigma_f^1 \phi_1 + \Sigma_f^2 \phi_2\right) E_p V_{ijk}\right) \qquad (\mathbf{3}.99)$$

3.2.5.2 Decay Heat

The decay heat calculation in TINTE is based on the DIN 25 485 standard [21]. In the standard, five contributions to the decay heat are specified, namely:

a. The contribution of the fission products $\dot{Q}_S(t,T)$.

b. The contribution of the actinides ^{239}U and ^{239}Np $\dot{Q}_B(t,T)$. In TINTE the actinides ^{233}Th and ^{233}Pa are included in this contribution.

c. The contribution of the remaining actinides $\dot{Q}_A(t,T)$.

d. The contribution of the ^{134}Cs capture reaction $\dot{Q}_{Cs}(t,T)$.

e. The contribution of the remaining capture reactions $\dot{Q}_E(t,T)$.

where t is the decay period (after reactor shutdown) and T the operating period.

The total decay heat may be written as:

$$\dot{Q}_d = \dot{Q}_S + \dot{Q}_B + \dot{Q}_A + \dot{Q}_{Cs} + \dot{Q}_E$$

The contribution $\dot{Q}_A$ is calculated using:

$$\dot{Q}_A(t,T) = K_A A(t) \cdot \dot{Q}_S(t,T)$$

where

$$K_A = 1 - 3.826 \times 10^{-3}(140 - BU) + 4.544 \times 10^{-2}(2.5 - L) - 7.08 \times 10^{-2}(12 - SM) \qquad (\mathbf{3}.100)$$

BU is the average discharge burn-up of the fuel in MWd / kg.

L is the power density in MW / m^3.

SM is the mean heavy metal content of the fuel (including fuel free spheres) in g per fuel sphere.

$A(t)$ is a tabulated function.

The contribution $\dot{Q}_E(t,T)$ may be written as:

$$\dot{Q}_E(t,T) = H(t) \cdot \dot{Q}_S(t,T)$$

where $H(t)$ is a tabulated value.

The total decay heat may therefore be written as:

$$\dot{Q}_d = \dot{Q}_S\left(1 + H(t) + A(t)K_A\right) + \dot{Q}_B + \dot{Q}_{Cs} \qquad (\mathbf{3}.101)$$

TINTE specifies the fuel composition using more isotopes than is provided for in the DIN standard (refer to Table 6). For the isotopes not given in the DIN standard, values are assumed equal to those for ^{235}U.

3.2.5.2.1 Reactor life history

The composition and power generation within fuel, changes over the operation period of the fuel. These changes result from:

- the movement of the fuel through various power generation zones within the core;
- changes in total reactor power output;
- the formation and breakdown of fissionable isotopes.

This is taken into consideration by dividing the operational history of the fuel into a number of time intervals of constant power generation and constant power values for the fissionable isotopes, i.e. the power generation history is approximated by step functions.

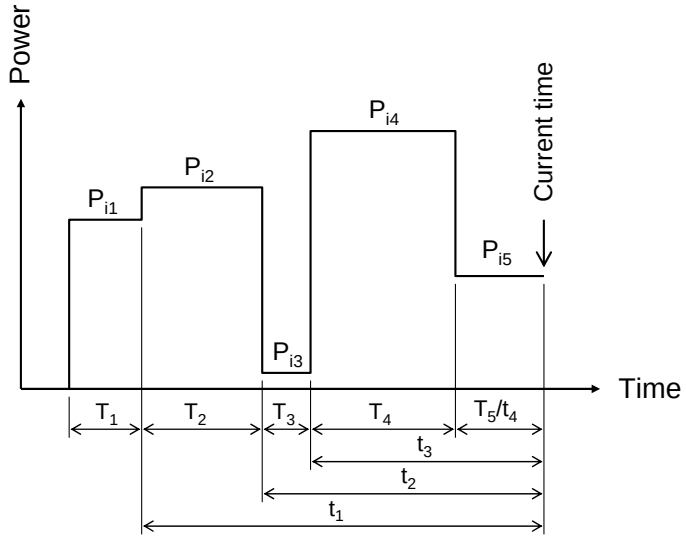

Figure 12: A Power Histogram

It is possible to determine each time offset t_k as a function of the reactor operation times T_k.

$$t_k = \sum_{j=k+1}^{m} T_j \qquad (\mathbf{3}.102)$$

and

$$t_m = 0$$

It is assumed that the user supplies the reactor life history. An option is available in TINTE to approximate the life history for the Once-Through-Then-Out (OTTO) fuel cycle, assuming no fuel isotopic changes. The option allowed the approximate construction of the reactor life history for multipath fuelling and was successfully used in the first models of the SIEMENS MODUL reactor. The option is now considered obsolete and therefore will not be discussed further in this document.

3.2.5.2.2 Fission product contribution

The contribution $\dot{Q}_S$ of the fission products to the decay heat is calculated by summing the individual $\dot{Q}_{S,i}$ values for the four fissionable isotopes (^{235}U, ^{238}U, ^{239}Pu and ^{241}Pu). If the reactor operation history can be divided into m constant power operating intervals, each with known fuel isotopic distributions, each $\dot{Q}_{S,i}$ value in turn consists of a sum of the decay heat contributions for m time intervals of reactor operation.

$$\dot{Q}_S = \sum_i \dot{Q}_{S,i} = \sum_{i=1}^{4} \sum_{k=1}^{m} \left[\frac{\dot{Q}_{ik}}{Q_i} \cdot \sum_{l=1}^{24} \left[\left(\frac{\alpha}{\lambda} \right)_{i,l} \left(1 - e^{-\lambda_{l,i} \cdot T_k} \right) e^{-\lambda_{l,i} \cdot t_k} \right] \right]$$

where $\dot{Q}_{ik} / Q_i$ is the ratio of thermal fission power to utilizable energy per fission for the ith fissionable isotope. This is equivalent to the fission rate $F_{i,k}$ for the isotope. This fission rate is related to the total fission rate in the material by $F_{i,k} = R_{i,k} F_k$, where $R_{i,k}$ is the ratio of fissions in the ith fissionable isotope to the total fission rate during the kth time interval.

The sum over l indicates the sum over the 24 decay heat precursor groups. The DIN standard, however, does not use the same group structures for all fissionable isotopes (^{235}U, ^{238}U, ^{239}Pu and ^{241}Pu). In order to optimize computational time, a single set of 24 precursor groups was chosen and associated $(\alpha_i / \lambda)_l$ values calculated [23] to closely replicate the DIN standard [21]. These values are given in Table 7. The resulting equation may be written as:

$$\dot{Q}_S = \sum_{k=1}^{m} \left[F_k \cdot \sum_{l=1}^{24} \left[\left(\sum_{i=1}^{4} R_{i,k} \left(\frac{\alpha_i}{\lambda} \right)_l \right) \left(1 - e^{-\lambda_l \cdot T_k} \right) e^{-\lambda_l \cdot t_k} \right] \right] \qquad (\mathbf{3}.103)$$

3.2.5.2.3 Contribution of the Actinides ^{239}U, ^{239}Np, ^{233}Th and ^{233}Pa

The two most important isotopes that can be produced by conversion ('breeding') are ^{233}U and ^{239}Pu. The reactions involved are as follows:

$$^{232}Th(n,\gamma)\,^{233}Th \xrightarrow{\beta-} {}^{233}Pa \xrightarrow{\beta-} {}^{233}U \qquad (\mathbf{3}.104)$$

$$^{238}U(n,\gamma)\,^{239}U \xrightarrow{\beta-} {}^{239}Np \xrightarrow{\beta-} {}^{239}Pu \qquad (\mathbf{3}.105)$$

The heat produced by the β-decay of ^{233}Th, ^{233}Pa, ^{239}U and ^{239}Np is termed the 'breeding' heat production, $\dot{Q}_B$. This is calculated as the sum of the individual isotope contributions.

$$\dot{Q}_B = \dot{Q}_U + \dot{Q}_{Np} + \dot{Q}_{Th} + \dot{Q}_{Pa} \qquad (\mathbf{3}.106)$$

where

$$\dot{Q}_U = E_U \sum_{k=1}^{m} F_k R_{U,k} \left(1 - e^{-\lambda_U \cdot T_k} \right) e^{-\lambda_U \cdot t_k} \quad \text{for } ^{239}\text{U} \qquad (\mathbf{3}.107)$$

$$\dot{Q}_{Np} = E_{Np} \sum_{k=1}^{m} F_k R_{U,k} \left[\frac{\lambda_U}{\lambda_U - \lambda_{Np}} \left(1 - e^{-\lambda_{Np} \cdot T_k} \right) e^{-\lambda_{Np} \cdot t_k} - \frac{\lambda_{Np}}{\lambda_U - \lambda_{Np}} \left(1 - e^{-\lambda_U \cdot T_k} \right) e^{-\lambda_U \cdot t_k} \right] \text{ for } ^{239}\text{Np} \qquad (\mathbf{3}.108)$$

$$\dot{Q}_{Th} = E_{Th}\sum_{k=1}^{m} F_k R_{Th,k}\left(1-e^{-\lambda_{Th}\cdot T_k}\right)e^{-\lambda_{Th}\cdot t_k} \quad \text{for } ^{233}\text{Th} \qquad (\mathbf{3}.109)$$

$$\dot{Q}_{Np} = E_{Pa}\sum_{k=1}^{m} F_k R_{Th,k}\left[\frac{\lambda_{Th}}{\lambda_{Th}-\lambda_{Pa}}\left(1-e^{-\lambda_{Pa}\cdot T_k}\right)e^{-\lambda_{Pa}\cdot t_k} - \frac{\lambda_{Pa}}{\lambda_{Th}-\lambda_{Pa}}\left(1-e^{-\lambda_{Th}\cdot T_k}\right)e^{-\lambda_{Th}\cdot t_k}\right] \text{ for } ^{233}\text{Pa} \qquad (\mathbf{3}.110)$$

where

$E_U = 0.474MeV$, the mean decay energy of ^{239}U

$E_{Np} = 0.419MeV$, the mean decay energy of ^{239}Np

E_{Th} , the mean decay energy of ^{233}Th, assumed equal to E_U

E_{Pa} , the mean decay energy of ^{233}Pa, assumed equal to E_{Np}

$\lambda_U = 4.91\times10^{-4}\,s^{-1}$, the decay constant of ^{239}U

$\lambda_{Np} = 3.41\times10^{-6}\,s^{-1}$, the decay constant of ^{239}Np

$\lambda_{Th} = 5.18\times10^{-4}\,s^{-1}$, the decay constant of ^{233}Th

$\lambda_{Pa} = 2.971\times10^{-7}\,s^{-1}$, the decay constant of ^{233}Pa

$R_{U,k}$ and $R_{Th,k}$, the ratios of the neutron capture rates of ^{239}U and ^{233}Th to the total fission rate at the end of the kth time interval

3.2.5.2.4 Total decay heat production

The contribution of ^{134}Cs to decay heat production is ignored. Taking this into account, the total decay heat production at a given time may be written as:

$$\dot{Q}_d = \sum_{k=1}^{m} F_k \left[\begin{array}{l} \displaystyle\sum_{l=1}^{24}\left[\left(\sum_{i=1}^{4} R_{i,k}\left(\frac{\alpha_i}{\lambda}\right)_l\left(1+H(t_k)+A(t_k)K_A\right)\right)\left(1-e^{-\lambda_l\cdot T_k}\right)e^{-\lambda_l\cdot t_k}\right] \\ + E_U R_{U,k}\left(1-e^{-\lambda_U\cdot T_k}\right)e^{-\lambda_U\cdot t_k} \\ + E_{Np} R_{U,k}\left(\frac{\lambda_U}{\lambda_U-\lambda_{Np}}\left(1-e^{-\lambda_{Np}\cdot T_k}\right)e^{-\lambda_{Np}\cdot t_k} - \frac{\lambda_{Np}}{\lambda_U-\lambda_{Np}}\left(1-e^{-\lambda_U\cdot T_k}\right)e^{-\lambda_U\cdot t_k}\right) \\ + E_{Th} R_{Th,k}\left(1-e^{-\lambda_{Th}\cdot T_k}\right)e^{-\lambda_{Th}\cdot t_k} \\ + E_{Pa} R_{Th,k}\left(\frac{\lambda_{Th}}{\lambda_{Th}-\lambda_{Pa}}\left(1-e^{-\lambda_{Pa}\cdot T_k}\right)e^{-\lambda_{Pa}\cdot t_k} - \frac{\lambda_{Pa}}{\lambda_{Th}-\lambda_{Pa}}\left(1-e^{-\lambda_{Th}\cdot T_k}\right)e^{-\lambda_{Th}\cdot t_k}\right) \end{array}\right] \qquad (\mathbf{3}.111)$$

In order to simplify the calculation, the term $(\alpha_i/\lambda)_l\left(1+H(t_k)+A(t_k)K_A\right)$ is written as $\left(\left(1+H^+(t)\right)\alpha_i/\lambda\right)_l + K_A\left(A(t)\alpha_i/\lambda\right)_l$ and a set of constants for $\left(\left(1+H^+(t)\right)\alpha_i/\lambda\right)_l$ and $\left(A(t)\alpha_i/\lambda\right)_l$ calculated. This approximation is discussed in detail in Appendix A, as well as

the method used to calculate the constants[**]. The constants $\left(\left(1+H^{+}(t)\right)\alpha_i/\lambda\right)_l$ and $\left(A(t)\alpha_i/\lambda\right)_l$ are tabulated in Table 7 and Table 8. Because the DIN standard [21] does not provide values for the isotopes ^{232}Th, ^{233}U, ^{234}U, ^{236}U, ^{240}Pu and ^{242}Pu, these are assumed equal to the values for ^{235}U.

Table 7: Decay Heat Group Constants used in TINTE, Contribution of Fission Products and Remaining Capture Reactions

Group	Decay Constant λ [1/s]	$\left(\left(1+H^{+}(t)\right)\alpha_i/\lambda\right)_l$ [MeV/fission]			
		^{235}U	^{238}U	^{239}Pu	^{241}Pu
1	9.46529900E-11	9.826E-02	1.000E-05	4.919E-03	1.134E-01
2	8.70105772E-11	6.366E-02	1.000E-05	1.020E-05	9.636E-06
3	7.13382487E-11	1.209E-05	1.769E-05	1.378E-05	7.954E-06
4	2.49801153E-11	3.796E-02	4.045E-01	3.575E-01	6.582E-03
5	1.12361217E-09	7.563E-02	5.786E-02	5.076E-02	4.251E-02
6	1.76517465E-08	1.000E-05	1.589E-02	2.848E-02	4.322E-02
7	2.63223467E-08	8.487E-02	1.045E-01	1.073E-01	1.274E-01
8	1.02468769E-07	7.239E-02	2.346E-02	8.340E-03	1.000E-05
9	1.31947711E-07	1.620E-01	1.762E-01	1.689E-01	1.433E-01
10	5.96407672E-07	2.298E-02	1.000E-05	4.865E-03	3.987E-02
11	6.66693113E-07	2.715E-01	2.781E-01	2.788E-01	2.501E-01
12	2.53418850E-06	2.113E-01	2.392E-01	2.514E-01	2.145E-01
13	7.80728971E-06	1.000E-05	6.312E-02	1.050E-01	1.917E-01
14	1.00849415E-05	2.650E-01	1.644E-01	1.119E-01	1.000E-05
15	2.03242415E-05	3.591E-01	3.667E-01	4.015E-01	3.972E-01
16	5.05207819E-05	5.771E-01	4.453E-01	3.516E-01	3.047E-01
17	1.57960705E-04	9.045E-01	8.383E-01	7.387E-01	8.415E-01
18	4.61398841E-04	1.166	1.258	1.293	1.223
19	1.23477143E-03	1.221	1.070	1.217	1.230
20	4.71254051E-03	1.179	1.498	9.214E-01	1.080
21	1.53414304E-02	2.307	2.831	1.871	2.410
22	5.89464404E-02	1.977	2.611	1.399	1.945
23	2.19475243E-01	2.285	2.593	1.540	2.262
24	8.83998586E-01	5.457E-01	1.952	4.715E-01	8.838E-01

[**] Note that the terms λ_l, $\left(\left(1+H^{+}(t)\right)\alpha_i/\lambda\right)_l$ and $\left(A(t)\alpha_i/\lambda\right)_l$, used in this chapter, refer to the constants Λ_l, β_{il} and γ_{il}, derived in Appendix A, respectively. The original variable names, as given in the DIN standard, are kept the same to improve readability.

Table 8: Decay Heat Group Constants used in TINTE, Contribution of the Remaining Actinides

Group	Decay Constant λ [1/s]	$(A(t)\alpha_i/\lambda)_l$ [MeV/fission]			
		^{235}U	^{238}U	^{239}Pu	^{241}Pu
1	9.46529900E-11	8.606E-06	2.031E-01	1.321E-01	1.940E-05
2	8.70105772E-11	3.181E-01	4.386E-02	7.297E-02	6.513E-02
3	7.13382487E-11	5.806E-02	4.193E-02	4.682E-02	1.552E-01
4	2.49801153E-11	1.351E-01	1.000E-05	3.682E-02	1.605E-01
5	1.12361217E-09	1.000E-05	1.000E-05	1.000E-05	1.000E-05
6	1.76517465E-08	6.248E-03	1.786E-02	2.314E-02	3.056E-02
7	2.63223467E-08	6.620E-03	1.849E-03	1.000E-05	1.000E-05
8	1.02468769E-07	3.342E-02	2.840E-02	2.421E-02	1.974E-02
9	1.31947711E-07	1.000E-05	1.000E-05	9.120E-04	1.000E-05
10	5.96407672E-07	5.854E-03	1.088E-02	1.330E-02	2.197E-02
11	6.66693113E-07	1.526E-02	9.275E-03	7.780E-03	1.000E-05
12	2.53418850E-06	1.086E-02	1.392E-02	1.461E-02	1.235E-02
13	7.80728971E-06	4.939E-03	4.099E-03	6.538E-03	1.214E-02
14	1.00849415E-05	1.118E-02	1.007E-02	7.135E-03	8.118E-05
15	2.03242415E-05	1.759E-02	1.661E-02	1.822E-02	1.837E-02
16	5.05207819E-05	1.936E-02	1.462E-02	1.026E-02	8.534E-03
17	1.57960705E-04	2.427E-02	2.316E-02	2.143E-02	2.537E-02
18	4.61398841E-04	2.013E-02	2.365E-02	2.428E-02	2.053E-02
19	1.23477143E-03	1.318E-02	8.913E-03	1.246E-02	1.329E-02
20	4.71254051E-03	1.384E-02	1.921E-02	1.015E-02	1.301E-02
21	1.53414304E-02	1.944E-02	2.367E-02	1.596E-02	2.078E-02
22	5.89464404E-02	1.328E-02	1.778E-02	8.924E-03	1.274E-02
23	2.19475243E-01	1.327E-02	1.507E-02	9.208E-03	1.398E-02
24	8.83998586E-01	2.210E-03	1.032E-02	2.005E-03	4.163E-03

3.2.5.2.5 Extending the operational time

In order to extend the operational history by additional constant power intervals, it is necessary to calculate the relationship between the decay heat at the end of subsequent time intervals, given known initial conditions. Equation (**3**.111) may generically be written as:

$$\dot{Q}_d = \sum_{k=1}^{m} F_k \sum_{l=1}^{30} \alpha'_l \left(1 - e^{-\lambda_l T_k}\right) e^{-\lambda_l t_k}$$
$$= \sum_{l=1}^{30} \alpha'_l \sum_{k=1}^{m} F_k \left(1 - e^{-\lambda_l T_k}\right) e^{-\lambda_l t_k}$$

where l is used to denote the 24 decay groups as well as the six additional exponential terms in Equation (**3**.111). Equation (**3**.102) is used to replace t_k as follows:

$$\dot{Q}_d = \sum_{l=1}^{30} \alpha'_l \sum_{k=1}^{m} F_k \left(1 - e^{-\lambda_l T_k}\right) e^{-\sum_{j=k+1}^{m} \lambda_l T_j}$$
$$= \sum_{l=1}^{30} \alpha'_l \sum_{k=1}^{m} F_k \left(1 - e^{-\lambda_l T_k}\right) \prod_{j=k+1}^{m} e^{-\lambda_l T_j}$$

where $T_{m+1}=0$. By expanding the final few terms of the sum over k, it is clear that the delayed heat production after interval m may be written as a function of that after interval $m-1$.

$$\dot{Q}_d = \sum_{l=1}^{30}\left[\alpha'_l\left(\begin{array}{l}\left[\sum_{k=1}^{m-3}F_k\left(1-e^{-\lambda_l T_k}\right)\left(\prod_{j=k+1}^{m}e^{-\lambda_l T_j}\right)e^{-\lambda_l T_m}\right]\\ +F_{m-2}\left(1-e^{-\lambda_l T_{m-2}}\right)e^{-\lambda_l T_{m-1}}e^{-\lambda_l T_m}\\ +F_{m-1}\left(1-e^{-\lambda_l T_{m-1}}\right)e^{-\lambda_l T_m}\\ +F_m\left(1-e^{-\lambda_l T_m}\right)\end{array}\right)\right]$$

$$= \sum_{l=1}^{30}\left[\left(\alpha'_l\sum_{k=1}^{m-1}F_k\left(1-e^{-\lambda_l T_k}\right)\prod_{j=k+1}^{m}e^{-\lambda_l T_j}\right)e^{-\lambda_l T_m}+\alpha'_l F_m\left(1-e^{-\lambda_l T_m}\right)\right]$$

By denoting $\dot{Q}_d(t)=\sum_{l=1}^{30}\dot{Q}_{d,l}(t)$, and assuming constant power over a time interval Δ.

$$\dot{Q}_{d,l}(t_0+\Delta)=\dot{Q}_{d,l}(t_0)e^{-\lambda_l\Delta}+\alpha'_l F\left(1-e^{-\lambda_l\Delta}\right) \qquad (\mathbf{3}.112)$$

This approximation is used to extend the decay heat production at the end of a given life histogram by a short time period. This would typically be half a burn-up cycle, in the order of several days.

3.2.5.2.6 Time-dependent decay heat production

The DIN standard assumes a constant fission rate for each time interval. For the time-dependent case, this zeroth order approximation is not particularly suited and a modified form of Equation (**3**.111) is sought out. It is noted that Equation (**3**.112) is the solution to the differential equation

$$\frac{d\dot{Q}_{d,l}}{dt}=\alpha'_l\lambda_l F-\lambda_l\dot{Q}_{d,l} \qquad (\mathbf{3}.113)$$

assuming constant fission rate. The general solution to this equation is:

$$\dot{Q}_{d,l}=e^{-\lambda_l(t-t_0)}\left\{\dot{Q}_{d,l}(t_0)+\alpha'_l\lambda_l\int_{t_0}^{t}dt'\,F(t')e^{\lambda_l(t'-t_0)}\right\} \qquad (\mathbf{3}.114)$$

If the fission rate is assumed linear ($F(t)=F_0+\frac{t-t_0}{\Delta}(F_1-F_0)$), (**3**.114) may be solved to yield the general solution form for a direct fission decay heat precursor.

$$\dot{Q}_{d,l}(t) = e^{-\lambda_l (t-t_0)} \left\{ \dot{Q}_{d,l}(t_0) + \alpha'_l \lambda_l \int_{t_0}^{t} dt' \left[F_0 + \frac{t'-t_0}{\Delta}(F_1 - F_0) \right] e^{\lambda_l (t'-t_0)} \right\}$$

$$= e^{-\lambda_l (t-t_0)} \left\{ \dot{Q}_{d,l}(t_0) + \alpha'_l \lambda_l \left[F_0 \int_{t_0}^{t} e^{\lambda_l (t'-t_0)} dt' + \frac{F_1 - F_0}{\Delta} \int_{t_0}^{t} (t'-t_0) e^{\lambda_l (t'-t_0)} dt' \right] \right\}$$

$$= e^{-\lambda_l (t-t_0)} \left\{ \dot{Q}_{d,l}(t_0) + \alpha'_l \lambda_l \left[F_0 \frac{1}{\lambda_l} \left(e^{\lambda_l (t-t_0)} - 1 \right) + \frac{F_1 - F_0}{\Delta} \frac{1}{\lambda_l^{\,2}} \left(1 + e^{\lambda_l (t-t_0)} \left(\lambda_l (t-t_0) - 1 \right) \right) \right] \right\}$$

$$= \dot{Q}_{d,l}(t_0) e^{-\lambda_l (t-t_0)} + \alpha'_l F_0 \left(1 - e^{-\lambda_l (t-t_0)} \right) + \alpha'_l \frac{F_1 - F_0}{\Delta} \frac{1}{\lambda_l^{\,2}} \left(e^{-\lambda_l (t-t_0)} + \lambda_l (t-t_0) - 1 \right)$$

$$\dot{Q}_{d,l}(t) = \dot{Q}_{d,l}(t_0) e^{-\lambda_l (t-t_0)} + \alpha'_l F_0 \left(1 - \frac{t-t_0}{\Delta} - e^{-\lambda_l (t-t_0)} + \frac{1 - e^{-\lambda_l (t-t_0)}}{\lambda_l \Delta} \right) + \alpha'_l F_1 \left(\frac{t-t_0}{\Delta} - \frac{1 - e^{-\lambda_l (t-t_0)}}{\lambda_l \Delta} \right) \quad (\mathbf{3}.115)$$

The individual decay heat precursors at the end of a time interval Δ are therefore found to be:

$$\dot{Q}_{S,l}(t_0 + \Delta) = \dot{Q}_{S,l}(t_0) e^{-\lambda_l \Delta} - \alpha_l' F_0 \left(e^{-\lambda_l \Delta} - \frac{1 - e^{-\lambda_l \Delta}}{\lambda_l \Delta} \right) + \alpha_l' F_1 \left(1 - \frac{1 - e^{-\lambda_l \Delta}}{\lambda_l \Delta} \right) \quad (\mathbf{3}.116)$$

$$\dot{Q}_{U}(t_0 + \Delta) = \dot{Q}_{U}(t_0) e^{-\lambda_U \Delta} - \alpha_U' F_0 \left(e^{-\lambda_U \Delta} - \frac{1 - e^{-\lambda_U \Delta}}{\lambda_U \Delta} \right) + \alpha_U' F_1 \left(1 - \frac{1 - e^{-\lambda_U \Delta}}{\lambda_U \Delta} \right) \quad (\mathbf{3}.117)$$

$$\dot{Q}_{Th}(t_0 + \Delta) = \dot{Q}_{Th}(t_0) e^{-\lambda_{Th} \Delta} - \alpha_{Th}' F_0 \left(e^{-\lambda_{Th} \Delta} - \frac{1 - e^{-\lambda_{Th} \Delta}}{\lambda_{Th} \Delta} \right) + \alpha_{Th}' F_1 \left(1 - \frac{1 - e^{-\lambda_{Th} \Delta}}{\lambda_{Th} \Delta} \right) \quad (\mathbf{3}.118)$$

In the case of the actinides ^{239}Np and ^{233}Pa (isotopes formed through breeding), the differential equation to be solved is given below (for the specific case of ^{239}Np).

$$\frac{d\dot{Q}_{Np}}{dt} = \frac{\alpha'_{Np}}{\alpha'_{U}} \lambda_{Np} \dot{Q}_U - \lambda_{Np} \dot{Q}_{Np} \quad (\mathbf{3}.119)$$

For the solution of Equation (**3**.119), partial integration is used.

$$\dot{Q}_{Np}(t) = e^{-\lambda_{Np}(t-t_0)}\left\{\dot{Q}_{Np}(t_0) + \frac{\alpha'_{Np}}{\alpha'_U}\lambda_{Np}\int_{t_0}^{t} dt'\,\dot{Q}_U(t')e^{\lambda_{Np}(t-t_0)}\right\}$$

$$= e^{-\lambda_{Np}(t-t_0)}\left\{\dot{Q}_{Np}(t_0) + \alpha'_{Np}\,\lambda_{Np}\int_{t_0}^{t} dt'\,F(t')e^{\lambda_{Np}(t-t_0)} + \frac{\alpha'_{Np}\,\lambda_{Np}}{\alpha'_U\,\lambda_U}\left(\dot{Q}_U(t_0)e^{-\lambda_{Np}(t-t_0)} - \dot{Q}_U(t)\right)\right\}$$

$$= e^{-\lambda_{Np}(t-t_0)}\left\{\dot{Q}_{Np}(t_0) + \alpha'_{Np}\,\lambda_{Np}\int_{t_0}^{t} dt'\,F(t')e^{\lambda_{Np}(t-t_0)} + \frac{\alpha'_{Np}\,\lambda_{Np}}{\alpha'_U\,\lambda_U}\left(\dot{Q}_U(t_0)e^{-\lambda_{Np}(t-t_0)} - \dot{Q}_U(t)\right)\right\}$$

$$= e^{-\lambda_{Np}(t-t_0)}\left\{\dot{Q}_{Np}(t_0) + \alpha'_{Np}\,\lambda_{Np}\int_{t_0}^{t} dt'\left[F_0 + \frac{t-t_0}{\Delta}(F_1 - F_0)\right]e^{\lambda_{Np}(t-t_0)}\right\}$$

$$+ \frac{\alpha'_{Np}\,\lambda_{Np}}{\alpha'_U\,\lambda_U}\left(\dot{Q}_U(t_0)e^{-\lambda_{Np}(t-t_0)} - \dot{Q}_U(t)\right)$$

Using the identical methodology as was used in the derivation of Equation (**3**.115), the integral part of the above equation is reduced, resulting in the following general expression for the time-dependent breeding decay heat of an isotope (for the case of ^{239}Np).

$$\dot{Q}_{Np}(t) = \dot{Q}_{Np}(t_0)e^{-\lambda_{Np}\Delta} + \alpha'_{Np}\,F_0\left[1 - \frac{t-t_0}{\Delta} - e^{-\lambda_{Np}(t-t_0)} + \frac{1-e^{-\lambda_{Np}(t-t_0)}}{\lambda_{Np}\Delta}\right]$$
$$+ \alpha'_{Np}\,F_1\left(\frac{t-t_0}{\Delta} - \frac{1-e^{-\lambda_{Np}(t-t_0)}}{\lambda_{Np}\Delta}\right) - \frac{\alpha'_{Np}\,\lambda_{Np}}{\alpha'_U\,\lambda_U}\left(\dot{Q}_U(t_0)e^{-\lambda_{Np}(t-t_0)} - \dot{Q}_U(t)\right) \quad (\mathbf{3}.120)$$

Using this, the expressions for the decay heat production of the isotopes ^{239}Np and ^{233}Pa at the end of a time interval Δ can be written as:

$$\dot{Q}_{Np}(t_0+\Delta) = \dot{Q}_{Np}(t_0)e^{-\lambda_{Np}\Delta} - \alpha'_{Np}\,F_0\left(e^{-\lambda_{Np}\Delta} - \frac{1-e^{-\lambda_{Np}\Delta}}{\lambda_{Np}\Delta}\right) + \alpha'_{Np}\,F_1\left(1 - \frac{1-e^{-\lambda_{Np}\Delta}}{\lambda_{Np}\Delta}\right)$$
$$- \frac{\alpha'_{Np}\,\lambda_{Np}}{\alpha'_U\,\lambda_U}\left(\dot{Q}_U(t_0)e^{-\lambda_{Np}\Delta} - \dot{Q}_U(t_0+\Delta)\right) \quad (\mathbf{3}.121)$$

$$\dot{Q}_{Pa}(t_0+\Delta) = \dot{Q}_{Pa}(t_0)e^{-\lambda_{Pa}\Delta} - \alpha'_{Pa}\,F_0\left(e^{-\lambda_{Pa}\Delta} - \frac{1-e^{-\lambda_{Pa}\Delta}}{\lambda_{Pa}\Delta}\right) + \alpha'_{Pa}\,F_1\left(1 - \frac{1-e^{-\lambda_{Pa}\Delta}}{\lambda_{Pa}\Delta}\right)$$
$$- \frac{\alpha'_{Pa}\,\lambda_{Pa}}{\alpha'_{Th}\,\lambda_{Th}}\left(\dot{Q}_{Th}(t_0)e^{-\lambda_{Pa}\Delta} - \dot{Q}_{Th}(t_0+\Delta)\right) \quad (\mathbf{3}.122)$$

The total decay heat production at the end of the time interval may be calculated as the sum of the individual decay heat components.

$$\dot{Q}_d(t+\Delta) = \left[\sum_{l=1}^{24}\dot{Q}_{S,l}(t+\Delta)\right] + \dot{Q}_U(t+\Delta) + \dot{Q}_{Np}(t+\Delta) + \dot{Q}_{Th}(t+\Delta) + \dot{Q}_{Pa}(t+\Delta) \quad (\mathbf{3}.123)$$

The mean for a time interval Δ may be calculated as:

$$\overline{\dot{Q}} = \frac{1}{t-t_0}\int_{t_0}^{t}\dot{Q}(t')dt'$$

Using Equations (**3**.115) and (**3**.120), the integral may be solved.

$$\overline{\dot{Q}}_{d,l} = \frac{1}{t-t_0}\left[\int_{t_0}^{t} dt'\,\dot{Q}_{d,l0}e^{-\lambda_l(t'-t_0)} + \int_{t_0}^{t} dt'\,\alpha'_l\,F_0\left[1-\frac{t'-t_0}{\Delta}-e^{-\lambda_l(t'-t_0)}+\frac{1-e^{-\lambda_l(t'-t_0)}}{\lambda_l\Delta}\right]\right.$$
$$\left. + \int_{t_0}^{t} dt'\,\alpha'_l\,F_1\left(\frac{t'-t_0}{\Delta}+\frac{e^{-\lambda_l(t'-t_0)}-1}{\lambda_l\Delta}\right)\right]$$

$$= \frac{1}{\Delta}\left[\dot{Q}_{d,l}(t_0)\int_{t_0}^{t} dt'\,e^{-\lambda_l(t'-t_0)} + \alpha'_l\,F_0\int_{t_0}^{t} dt'\left[1-\frac{t'-t_0}{\Delta}-e^{-\lambda_l(t'-t_0)}+\frac{1-e^{-\lambda_l(t'-t_0)}}{\lambda_l\Delta}\right]\right.$$
$$\left. + \alpha'_l\,F_1\int_{t_0}^{t} dt\left(\frac{t'-t_0}{\Delta}-\frac{1-e^{-\lambda_l(t'-t_0)}}{\lambda_l\Delta}\right)\right]$$

$$= \frac{1}{\Delta}\left[\dot{Q}_{d,l}(t_0)\frac{1-e^{-\lambda_l(t-t_0)}}{\lambda_l}\right.$$
$$+ \alpha'_l\,F_0\left[t-t_0-\frac{1}{\Delta}\left(\frac{t^2-{t_0}^2}{2}-t_0t+{t_0}^2\right)+\frac{1}{\lambda_l}\left(e^{-\lambda_l(t-t_0)}-1\right)+\frac{t-t_0}{\lambda_l\Delta}\right.$$
$$\left.\left. + \frac{1}{{\lambda_l}^2\Delta}\left(1-e^{-\lambda_l(t-t_0)}\right)\right]\right.$$
$$\left. + \alpha'_l\,F_1\left[\frac{1}{\Delta}\left(\frac{t^2-{t_0}^2}{2}-t_0t+{t_0}^2\right)-\frac{t-t_0}{\lambda_l\Delta}-\frac{1}{{\lambda_l}^2\Delta}\left(1-e^{-\lambda_l(t-t_0)}\right)\right]\right]$$

$$= \frac{1}{\Delta}\left[\dot{Q}_{d,l}(t_0)\frac{1-e^{-\lambda_l\Delta}}{\lambda_l} + \alpha'_l\,F_0\left[\frac{\Delta}{2}+\frac{e^{-\lambda_l\Delta}+\frac{1-e^{-\lambda_l\Delta}}{\lambda_l\Delta}}{\lambda_l}\right] + \alpha'_l\,F_1\left[\frac{\Delta}{2}-\frac{1-\frac{1-e^{-\lambda_l\Delta}}{\lambda_l\Delta}}{\lambda_l}\right]\right]$$

$$= \dot{Q}_{d,l}(t_0)\frac{1-e^{-\lambda_l\Delta}}{\lambda_l\Delta} + \alpha'_l\,F_0\left[\frac{1}{2}+\frac{e^{-\lambda_l\Delta}+\frac{1-e^{-\lambda_l\Delta}}{\lambda_l\Delta}}{\lambda_l\Delta}\right] + \alpha'_l\,F_1\left[\frac{1}{2}-\frac{1-\frac{1-e^{-\lambda_l\Delta}}{\lambda_l\Delta}}{\lambda_l\Delta}\right]$$

Similarly, the additional term $\frac{\alpha'_{Np}\,\lambda_{Np}}{\alpha'_U\,\lambda_U}\left(\dot{Q}_U(t_0)e^{-\lambda_{Np}(t-t_0)}-\dot{Q}_U(t)\right)$ in (**3**.120) may be integrated to obtain the following:

$$\frac{1}{t-t_0}\int_{t_0}^{t} dt'\,\frac{\alpha'_{Np}\,\lambda_{Np}}{\alpha'_U\,\lambda_U}\left(\dot{Q}_U(t_0)e^{-\lambda_{Np}(t'-t_0)}-\dot{Q}_U(t')\right) = \frac{1}{\Delta}\frac{\alpha'_{Np}\,\lambda_{Np}}{\alpha'_U\,\lambda_U}\left[\dot{Q}_U(t_0)\int_{t_0}^{t} dt'\,e^{-\lambda_{Np}(t'-t_0)} - \int_{t_0}^{t} dt'\,\dot{Q}_U(t')\right]$$
$$= \frac{\alpha'_{Np}\,\lambda_{Np}}{\alpha'_U\,\lambda_U}\left[\dot{Q}_U(t_0)\frac{1-e^{-\lambda_{Np}(t-t_0)}}{\lambda_{Np}\Delta} - \frac{1}{t-t_0}\int_{t_0}^{t} dt'\,\dot{Q}_U(t')\right]$$
$$= \frac{\alpha'_{Np}\,\lambda_{Np}}{\alpha'_U\,\lambda_U}\left[\dot{Q}_U(t_0)\frac{1-e^{-\lambda_{Np}\Delta}}{\lambda_{Np}\Delta} - \overline{\dot{Q}}_U\right]$$

The mean component decay heat precursor values for a time interval Δ may therefore be written as:

$$\overline{\dot{Q}}_{S,l} = \dot{Q}_{S,l}(t_0)\frac{1-e^{-\lambda_l \Delta}}{\lambda_l \Delta} + \alpha_l' F_0 \left(\frac{1}{2} + \frac{e^{-\lambda_l \Delta} - \frac{1-e^{-\lambda_l \Delta}}{\lambda_l \Delta}}{\lambda_l \Delta} \right) + \alpha_l' F_1 \left(\frac{1}{2} - \frac{1 - \frac{1-e^{-\lambda_l \Delta}}{\lambda_l \Delta}}{\lambda_l \Delta} \right) \quad (\mathbf{3}.124)$$

$$\overline{\dot{Q}}_{U} = \dot{Q}_{U}(t_0)\frac{1-e^{-\lambda_U \Delta}}{\lambda_U \Delta} + \alpha_U' F_0 \left(\frac{1}{2} + \frac{e^{-\lambda_U \Delta} - \frac{1-e^{-\lambda_U \Delta}}{\lambda_U \Delta}}{\lambda_U \Delta} \right) + \alpha_U' F_1 \left(\frac{1}{2} - \frac{1 - \frac{1-e^{-\lambda_U \Delta}}{\lambda_U \Delta}}{\lambda_U \Delta} \right) \quad (\mathbf{3}.125)$$

$$\overline{\dot{Q}}_{Np} = \dot{Q}_{Np}(t_0)\frac{1-e^{-\lambda_{Np} \Delta}}{\lambda_{Np} \Delta} + \alpha'_{Np} F_0 \left(\frac{1}{2} + \frac{e^{-\lambda_{Np} \Delta} - \frac{1-e^{-\lambda_{Np} \Delta}}{\lambda_{Np} \Delta}}{\lambda_{Np} \Delta} \right) + \alpha'_{Np} F_1 \left(\frac{1}{2} - \frac{1 - \frac{1-e^{-\lambda_{Np} \Delta}}{\lambda_{Np} \Delta}}{\lambda_{Np} \Delta} \right) \quad (\mathbf{3}.126)$$

$$- \frac{\alpha'_{Np} \lambda_{Np}}{\alpha'_{U} \lambda_{U}} \left(\dot{Q}_{U}(t_0)\frac{1-e^{-\lambda_{Np} \Delta}}{\lambda_{Np} \Delta} - \overline{\dot{Q}}_{U} \right)$$

$$\overline{\dot{Q}}_{Th} = \dot{Q}_{Th}(t_0)\frac{1-e^{-\lambda_{Th} \Delta}}{\lambda_{Th} \Delta} + \alpha_{Th}' F_0 \left(\frac{1}{2} + \frac{e^{-\lambda_{Th} \Delta} - \frac{1-e^{-\lambda_{Th} \Delta}}{\lambda_{Th} \Delta}}{\lambda_{Th} \Delta} \right) + \alpha_{Th}' F_1 \left(\frac{1}{2} - \frac{1 - \frac{1-e^{-\lambda_{Th} \Delta}}{\lambda_{Th} \Delta}}{\lambda_{Th} \Delta} \right) \quad (\mathbf{3}.127)$$

$$\overline{\dot{Q}}_{Pa} = \dot{Q}_{Pa}(t_0)\frac{1-e^{-\lambda_{Pa} \Delta}}{\lambda_{Pa} \Delta} + \alpha'_{Pa} F_0 \left(\frac{1}{2} + \frac{e^{-\lambda_{Pa} \Delta} - \frac{1-e^{-\lambda_{Pa} \Delta}}{\lambda_{Pa} \Delta}}{\lambda_{Pa} \Delta} \right) + \alpha'_{Pa} F_1 \left(\frac{1}{2} - \frac{1 - \frac{1-e^{-\lambda_{Pa} \Delta}}{\lambda_{Pa} \Delta}}{\lambda_{Pa} \Delta} \right) \quad (\mathbf{3}.128)$$

$$- \frac{\alpha'_{Pa} \lambda_{Pa}}{\alpha'_{Th} \lambda_{Th}} \left(\dot{Q}_{Th}(t_0)\frac{1-e^{-\lambda_{Pa} \Delta}}{\lambda_{Pa} \Delta} - \overline{\dot{Q}}_{Th} \right)$$

The total mean decay heat production for a time interval may be calculated as:

$$\overline{\dot{Q}}_{d} = \left[\sum_{l=1}^{24} \overline{\dot{Q}}_{S,l} \right] + \overline{\dot{Q}}_{B} \quad (\mathbf{3}.129)$$

3.2.5.2.7 Effective steady-state heat production

The total energy per fission specifies the energy release at equilibrium operating conditions, i.e. decay heat is constant ($T \to \infty$). If we write the total energy release per fission as the sum of prompt and decay components, Equation (**3**.111).

$$
\begin{aligned}
E_{f,eq} &= E_p + E_d \\
&= E_p + \left(\frac{\dot{Q}_d}{F}\right)_{T\to\infty,t\to 0} \\
&= E_p + \left[\begin{array}{l} \sum_{l=1}^{24}\left[\left(\sum_{i=1}^{4} R_{i,k}\left(\frac{\alpha_i}{\lambda}\right)_l\left(1+H^+ + AK_A\right)\right)\right] \\ + E_U R_{U,k} + E_{Np} R_{U,k} + E_{Th} R_{Th,k} + E_{Pa} R_{Th,k} \end{array}\right]
\end{aligned}
$$

The prompt energy per fission may thus be expressed as follows:

$$
E_p = E_{f,eq} - \left[\begin{array}{l} \sum_{l=1}^{24}\left[\left(\sum_{i=1}^{4} R_{i,k}\left(\frac{\alpha_i}{\lambda}\right)_l\left(1+H^+ + AK_A\right)\right)\right] \\ + E_U R_{U,k} + E_{Np} R_{U,k} + E_{Th} R_{Th,k} + E_{Pa} R_{Th,k} \end{array}\right] \tag{3.130}
$$

The real reactor, however, will never reach true infinite equilibrium conditions and the effective energy release per fission, which now takes into account the life history of the fuel is:

$$
E_f = E_p + \frac{\dot{Q}_d}{F} \tag{3.131}
$$

where E_p is a known value for each fissionable isotope. In this case, the decay heat (calculated using (**3**.111)) is substituted in to obtain the effective energy per fission.

3.2.5.3 Locality of heat production

During the heat production, which is caused by fission, most of the feedback energy of the heavy fission fragments is converted to heat at the site where fission took place. β-radiation also does not travel far and can be assumed to remain at the site of fission.

In contrast, the high-energy neutrons, as well as prompt and decay γ-radiation will cover large distances before depositing their energy in the reactor materials.

Two types of heat production may therefore be distinguished with respect to their locality of energy deposition:

- Local heat sources – Recoil energy of fission fragments (prompt) and β-radiation (decay).
- Non-local heat sources – High-energy neutron moderation and capture, neutron,γ interactions and γ-radiation.

3.2.5.3.1 Local heat sources

The ratios χ_p and χ_d are defined as the ratio of local to total heat production for the prompt and decay heat cases respectively. The local power of the reactor may then be written as:

$$
\dot{Q}_l = \chi_p \dot{Q}_p + \chi_d\left(\dot{Q}_d - \dot{Q}_B\right) \tag{3.132}
$$

The breeding term $\dot{Q}_B$ is assumed to be non-local, hence its exclusion from the decay power term in Equation (**3**.132).

Using Equations (**3**.95) and (**3**.96), the locally deposited contributions of the prompt and decay energies-per-fission are E_r and E_β respectively; therefore $\chi_p = \frac{E_r}{E_p}$ and $\chi_d = \frac{E_\beta}{E_d}$.

3.2.5.3.2 Non-local heat sources

Non-local heat production is due to a number of interactions, namely:

- scattering interactions during moderation;
- neutron,γ-reactions; and
- γ-reactions.

The kinetic energy of the high-energy neutrons is generally converted to heat during moderation and absorption. The moderation and absorption heat production is calculated from the effective heat-production per moderation interaction, E_{mod}.

$$\dot{Q}'''_{\text{mod}} = E_{\text{mod}}\left(\Sigma_{a1} + \Sigma_s^{1\to 2}\right)\phi_1 \qquad (\mathbf{3}.133)$$

Because of the unique composition of fuel-containing regions of the reactor, a unique fast neutron spectrum exists in all regions. The energy per moderation is therefore spatially-dependent, depending on the fraction of each fissionable isotope within the region.

$$E_{\text{mod},i} = \left[E_{\text{mod}}^{U5}F_{U5,i} + E_{\text{mod}}^{Th2}F_{Th2,i} + \ldots + E_{\text{mod}}^{Pu2}F_{Pu2,i}\right]\frac{1}{F_{U5,i} + F_{Th2,i} + \ldots + F_{Pu2,i}} \qquad (\mathbf{3}.134)$$

The fractions $\frac{F_{U5,i}}{F_{U5,i} + F_{Th2,i} + \ldots + F_{Pu2,i}} \equiv R_{U5,i}$, etc., representing the fraction of fissions taking place in a fissionable isotope, for each nuclear material, are assumed to be user-supplied parameters. It should be noted that because of the non-locality of the heat production due to moderation and absorption, regions within the reactor cannot be treated individually according to their unique composition. This is because neutrons born in one region of the reactor may travel some distance before being moderated or absorbed. The assumption is made that all regions of the reactor have the same homogenized energy per moderation. The homogenized energy per moderation/absorption is calculated as the volume-weighted average of that for all fuel-containing regions.

$$E_{\text{mod}} = \frac{\sum_{core} E_{\text{mod},i}V_i}{\sum_{core} V_i} \qquad (\mathbf{3}.135)$$

n,γ-reactions are treated in a similar fashion using an effective heat-production per n,γ-interaction.

$$\dot{Q}'''_{n,\gamma} = E_{n.,\gamma}\left[\left(\Sigma_{a1} - \Sigma_{f1}\right)\phi_1 + \left(\Sigma_{a2} - \Sigma_{f2}\right)\phi_2\right] \qquad (\mathbf{3}.136)$$

where $E_{n,\gamma}$ is assumed a constant value of 6.1 MeV per reaction (Table 1 of DIN 25 485 [21]).

The distribution of heat produced by γ-reactions can be determined by means of transport theory methods, which is not practical in this case, as these calculations require a large amount of computational effort. Because the effective cross sections of the γ-quanta, which

arise from the fission process, are similar to those of the fast neutrons in the HTR, it is assumed that the γ-heat is distributed in the same profile as the fast neutron destruction rate.

An effective γ-cross-section is defined as:

$$\Sigma_\gamma = \Sigma_a^2 - \Sigma_f^2 + \Sigma_s^{1\to 2} \tag{3.137}$$

taking into account γ-reactions and scattering. This expression for the effective γ-cross-section was determined arbitrarily to match experimental data. No documented validation of the expression is currently available. The cross section is used to create a normalized value at each location.

$$\zeta_\gamma''' \equiv \frac{\Sigma_\gamma \phi_1'''}{\dot{Q}_\gamma} \tag{3.138}$$

The discretized form of the above equation is given below.

$$\zeta_{\gamma,ijk}''' \equiv \frac{\Sigma_\gamma \phi_{1,ijk}}{V_{ijk}\dot{Q}_\gamma} \tag{3.139}$$

The γ-heat production at each location is then calculated according to

$$\dot{Q}_\gamma''' = \zeta_\gamma''' \dot{Q}_\gamma \tag{3.140}$$

where $\dot{Q}_\gamma$ is the global γ heat production. If the total and local energy per fission are defined to exclude n-γ interactions as well as neutron moderation and absorption reactions, $\dot{Q}_\gamma$ can be calculated as the difference between the total and the local fission power, namely:

$$\dot{Q}_\gamma = \dot{Q}_f - \dot{Q}_l \tag{3.141}$$

3.2.6 Determining Feedback Values for Calculating Cross Sections

3.2.6.1 Time-dependent extrapolation

Because cross sections are required for the nuclear calculation, they must be determined before each nuclear calculation commences. Therefore, feedback parameters such as fuel and moderator temperatures, gas concentrations, graphite burn-up, etc. must be available before each nuclear calculation. This becomes a problem in the time-dependent case, because temperatures and gas flow parameters are only calculated after several nuclear time intervals (refer to Figure 16). This problem may be removed if the nuclear and temperature calculations are iterated over, however, this would greatly increase the required computational time.

Instead, the assumption is made that a number of parameters vary linearly with time and therefore their values may be extrapolated from the previous available time interval. For the following parameters, values for the previous nuclear time interval are extrapolated:

a. Local and non-local heat sources – The previous interval mean and end-of-interval values are extrapolated to estimate the new interval mean.

$$\overline{\dot{Q}_1'''} = \dot{Q}_1''' + \left(\dot{Q}_1''' - \overline{\dot{Q}_0'''}\right)\frac{\Delta t_{n1}}{\Delta t_{n0}} \qquad (\mathbf{3}.142)$$

This is illustrated in Figure 13.

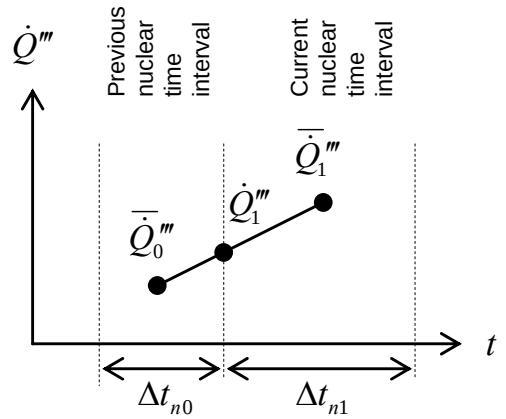

Figure 13: Time Extrapolation of the Nuclear Heat Sources

b. The fuel layer temperatures – The fuel layer temperature values are not directly available at the end of each nuclear calculation (they result from the temperature calculation). Additionally, the fuel temperatures may change rapidly in response to nuclear power changes. A simple extrapolation of the fuel layer temperatures is therefore insufficient to account for changing power levels. The method used to calculate the fuel layer temperatures (described in the TINTE thermal-hydraulic theory description **[6]**) is sufficiently fast that the values at the end of each nuclear time interval can be calculated directly. This calculation is done using the fuel layer temperatures and nuclear heat sources at the end of the previous nuclear time interval, as well as extrapolated nuclear heat sources (refer to (a) above) and extrapolated fuel surface boundary conditions (refer to (d) below). This method allows the fuel layer temperatures to be estimated, taking into account changes in power.

   For the following parameters, values from the previous temperature time interval are extrapolated:

c. Solid material temperatures – The reflectors and other solid materials are sufficiently far from the fuel elements themselves that changes in power will result in a relatively slow response in temperature. A simple time extrapolation of the solid material temperatures is therefore acceptable. This extrapolation uses the temperatures from the previous nuclear time interval and the rates of temperature change from the previous temperature time interval.

$$T_{s1} \approx T_{s0} + \left(\frac{\partial T_s}{\partial t}\right)_0 \Delta t_n \qquad (\mathbf{3}.143)$$

This is illustrated in Figure 14.

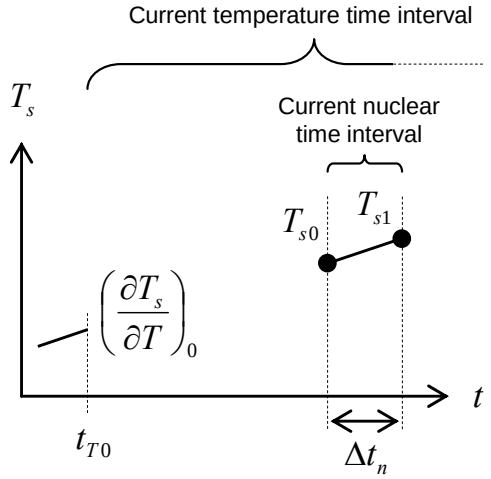

Figure 14: Time Extrapolation of the Solid Material Temperatures

d. The fuel surface boundary conditions – The heat transfer from the fuel surface to its surroundings is represented using two parameters, α^* and θ^*. Here α^* is an effective heat transfer coefficient and θ^* is the representative temperature of the surroundings. For the calculation of the fuel layer temperatures, these parameters provide the boundary conditions at the surface of the fuel sphere. The approximation is made that α^* and θ^* vary linearly with respect to time and that their values may be extrapolated using the same method described in (c) above.

$$\alpha_1^* \approx \alpha_0^* + \left(\frac{\partial \alpha^*}{\partial t}\right)_0 \Delta t_n \qquad (\mathbf{3}.144)$$

$$\theta_1^* \approx \theta_0^* + \left(\frac{\partial \theta^*}{\partial t}\right)_0 \Delta t_n \qquad (\mathbf{3}.145)$$

This simple extrapolation is sufficient for the case of non-changing surrounding temperatures. This is, however, not the case (refer to (c) above). Because the surrounding (solid material) temperatures are extrapolated, θ^* must be corrected. With reference to the TINTE Thermal-hydraulics Theory Report [6], the total heat transfer from the surface of a fuel sphere to its surroundings may be written as the sum of a number of individual heat transfers. In the discretized spatial domain this includes heat transfer from the surrounding meshes, as well as other influences such as gas temperature.

$$
\begin{aligned}
S &= \sum_i \alpha_i \left(T_p - T_i\right) \\
&= T_p \sum_i \alpha_i - \sum_i \alpha_i T_i \\
&= T_p \sum_i \alpha_i - \theta^* \sum_i \alpha_i \\
&= \alpha^* \left(T_p - \theta^*\right)
\end{aligned}
$$

where

$$
\alpha^* = \sum_i \alpha_i
$$

$$
\theta^* = \frac{\sum_i \alpha_i T_i}{\sum_i \alpha_i}
$$

If each temperature T_i changes by an amount ΔT_i, the updated value of θ^* is calculated as:

$$
\begin{aligned}
\theta' &= \frac{\sum_i \alpha_i \left(T_i + \Delta T_i\right)}{\sum_i \alpha_i} \\
&= \frac{\sum_i \alpha_i T_i}{\sum_i \alpha_i} + \frac{\sum_i \alpha_i \Delta T_i}{\sum_i \alpha_i} \\
&= \theta^* + \frac{\sum_i \alpha_i \Delta T_i}{\sum_i \alpha_i}
\end{aligned}
$$

where θ' is the corrected value. A total correction $\Delta\theta^*$ may be defined as:

$$
\Delta\theta^* = \frac{\sum_i \alpha_i \Delta T_i}{\sum_i \alpha_i} \qquad (\mathbf{3}.146)
$$

The correction to the change in a single surrounding temperature (i.e. neighbouring mesh) therefore becomes:

$$
\Delta\theta_i^* = \frac{\alpha_i \Delta T_i}{\sum_j \alpha_j} \qquad (\mathbf{3}.147)
$$

such that

$$
\theta' = \theta^* + \sum_i \Delta\theta_i^* \qquad (\mathbf{3}.148)
$$

The question arises that, if θ^* may be calculated directly using the extrapolated temperature, what is the reason for first extrapolating θ^* and then correcting the value. The reason is that θ^* is a function of both the surrounding temperatures T_i and the heat transfer coefficients α_i. A more accurate approximation is obtained using this method because it takes into account the change in heat transfer coefficients. This method is equivalent to extrapolating the individual heat transfer coefficients α_i in addition to the surrounding temperatures T_i and then, from these, calculating the extrapolated θ^*.

3.2.6.2 Coated particle overheating model

The fuel layer temperature calculation, described in the TINTE Thermal-hydraulics Theory Report **[6]**, does not account for the heterogeneity of the fuel spheres, specifically the many fuel-containing coated particles embedded within the fuel graphite matrix. Because of the very small size of the coated particles, the temperature difference between the fuel and the surrounding graphite is generally small, in the order of 3 to 6 °C. Therefore the additional complications that would arise by developing a very accurate model for the fuel, taking into account the double-heterogeneity of the core, would not provide a significant advantage over a simplified model.

A simplified lumped mass heat transfer model for the coated particles was chosen, as shown in Figure 15. Each coated particle is assumed to be a spatially independent point heat source with heat storage and conductive heat transfer to the surrounding matrix. This assumption introduces minimal error for a number of reasons:

- The coated particles have a very small diameter.
- The conductivity of the uranium dioxide fuel kernel is high relative to that of the very thin coating layers. The result of this is that the temperature profile through a typical coated particle is ‘top-hat’ shaped, i.e. approximately discontinuous at the coatings with very little temperature difference across the uranium dioxide kernel itself.
- The low density of the coating layers results in a low heat capacity and therefore the coatings have little influence on the time-dependent temperature response of fuel kernel.
- The thermal behaviour of the uranium dioxide kernels and coatings under extreme temperatures and neutron fluxes is not fully understood. For this reason, the accuracy of the material properties used in a more complex model would be questionable. Time-dependent experimental results would be needed to ‘tweak’ the parameters of any model, regardless of its complexity. This ‘tweaking’ of parameters is more easily carried out for a simple model.

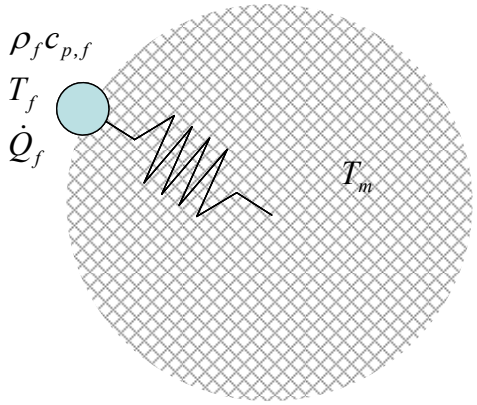

Figure 15: Lumped Particle Model for Particle Overheating

The coated particle (fuel) is at temperature T_f and the surrounding matrix (moderator) at temperature T_m. The nuclear power generation within the coated particle is $\dot{Q}_f'''$ and the particle has volumetric heat capacity $\rho_f c_{p,f}$. The following differential equation may be used to describe the system:

$$\rho_f c_{p,f} \dot{T}_f = \dot{Q}_f''' - \frac{1}{\alpha_f}\left(T_f - T_m\right) \quad (\mathbf{3}.149)$$

Here, α_f is an effective heat flux resistance for the coated particle (represented by the resistor element in Figure 15). This value is assumed constant for a given reactor. Note that the coated particle power density differs from the homogenized power density calculated in paragraph 3.2.5. We therefore introduce the ratio of coated particle power density to homogenized local power density $\dot{Q}_f''' / \dot{Q}_l'''$. Also note that the local power production is considered because we are concerned with the local heating within the fuel itself.

Rearranging Equation (**3**.149) yields the following:

$$\dot{T}_f = \frac{1}{\rho_f c_{p,f}} \frac{\dot{Q}_f'''}{\dot{Q}_l'''} \dot{Q}_l''' - \frac{1}{\alpha_f \rho_f c_{p,f}}\left(T_f - T_m\right)$$

We define a modified heat flux resistance:

$$\alpha'_f \equiv \frac{\dot{Q}_f'''}{\dot{Q}_l'''} \alpha_f \quad (\mathbf{3}.150)$$

and a time-dependence factor:

$$\lambda_f \equiv \frac{1}{\alpha_f \rho_f c_{p,f}} \quad (\mathbf{3}.151)$$

These may be substituted into the equation to yield the following:

$$\dot{T}_f = \alpha_f \lambda_f \frac{\dot{Q}_f'''}{\dot{Q}_l'''} \dot{Q}_l''' - \lambda_f \left(T_f - T_m\right)$$

$$\dot{T}_f = \alpha'_f \lambda_f \dot{Q}_l''' - \lambda_f \left(T_f - T_m\right)$$

$$\dot{T}_f + \lambda_f T_f = \lambda_f \left(\alpha'_f \dot{Q}_l''' + T_m\right) \quad (\mathbf{3}.152)$$

Here λ_f may be written in terms of the modified heat flux resistance α'_f.

$$\lambda_f = \frac{\dot{Q}_f'''}{\dot{Q}_l'''} \frac{1}{\alpha'_f \rho_f c_{p,f}} \quad (\mathbf{3}.153)$$

3.2.6.2.1 Steady-state case

For the steady-state case, the time-derivative term in Equation (**3**.152) is zero and the equation reduces to:

$$T_f = \alpha'_f \dot{Q}_l''' + T_m \quad (\mathbf{3}.154)$$

3.2.6.2.2 Time-dependent case

The heat generation is assumed linearly dependent on time, i.e. $\dot{Q}_l'''(t) = \dot{Q}_{l0}''' + \frac{t-t_0}{\Delta}\left(\dot{Q}_{l1}''' - \dot{Q}_{l0}'''\right)$. Similarly, the moderator temperature is assumed to vary linearly with time, i.e. $T_m(t) = T_{m0} + \frac{t-t_0}{\Delta}\left(T_{m1} - T_{m0}\right)$. The time-dependence of the term $\alpha'_f \dot{Q}_l''' + T_m$ may therefore be written as shown.

$$\left(\alpha'_f \dot{Q}_l''' + T_m\right)(t) = \left(\alpha'_f \dot{Q}_{l0}''' + T_{m0}\right) + \frac{t-t_0}{\Delta}\left[\left(\alpha'_f \dot{Q}_{l1}''' + T_{m1}\right) - \left(\alpha'_f \dot{Q}_{l0}''' + T_{m0}\right)\right]$$

We define the source terms:

$$A(t) \equiv \alpha'_f \dot{Q}_l'''(t) + T_m(t) \quad (\mathbf{3}.155)$$

$$A_1 \equiv \alpha'_f \dot{Q}_{l1}''' + T_{m1} \quad (\mathbf{3}.156)$$

$$A_0 = \alpha'_f \dot{Q}_{l0}''' + T_{m0} \quad (\mathbf{3}.157)$$

Equation (**3**.152) may be rewritten as:

$$\dot{T}_f = \lambda_f A(t) - \lambda_f T_f \quad (\mathbf{3}.158)$$

The above equation has the same general form as Equation (**3**.113), for which the solution is known.

$$T_f(t) = T_f(t_0)e^{-\lambda_f(t-t_0)} + A_0\left(1 - \frac{t-t_0}{\Delta} - e^{-\lambda_f(t-t_0)} + \frac{1-e^{-\lambda_f(t-t_0)}}{\lambda_f \Delta}\right) + A_1\left(\frac{t-t_0}{\Delta} - \frac{1-e^{-\lambda_f(t-t_0)}}{\lambda_f \Delta}\right)$$

The coated particle overheating at the end of time interval Δ may therefore be written as:

$$T_f(t_0+\Delta) = T_{f0}e^{-\lambda_f \Delta} - A_0\left(e^{-\lambda_f \Delta} - \frac{1-e^{-\lambda_f \Delta}}{\lambda_f \Delta}\right) + A_1\left(1 - \frac{1-e^{-\lambda_f \Delta}}{\lambda_f \Delta}\right)$$

$$T_{f1} = A_1 + \left(T_{f0} - A_0\right)e^{-\lambda_f \Delta} + \left(A_0 - A_1\right)\frac{1-e^{-\lambda_f \Delta}}{\lambda_f \Delta} \quad (\mathbf{3}.159)$$

3.2.6.2.3 Coated particle parameters

The ratio $\dot{Q}_f''' / \dot{Q}_l'''$ in Equations (**3**.150) and (**3**.153) is equal to the inverse of the coated particle packing fraction, $1-\varepsilon_f$. This may be calculated using the fuel element geometry and design as follows.

We define the number of coated particle per fuel sphere, n_f. This, multiplied by volume per coated particle V_f, gives the volume of coated particles per fuel sphere, $n_f V_f$. The coated particle packing fraction is given by:

$$\frac{\dot{Q}_l'''}{\dot{Q}_f'''} = 1-\varepsilon_f = n_f \frac{V_f}{V_{be}}\left(1-\varepsilon_{be}\right) \tag{3.160}$$

where V_{be} is the volume per fuel sphere (ball element) and ε_{be} is the pebble bed void fraction. The volume per fuel sphere is calculated using the formula:

$$V_{be} = \frac{4}{3}\pi R_{be}{}^3 \tag{3.161}$$

where R_{be} is the fuel sphere radius.

A heavy metal loading per fuel sphere SM may be used to calculate the uranium dioxide loading per fuel sphere as $SM\frac{M_{UO_2}}{M_U}$, where M_{UO_2} and M_U are the molar masses of uranium dioxide fuel and low enriched uranium metal respectively. The coated particle density ρ_f may be expressed in terms of the fuel sphere heavy metal loading.

$$\rho_f = \frac{SM}{n_f V_f}\frac{M_{UO_2}}{M_U} \tag{3.162}$$

Using Equations (**3**.160) and (**3**.162), Equation (**3**.153) may now be rewritten as:

$$\begin{aligned}\lambda_f &= \frac{1}{1-\varepsilon_f}\frac{1}{\alpha'_f \rho_f c_{p,f}} \\ &= \frac{1}{n_f \frac{V_f}{V_{be}}\left(1-\varepsilon_{be}\right)}\frac{1}{\alpha'_f\left(\frac{SM}{n_f V_f}\frac{M_{UO_2}}{M_U}\right)c_{p,f}}\end{aligned}$$

$$\therefore \lambda_f = \frac{V_{be}}{SM\left(1-\varepsilon_{be}\right)}\frac{M_U}{M_{UO_2}}\frac{1}{\alpha'_f c_{p,f}} \tag{3.163}$$

Note that the above equation of λ_f is independent of the coated particle geometry and layout. Instead, the heavy metal loading, fuel sphere volume and pebble bed void fraction are used as these may be more accurately measured. The fuel data used in TINTE for calculating λ_f is summarized in Table 9.

Table 9: Fuel Data Assumed for the Coated Particle Overheating Model

Parameter	Value	Source	Comment
R_{be}	3 cm	**[25]**	PBMR Type A fuel
M_U	238 g/mol		Low-enriched Uranium (LEU) fuel
M_{UO_2}	270 g/mol		
$c_{P,f}$	0.3 kJ/kg/K	[24]	For UO_2 fuel. Calculated using temperature dependent equation at 500 °C.
SM	-		User supplied parameter
ε_{be}	-		User supplied parameter

Parameter	Value	Source	Comment
R_{be}	3 cm	**[25]**	PBMR Type A fuel
M_U	238 g/mol		Low-enriched Uranium (LEU) fuel
M_{UO_2}	270 g/mol		
$c_{P,f}$	0.3 kJ/kg/K	[24]	For UO_2 fuel. Calculated using temperature dependent equation at 500 °C.
α'_f	-		User-supplied parameter

An average coated particle temperature of approximately 500 °C is assumed for the value of $c_{P,f}$. For reactors operating with higher average fuel temperatures, such as the Pebble Bed Modular Reactor (PBMR) (900 °C, refer to **[20]**), a more accurate value would be 317 J/kg/K according to [24]. The value assumed neglects influences such as fuel burn-up and operational temperature.

The effective specific resistance α'_f of the coated particle may be calculated directly from Equation (**3**.154) if steady-state operational data for a reactor is available.

$$\alpha'_f = \frac{T_f - T_m}{\dot{Q}'''} \qquad (\mathbf{3}.164)$$

It is, however, a difficult task to measure the temperature difference in a reactor accurately and for this reason the value is more easily determined using the response of a reactor to transients such as control rod withdrawals. Typical values for α'_f are in the region of 0.5 K.cm^3/W to 0.9 K.cm^3/W. Recent work suggests that a value closer to 2.6 K.cm^3/W should be used for the PBMR reactor ([26] and [27]).

3.2.6.3 Determining representative fuel and moderator temperatures

The extrapolation methods discussed in paragraph 3.2.6.1 estimated temperature values. For out-of-core locations (reflectors, etc.), the homogenized solid material temperatures are estimated. Each out-of-core location therefore has a single representative moderator temperature value which may be used for the calculation of cross sections (refer to paragraph 3.2.2).

For locations within the core, the extrapolation methods discussed in paragraph 3.2.6.1 yield temperatures for all layers of all fuel types. In order to determine representative moderator temperatures for a given core location, volume-weighted averaging is applied over all fuel types and all layers within the fuel sphere.

$$T_m^* = \sum_n \left[\gamma_n \frac{\sum_i V_i T_{i,n}}{\sum_i V_i} \right] \qquad (\mathbf{3}.165)$$

The subscripts n and i denote the individual fuel types and fuel layers respectively. γ_n is the volume fraction of type n fuel elements in the relevant core region.

Fuel temperatures are calculated using the coated particle overheating model discussed in paragraph 3.2.6.2. For the calculation of the representative fuel temperature, the volume-weighted average fuel temperature is calculated in a similar manner to Equation (**3**.165).

The variables of Equations (**3**.154) and (**3**.159) for the calculation of fuel temperatures using the overheating model are considered.

- The heat production values $\dot{Q}'''_{f1}$ and $\dot{Q}'''_{f0}$ are dependent on the fuel type but are independent of the fuel layers, i.e. spatial self-shielding within the fuel zone is neglected.
- The temperatures T_{f0}, T_{m0} and T_{m1} are dependent on both the fuel type and layer.

For simplicity's sake, we denote the volume-weighted average, over the fuel-containing layers, of a variable x as $\Omega_f(x)$.

$$\Omega_f(x) = \frac{\sum_i V_i x_i}{\sum_i V_i} \text{ for } i \text{ in the fuel-containing layers} \qquad (\mathbf{3}.166)$$

Applying Equation (**3**.166) with substitution of Equations (**3**.156), (**3**.157) and (**3**.159) yields the following:

$$\Omega_f(T_{f1}) = \Omega\left(\begin{array}{l} T_{m1} + (T_{f0} - T_{m0})e^{-\lambda_f \Delta} + (T_{m0} - T_{m1})\dfrac{1-e^{-\lambda_f\Delta}}{\lambda_f\Delta} \\ \quad + \alpha'_f \dot{Q}'''_{f1} - \alpha'_f \dot{Q}'''_{f0} e^{-\lambda_f\Delta} + \alpha'_f (\dot{Q}'''_{f0} - \dot{Q}'''_{f1})\dfrac{1-e^{-\lambda_f\Delta}}{\lambda_f\Delta} \end{array}\right)$$

By manipulation of the above equation and application of the properties of sums, the volume-weighted average of the updated fuel temperature $\Omega_f(T_{f1})$, for a fuel type and location, may be written in terms of the volume-weighted sums of the initial fuel temperature and moderator temperatures.

$$\begin{aligned} \Omega_f(T_{f1}) = {} & \Omega_f(T_{f0})e^{-\lambda_f\Delta} + \Omega_f(T_{m1})\left(1 - \frac{1-e^{-\lambda_f\Delta}}{\lambda_f\Delta}\right) - \Omega_f(T_{m0})\left(e^{-\lambda_f\Delta} - \frac{1-e^{-\lambda_f\Delta}}{\lambda_f\Delta}\right) \\ & + \alpha'_f \dot{Q}'''_{f1} - \alpha'_f \dot{Q}'''_{f0} e^{-\lambda_f\Delta} + \alpha'_f (\dot{Q}'''_{f0} - \dot{Q}'''_{f1})\frac{1-e^{-\lambda_f\Delta}}{\lambda_f\Delta} \end{aligned} \qquad (\mathbf{3}.167)$$

This simple manipulation shows that for constant α'_f and λ_f, and assuming uniform heat sources (neglecting fuel spatial self shielding), the representative fuel temperature, at the end of a time interval Δ, for each fuel type in each location, may be calculated directly using the representative initial fuel ($\Omega_f(T_{f0})$) and moderator temperatures ($\Omega_f(T_{m0})$ and $\Omega_f(T_{m1})$). It is therefore not necessary to calculate the particle overheating for each layer individually. Note, however, that the representative moderator temperatures $\Omega_f(T_{m0})$ and $\Omega_f(T_{m1})$ in this case are for the fuel-containing layers only.

The TINTE nuclear calculation assumes a homogenous core, therefore the cross-section polynomials do not distinguish between fuel types. It is necessary to combine the representative fuel temperatures for each fuel type into a single representative fuel

temperature for each location. This is done using the volume fractions γ_n for each fuel type as in Equation (**3**.165).

$$T_f^* = \sum_n \left[\gamma_n \, \Omega_f \left(T_{f,n}\right)\right] \qquad (\mathbf{3}.168)$$

3.2.6.4 Determining representative molecular concentrations

The gas-mixing model in TINTE calculates the molecular concentrations of nitrogen (in the form of N_2), hydrogen (in the form of H_2O) and carbon (in the form of CO and CO_2). The presence of these molecules in the gas flow is potentially important for calculations including water ingress and graphite corrosion because of their influence on moderation. For this reason their concentrations are included as terms in the calculation of neutronic cross sections.

The calculation of gas mixing is discussed in detail in the TINTE Thermal-hydraulics Theory Report [6]. From the perspective of the nuclear calculation, it is necessary to calculate the homogenized molar densities of nitrogen, hydrogen and carbon in the material blocks. The gas-mixing calculation supplies the molar densities of gaseous N_2, CO, CO_2, H_2 and H_2O, as well as liquid H_2O (surface wetting).

The concentration of a particular species (a) in gas may be calculated from the gas concentration C_g (mol/m^3) and the species mol fraction x_a (mol$_a$/mol$_{gas}$).

$$C_a = x_a C_g$$

If a material block contains a fraction ε of solid material, a gas fraction of $1-\varepsilon$ is present and the homogenized concentration of species a becomes:

$$C_a = (1-\varepsilon) x_a C_g$$

For nitrogen gas, this becomes:

$$C_{N_2} = (1-\varepsilon) x_{N_2} C_g \qquad (\mathbf{3}.169)$$

For total carbon, this becomes:

$$C_{CO} + C_{CO_2} = (1-\varepsilon)\left(x_{CO} + x_{CO_2}\right) C_g$$

If we consider that a concentration C_B of graphite has been removed due to corrosion or other effects, the resulting loss in the concentration of carbon atoms ΔC_C is:

$$\begin{aligned} \Delta C_C &= C_B - \left(C_{CO} + C_{CO_2}\right) \\ &= C_B - (1-\varepsilon)\left(x_{CO} + x_{CO_2}\right) C_g \end{aligned}$$

This loss is expressed as a fraction of the initial graphite concentration in the material block C_s.

$$\frac{\Delta C_C}{C_s} = \frac{1}{C_s}\left(C_B - (1-\varepsilon)\left(x_{CO} + x_{CO_2}\right) C_g\right) \qquad (\mathbf{3}.170)$$

For gaseous H_2 and H_2O, as well as liquid water (vapour):

$$C_{H_2} + C_{H_2O,g} + C_{H_20,v} = (1-\varepsilon)\left(x_{H_2} + x_{H_2O,g} + x_{H_20,v}\right) C_g$$

To take into account surface wetting, we now introduce a surface wetting concentration $C_{H_2O,l}$, which is the number of moles of liquid water per mole of solid graphite in the material block. The total hydrogen-based molecule concentration in the material block becomes:

$$C_{H_2} = (1-\varepsilon)\left(x_{H_2} + x_{H_2O,g} + x_{H_20,v}\right)C_g + \varepsilon C_{H_2O,l} \qquad (\mathbf{3}.171)$$

The cross-section polynomials are derived directly in terms of the variables C_{N_2}, $\Delta C_C / C_s$ and C_{H_2}. The values calculated using Equations (**3**.169) through (**3**.171) may therefore be used directly to calculate the neutronic cross sections.

4. BASIC MODELLING EQUATIONS

Because of the large number of equations used and specific methods used for the coupled solution of these equations, a single list of modelling equations will serve little purpose for the reader of this document. For this reason, this chapter gives calculation algorithms that are used for the complete nuclear calculation. Each step in the solution process is referenced to a single equation within paragraph 3.2. Where a single equation is not used, but rather a solution method consisting of several coupled equations, a reference is provided to the relevant subsection within paragraph 3.2.

4.1 CALCULATIONAL STRUCTURE

The partial problems of a reactor calculation are solved separately in TINTE, i.e. the partial solutions are explicitly coupled. The disadvantage of this is that the solution of the full system of equations may only be solved by iteration. On the other hand, this method of solution allows the partial problems to be separated, thus simplifying the calculation structure.

The partial solutions include the following:

a. The nuclear calculation – A neutronic calculation is performed to determine the time-dependent flux distribution and the power distribution is calculated from this.
b. The temperature calculation – Heat transfer calculations are performed to determine time-dependent temperature distribution of the calculation domain. This includes gas flow, convection, solid conduction and radiation heat transfer calculations.
c. Chemistry calculation – Chemical reaction rates (graphite oxidation) are calculated, to determine changes in geometry and chemical composition.

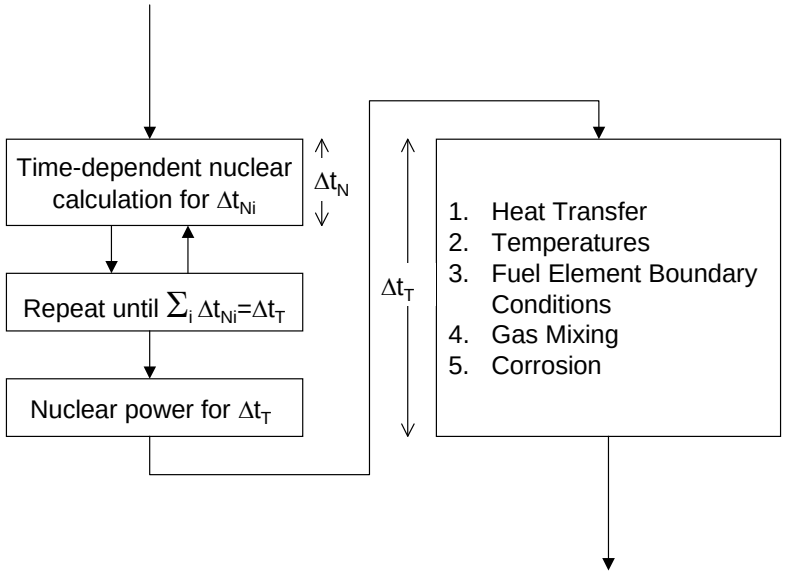

Figure 16: The Modular Structure of TINTE; the Principle of Time Discretization [3]

We term the iteration over the partial problems the outer iteration. Because of the relatively short periods associated with neutronic calculations, several nuclear time intervals are used within each temperature/chemistry calculation. This concept is shown in Figure 16. Separate temperature and nuclear time intervals are therefore defined. The choice of the time intervals is determined by the control module and will not be described in this document. In the context of this document, the generic time interval Δ refers to the nuclear time interval.

4.1.1 The Nuclear Calculation

Initially, fuel and moderator temperatures are required for the cross-section calculation. Because multiple nuclear time intervals are used per temperature interval, these values are available for the first nuclear interval. For the subsequent nuclear intervals within the temperature interval, the fuel and moderator temperatures are calculated by temporal extrapolation of previous temperatures. This extrapolation is considered part of the temperature calculation (although separate in a sense) and will not be discussed in any great detail within this document.

As stated above, the moderator and fuel temperatures are used to calculate nuclear cross sections. Then follows what is termed the neutron flux inner iteration. During this, the xenon (and other strong absorbers) concentrations are first adjusted according to the guessed neutron flux distribution for the time interval. These concentrations are used to update the neutron absorption of the material blocks. A flux calculation is then performed to update the flux distribution. The neutron flux inner iteration is repeated until convergence of the flux distribution is obtained.

The spatial fission power distribution for the time-interval is then calculated. In transient cases, the power distribution is fed back into the fuel and moderator temperature calculation. Therefore, an intermediate power iteration is repeated until convergence is obtained.

This represents the converged solution for a single nuclear time interval. This is repeated for all nuclear intervals within the current temperature time interval. The effective nuclear power in each material mesh block, for the temperature interval, is then calculated as the average power for all the nuclear subintervals.

This calculation structure is depicted in Figure 17.

4.1.2 Calculation Algorithms

The individual nuclear calculation algorithm for the steady-state case is depicted in Figure 18. This represents the nuclear calculation for a single pseudo-time-interval (the concept is described in paragraph 3.2.3.5). Figure 19 depicts the algorithm for the time-dependent case. This represents the solution algorithm for a single nuclear time-interval. Note that the inner flux iteration (refer to Figure 20) is shared between both cases. The detail of each of the blocks in the Figure 18 through Figure 20 is explored in the subsequent chapters of this document.

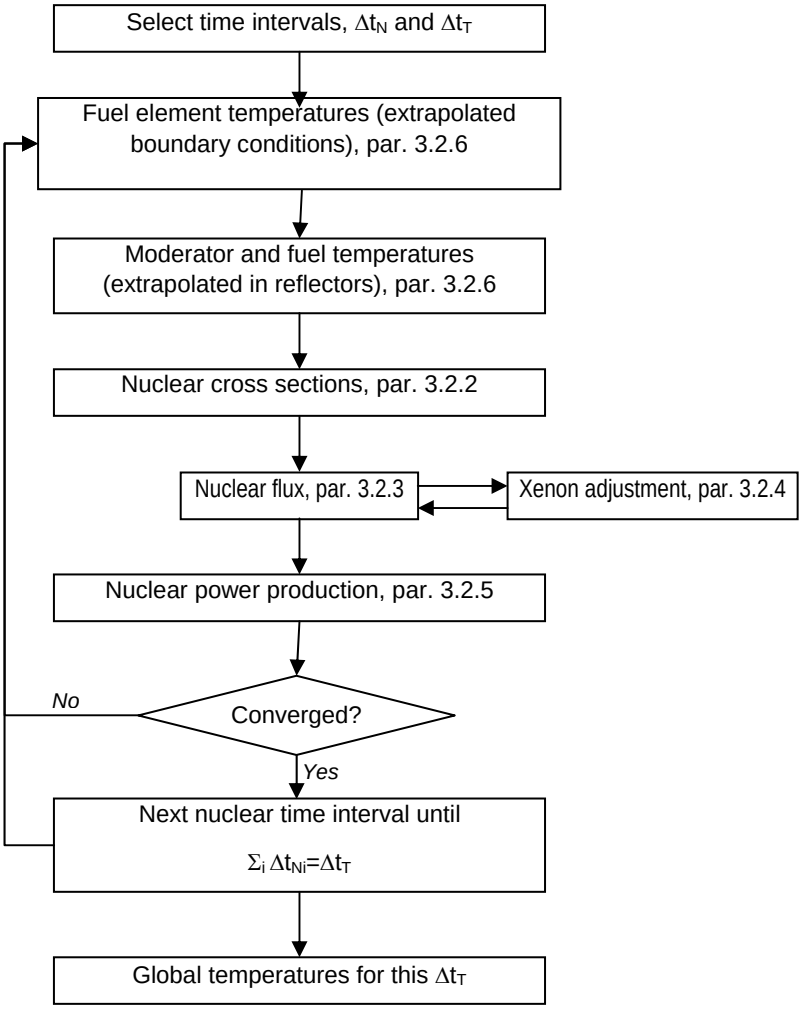

Figure 17: The TINTE Nuclear Calculation [3]

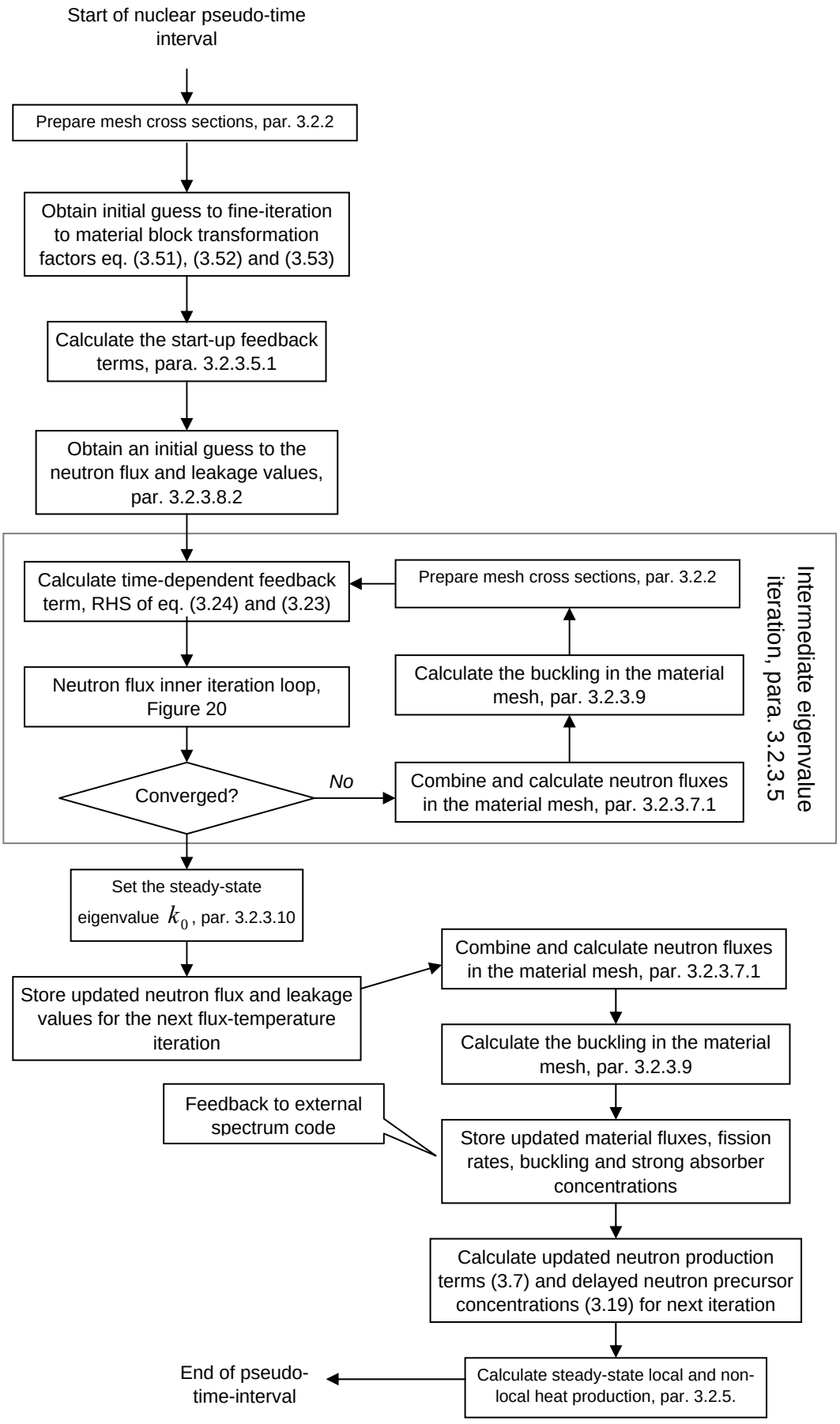

Figure 18: Flow Diagram for the Steady-State Nuclear Calculation

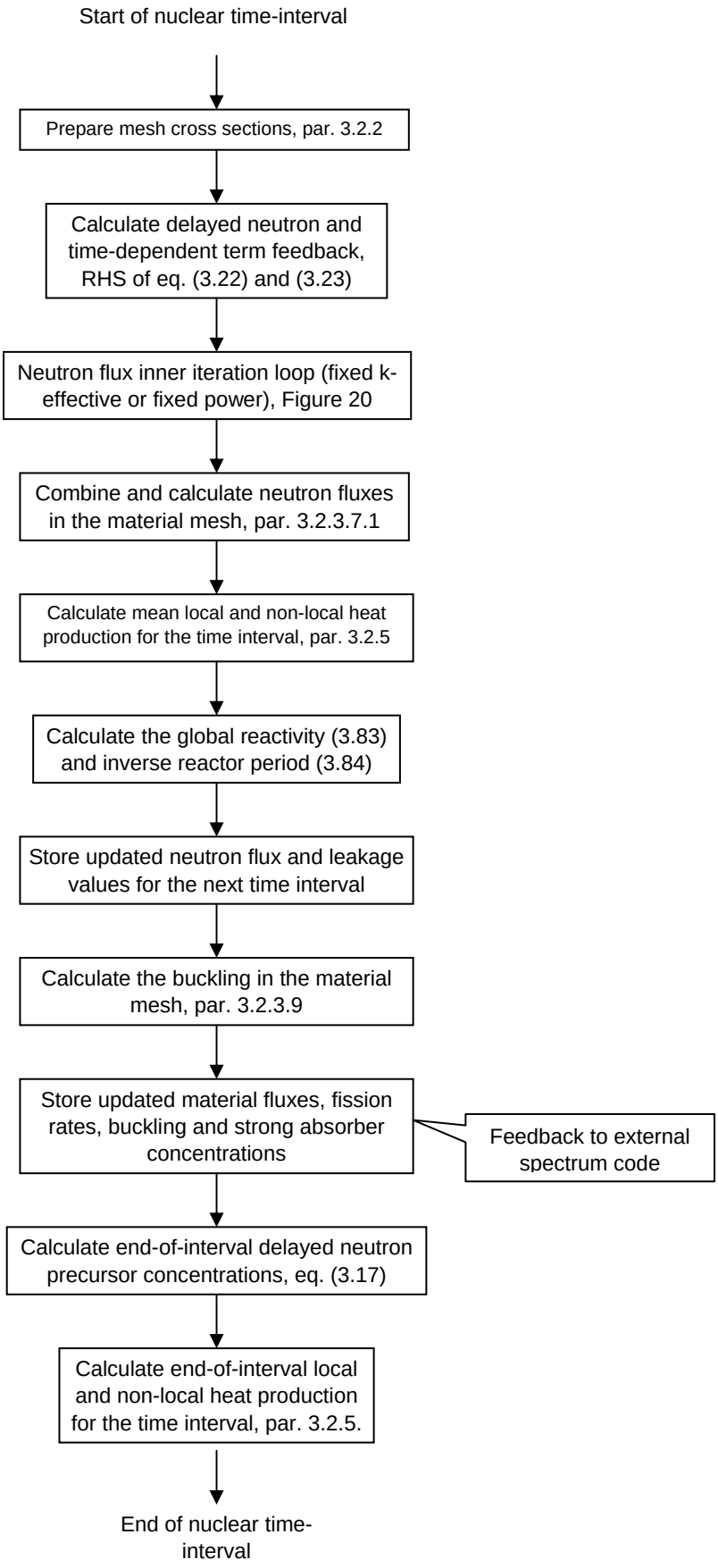

Figure 19: Flow Diagram for the Time-dependent Nuclear Calculation

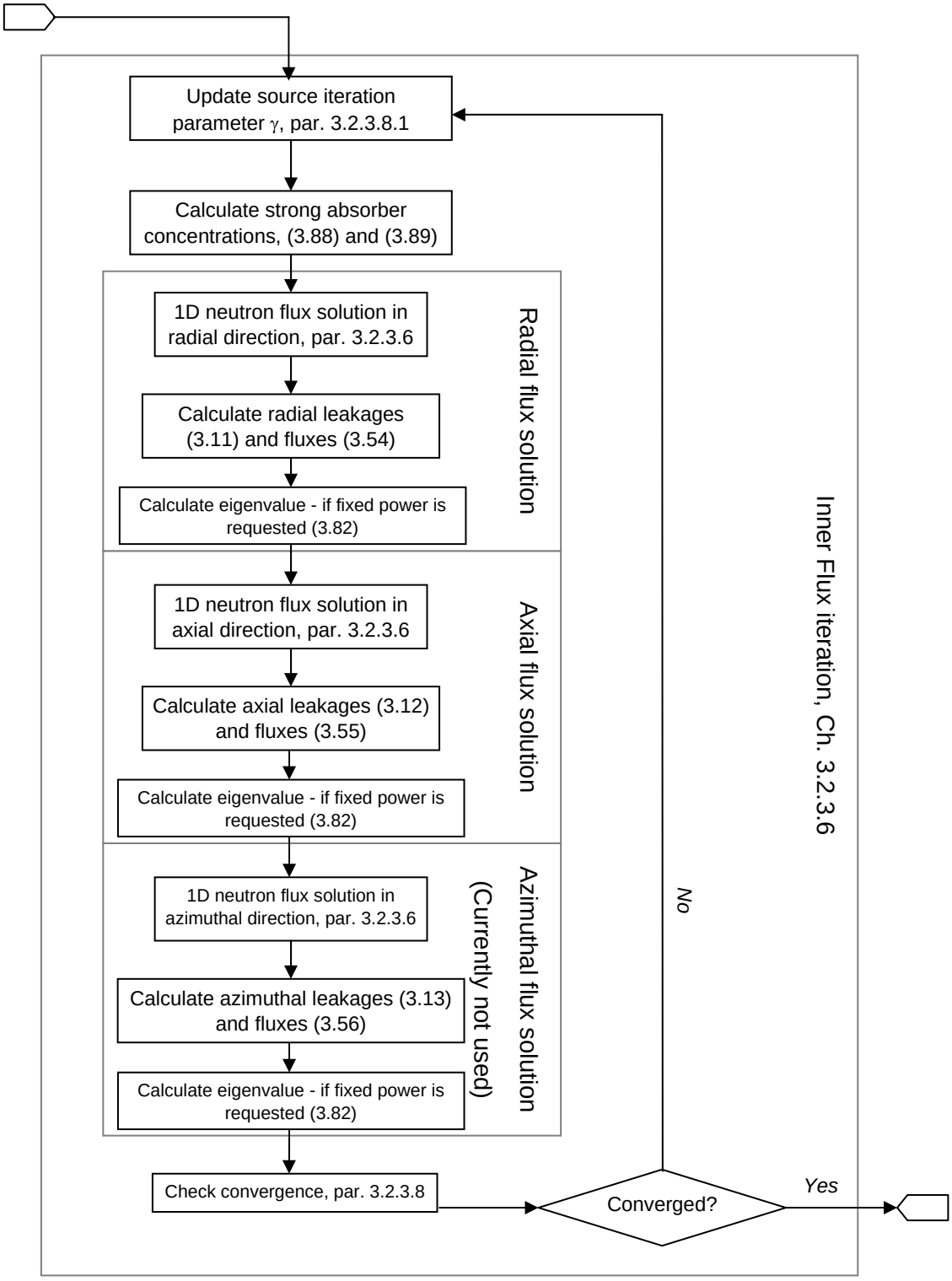

Figure 20: Flow Diagram for the Neutron Flux Inner Iteration

4.2 OUTSTANDING ISSUES

The impacts of the following assumptions have yet to be validated.

- The delayed neutron production – The delayed neutron yields and group data were originally taken from ENDF/B IV [12], BNL-325 [18], as well as a number of other sources. In the absence of some of the original documentation, the values used in TINTE are compared with the more recent ENDF/B VI [14]. This comparison is detailed in Appendix B. The effects of differences in the source data have been shown, using a simplified steady-state approximation, to be below 1%. The full impact on strong transient calculations (power excursions, etc.), however, has yet to be quantified. Possibly of greater importance is that no attempt has been made to account for the differences in the yield spectra of prompt and delayed neutrons for the two-group diffusion calculation, i.e. no attempt has been made to calculate effective β values from the physical values.
- The saturation fission products (neutron poisons) – Decay constants and fission yields for the saturation fission products were originally taken from ENDF/B IV [12]. In the absence of the original data, the values used in TINTE are compared with the more recent ENDF/B VI [14]. This comparison is detailed in Appendix D. A number of significant differences have been noted, however, the effects of these differences have not been fully quantified. Differences were noted between Equation (**3**.89) and Equation (3.52) of [3]. Equation (**3**.89) is, however, consistent with the original German version of [3] and the TINTE source code.
- The decay heat calculation - Assumptions made to DIN 25 485 [21] are discussed in Appendix A. In this paragraph, it is shown that the assumptions made are conservative, however, the amount of conservatism has yet to be quantified. Also, the DIN standard does not specify decay heat data for the isotopes ^{232}Th, ^{233}U, ^{234}U, ^{236}U, ^{240}Pu and ^{242}Pu; these are assumed equal to the values for ^{235}U. The effect of this assumption has not been quantified.
- The locality of heat production – An effective gamma cross section is assumed in Equation (**3**.137). This assumption was based on previous data for a pebble-bed-type reactor. No derivation is available; therefore the assumption is currently not fully validated in accordance with the requirements of [1].
- The overheating model for the fuel coated particle temperatures, discussed in paragraph 3.2.6.2, has not been fully validated. In particular, the choice of an accurate value for the effective specific resistance requires experimental data. Current progress within the Data Methods and Code Development (DMACD) group on an updated coated particle overheating model [28] should resolve this issue.

5. APPENDICES

5.1 APPENDIX A: THE DECAY HEAT CONSTANTS AS APPLIED IN TINTE

This appendix summarizes Chapter 4.1 of [23]. This document describes the treatment of decay heat production in TINTE and the methods used to obtain the constants used from the DIN standard [21]. Chapter 4.1 of [23] discusses the adjustment of the DIN standard for use in a dynamic program such as TINTE.

It is appropriate and convenient to model the decay heat production of a reactor using methods similar to those used for the decay chains of the neutron poisons Xe-135, Sm-149, etc., discussed in paragraph 3.2.4 of the current document. The decay heat production is therefore described using ordinary differential equations, which can be solved numerically with minimal computational effort. This method of solution applies to the fission product contribution $\dot{Q}_S$ (refer to paragraph 3.2.5.2.2) and the contributions $\dot{Q}_U$, $\dot{Q}_{Np}$, $\dot{Q}_{Th}$ and $\dot{Q}_{Pa}$ of the actinides ^{239}U, ^{239}Np, ^{233}Th and ^{233}Pa respectively (refer to paragraph 3.2.5.2.3).

The neutron captures of caesium isotopes can similarly be described using ordinary differential equations. Supplement 1 of the DIN standard [21] discusses the decay heat contribution of ^{133}Cs and ^{134}Cs. For reactor operation periods of greater than 50 d and reactor shutdown periods of less than 100 d, both isotopes have negligible influence on the decay heat. 1 d after reactor shutdown, these isotopes contribute approximately 0.2% of the total decay heat. After 5 d, this value is approximately 0.5%, which again may be considered negligible.

The DIN standard is not written in the form of dynamic differential equations suitable for use both during and after reactor shutdown. The functions $A(t)$ and $H(t)$ are dependent on the time after reactor shutdown. Implementing such a method in a dynamic code would require additional intervals to be added to the operational histogram each time the power level and/or flux profile changes, even if only by small amounts. For certain transients this would result in a reactor history consisting of many thousands of time intervals for all locations in the core, which is not feasible. An adaptation of the standard is required that will allow the decay heat data, during the time-dependent calculation, to be calculated independently of the reactor's operational history, using only the decay heat values from the previous iteration.

The following procedure is used to achieve this: The function $A(t)$ rises continuously up to a shutdown time of 10^9 s (refer to Figure 21), which is greater than the operational life of the fuel elements. If the time zero of the function $A(t)$ is redefined as the time of fission, a conservative estimate of the decay heat is obtained. Unlike $A(t)$, the function $H(t)$ does not rise continuously, but includes a number of small oscillations. Applying the same technique to this function would therefore not necessarily be conservative, because the function decreases with time in some places. A further conservative assumption is therefore made. A function $H^+(t)$ is defined such that it envelopes $H(t)$, but does not decrease with time as shown in Figure 21. One can then conservatively redefine the time zero of $H^+(t)$ as the time of fission.

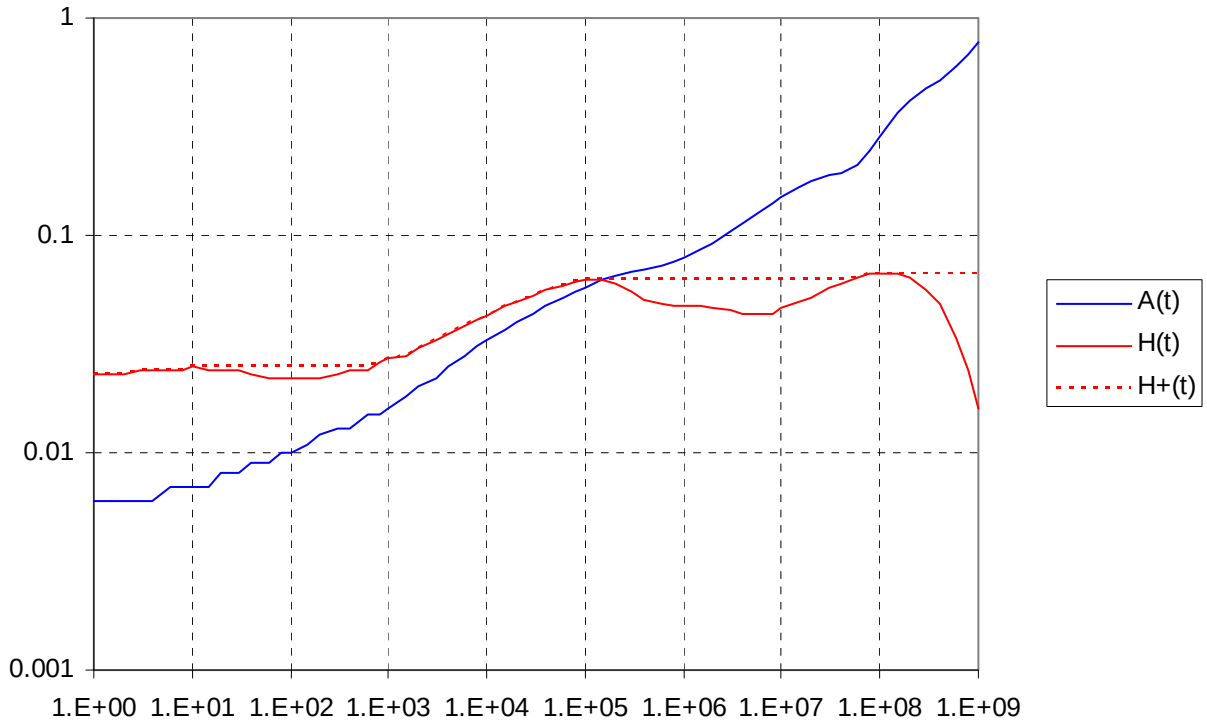

Figure 21: The Decay Heat Functions A(t) and H(t) from DIN 25 485

With reference to Equation (**3**.103), the contributions $\dot{Q}_S(t,T)+\dot{Q}_E(t,T)$ and $\dot{Q}_A(t,T)$ may now be rewritten, setting $A(t)=A(T+t)$ and $H(t)=H^+(T+t)$.

$$\begin{Bmatrix} \dot{Q}_S(t,T)+\dot{Q}_E(t,T) \\ \dot{Q}_A(t,T) \end{Bmatrix} = \begin{Bmatrix} 1+H^+(T+t) \\ K_A A(T+t) \end{Bmatrix} \dot{Q}_S(t,T) \qquad (\mathbf{5}.1)$$

Equation (2) of the DIN standard [21] is now introduced for a single operational time ($T_k = T$ and $t_k = \tau$).

$$\begin{Bmatrix} \dot{Q}_{S,i}(t,T)+\dot{Q}_{E,i}(t,T) \\ \dot{Q}_{A,i}(t,T) \end{Bmatrix} = \int_{-\tau}^{0} dT\ F_i(T) \sum_{l=1}^{24} \begin{Bmatrix} 1+H^+(-T+\tau) \\ K_A A(-T+\tau) \end{Bmatrix} \alpha_{il} e^{-\lambda_{l,i}(-T+\tau)} \qquad (\mathbf{5}.2)$$

The data for each isotope $\left(\frac{\alpha_i}{\lambda}\right)_l$ is specified in the DIN standard using differing decay constants. In order to reduce computational and coding effort as well as storage requirements, a new set of decay constants is chosen and new sets of decay group data for each isotope for use in TINTE are calculated. The decay groups are chosen such that all isotopes share a common set of decay constants. This allows a certain amount of precalculation to be carried out and, as such, reduces the computational effort required. The new decay heat constants Λ_l, β_{il} and γ_{il} are chosen such that the following relationship applies:

$$\int_{-\tau}^{0} dT\ S_i(T) \sum_{l=1}^{24} \begin{Bmatrix} 1+H^+(-T+t) \\ K_A A(-T+t) \end{Bmatrix} \alpha_{il} e^{-\lambda_{l,i}(-T+t)} = \int_{-\tau}^{0} dT\ S_i(T) \sum_{l} \begin{Bmatrix} \beta_{il} \\ \gamma_{il} \end{Bmatrix} \Lambda_l e^{-\Lambda_l(-T+t)} \qquad (\mathbf{5}.3)$$

The above relationship should be independent of the integral portion and as such may be simplified to the following:

$$\sum_{l=1}^{24}\begin{Bmatrix}1+H^{+}(t)\\ K_A A(t)\end{Bmatrix}\alpha_{il}e^{-\lambda_{l,i}(t)} = \sum_{l}\begin{Bmatrix}\beta_{il}\\ \gamma_{il}\end{Bmatrix}\Lambda_l e^{-\Lambda_l t} \qquad (\mathbf{5}.4)$$

This relationship must be accurate for both large and small values of t. Because the exponential functions will quickly fall to very small values, the percentage error rather than the absolute error is reduced to ensure the inherent trend of the decay is maintained. This is more easily achieved using the following form of (**5**.4).

$$\log\sum_{l=1}^{24}\begin{Bmatrix}1+H^{+}(t)\\ K_A A(t)\end{Bmatrix}\alpha_{il}e^{-\lambda_{l,i}(t)} = \log\sum_{l}\begin{Bmatrix}\beta_{il}\\ \gamma_{il}\end{Bmatrix}\Lambda_l e^{-\Lambda_l t} \qquad (\mathbf{5}.5)$$

In order to minimize the loss in accuracy, the number of decay groups is chosen equal to that specified in the DIN standard, 24. Nonlinear involution has been used to generate the necessary values. Details on this method will not be discussed, but rather comparisons with the DIN standard are shown to illustrate the accuracy of the newly developed decay heat data. The comparisons are shown in Figure 22 through Figure 25. Where small differences occur, e.g. in Figure 22 between 10^6 and 10^7 s, these are conservative.

The fitted data values are given in tabular form in Table 7 and Table 8, on pages 50 and 51 respectively. Note that the terms λ_l, $\left(\left(1+H^{+}(t)\right)\alpha_i/\lambda\right)_l$ and $\left(A(t)\alpha_i/\lambda\right)_l$, in the context of paragraph 3.2.5.2, refer to the derived constants Λ_l, β_{il} and γ_{il} respectively.

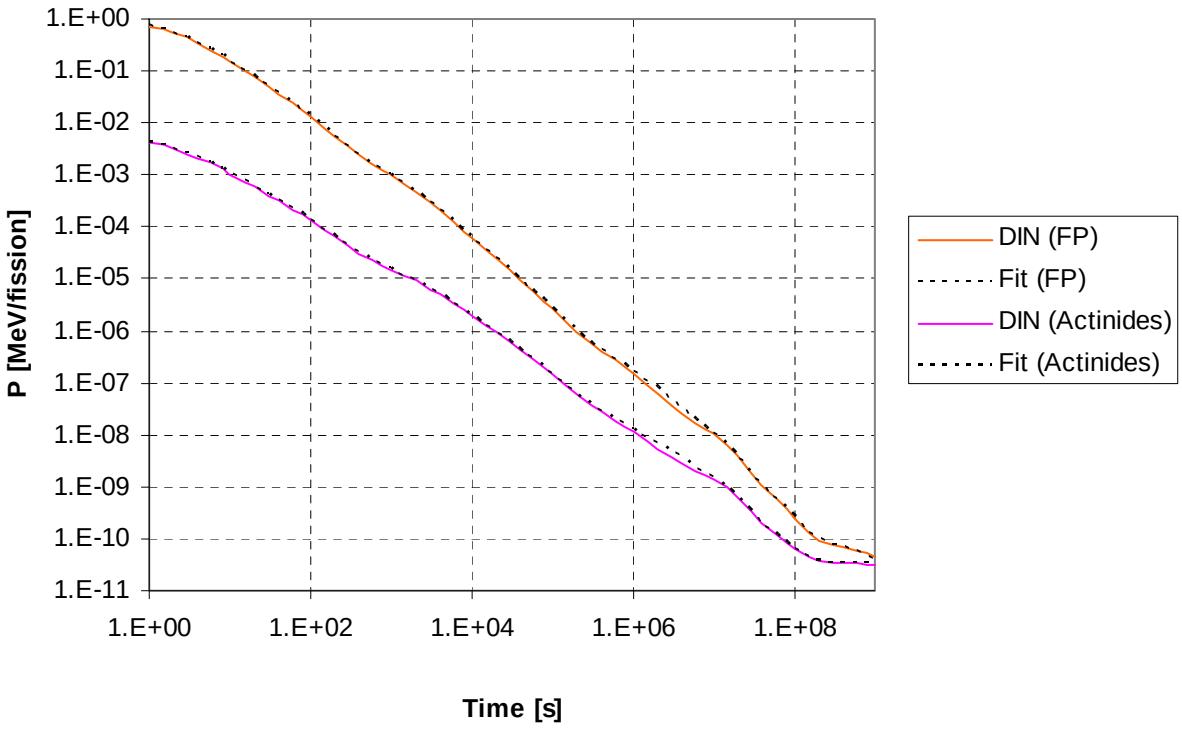

Figure 22: Comparison of the Decay Heat Release of ^{235}U for the DIN Decay Data and Fitted Values

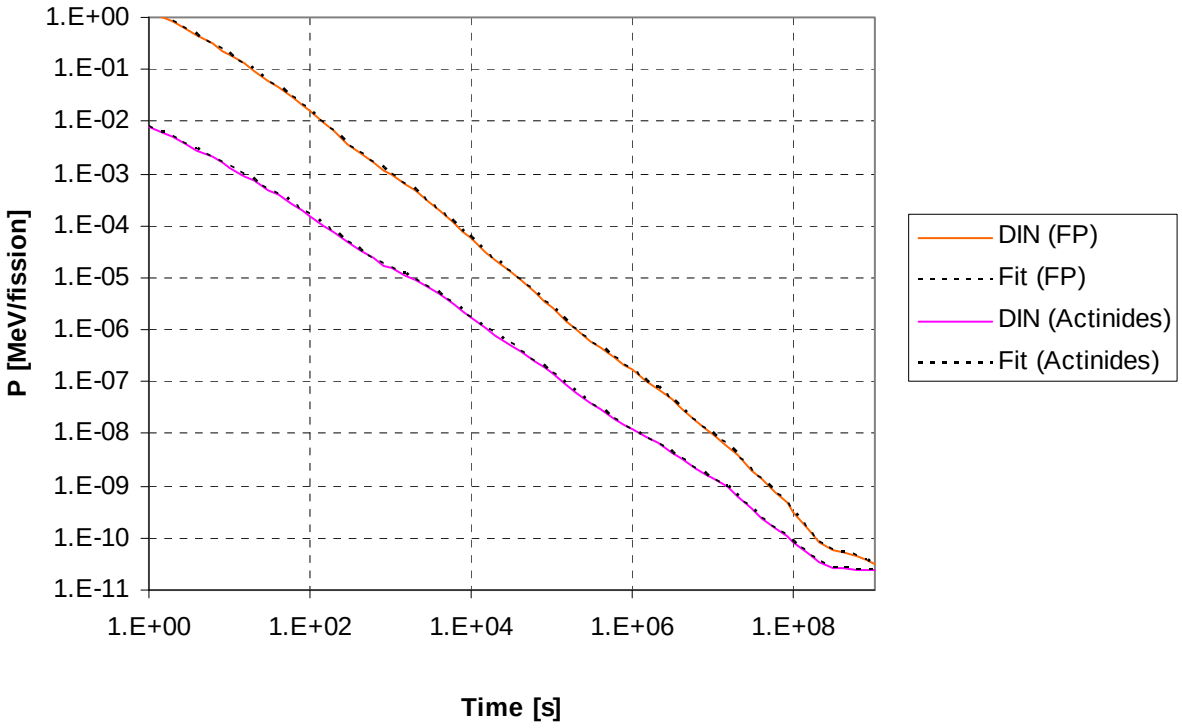

Figure 23: Comparison of the Decay Heat Release of ^{238}U for the DIN Decay Data and Fitted Values

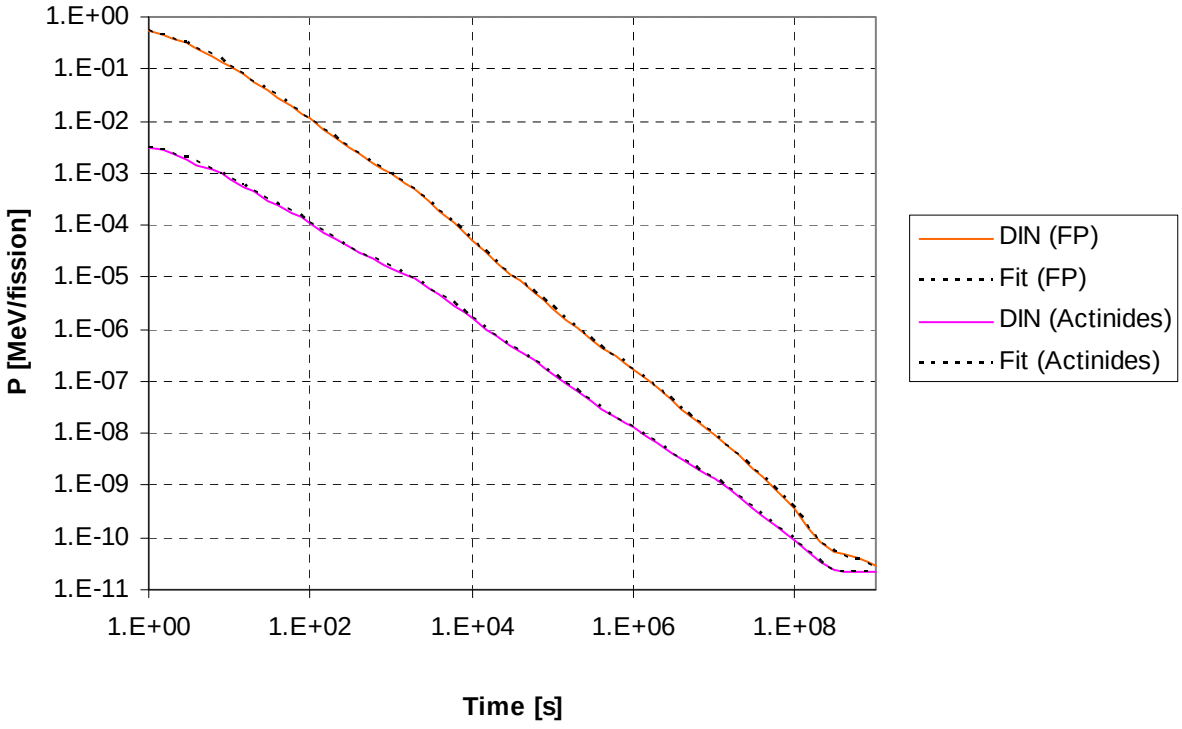

Figure 24: Comparison of the Decay Heat Release of ^{239}Pu for the DIN Decay Data and Fitted Values

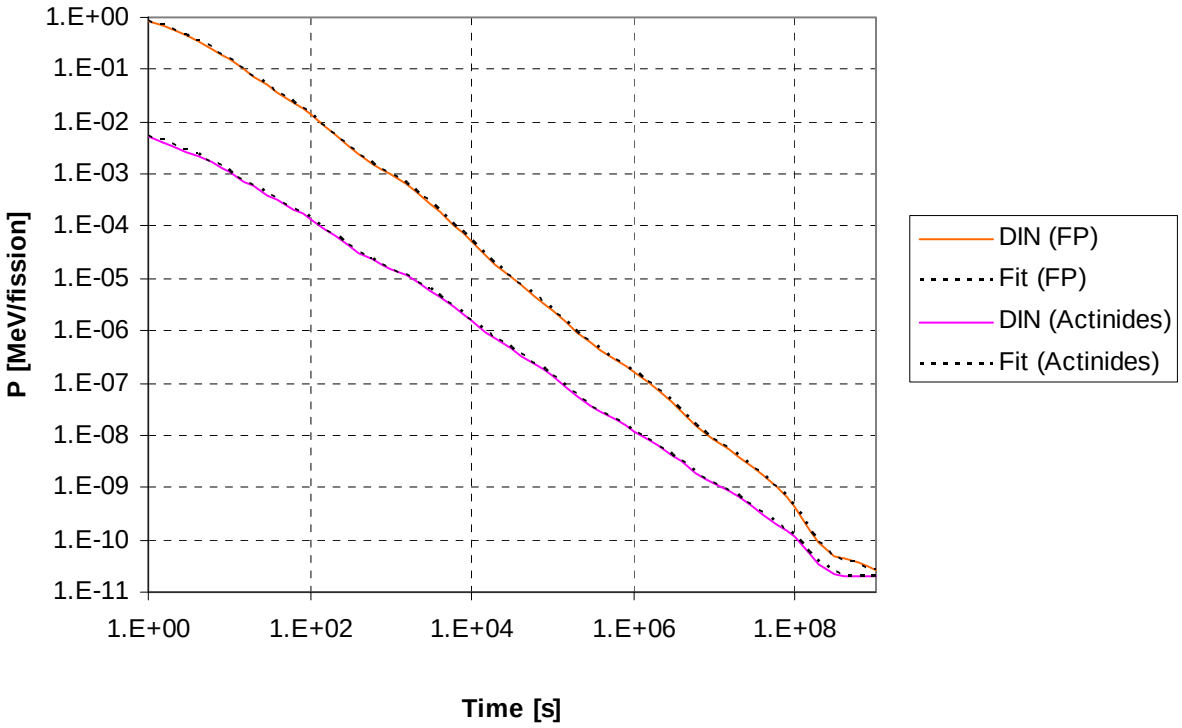

Figure 25: Comparison of the Decay Heat release of ^{241}Pu for the DIN Decay Data and Fitted Values

5.2 APPENDIX B: MODIFICATION OF THE ABSOLUTE DELAYED NEUTRON YIELDS FOR USE IN TINTE

The source for the original data for the absolute delayed neutron yields is specified in the TINTE source code as ENDF/B IV [12], for the isotopes ^{235}U, ^{232}Th, ^{233}U, ^{238}U, ^{239}Pu, ^{240}Pu and ^{241}Pu, and INDC(NDS)-107/G+Special [16] (Table III, p. 61) for the isotopes ^{234}U, ^{236}U and ^{242}Pu. In the absence of the original ENDF/B data, ANL/NDM-5 [15] was referred to. Both [15] and [16] contain delayed neutron yield ν_d values. BNL-325 [18] is referenced for the total neutron yield ν_t of each isotope, however, this original data source could not be obtained to verify the data used in TINTE.

In order to verify the data used, ENDF/B VI [12] data is compared with the values used in TINTE. This comparison is shown in Table 10.

Table 10: Comparison of TINTE and ENDF/B VI Total Delayed Neutron Yields

Isotope	ENDF/B VI			TINTE	Difference
	ν_d	ν_t	β [%]	β [%]	
^{235}U	1.67E-02	2.4367	0.6854	0.6904	0.0050
^{232}Th	**5.27E-02**	**1.9487**	**2.7044**	**2.3981**	**0.3063**
^{233}U	0.0074	2.4947	0.2966	0.2962	0.0004
^{234}U	0.0129	2.3520	0.5485	0.4342	0.1143
^{236}U	0.0232	2.3170	1.0013	1.1693	0.1680
^{238}U	0.0440	2.4921	1.7656	1.7510	0.0146
^{239}Pu	0.0065	2.8789	0.2240	0.2245	0.0005
^{240}Pu	0.0090	2.803	0.3211	0.2850	0.0361
^{241}Pu	0.0162	2.9453	0.5500	0.5354	0.0146
^{242}Pu	**0.0197**	**2.81**	**0.7011**	**1.0524**	**0.3513**

The isotopes ^{235}U, ^{233}U, ^{238}U, ^{239}Pu and ^{241}Pu compare well. Differences are seen in the values for the other isotopes, in particular the isotopes ^{232}Th and ^{242}Pu (shown in bold) show large differences. This may be attributed to a lack of experimental data at the time.

In a typical pebble-bed-type thermal reactor, operating on Low-enriched Uranium (LEU) fuel, more than 99% of the fission reactions take place in the isotopes ^{235}U, ^{239}Pu and ^{241}Pu[††]. The remaining fissionable isotopes contribute less than 1% in total to the fission rate. In particular, the isotopes ^{232}Th and ^{233}U are not formed or found in LEU fuels in even small amounts. The isotope ^{242}Pu is created very slowly as fuel is burned and the isotope has a very small fission cross section at thermal energies, therefore even with very high fuel burn-up values, the fraction of fissions in this isotope is negligible (0.004%)[††]. For these reasons, the differences in the total delayed neutron yields will have a negligible effect on the calculation, for the case of LEU fuel. Therefore, the data specified in Table 2 is acceptable for calculations involving LEU fuel.

[††] Data is obtained using VSOP [19] output data for the 400 MW PBMR reactor [20].

5.3 APPENDIX C: MODIFICATION OF THE DELAYED NEUTRON PRECURSOR GROUPS FOR USE IN TINTE

Group delayed neutron data is taken from ENDF/B IV [12] for the isotopes ^{235}U, ^{232}Th, ^{233}U, ^{238}U, ^{239}Pu, ^{240}Pu and ^{241}Pu. A further confirmation of this data is found in ANL/NDM-5 [15]. The group delayed neutron data for the isotope ^{242}Pu is taken from AERE-R 6993 [17]. This data is summarized in Table 11 and Table 12.

Table 11: Group Delayed Neutrons Data (β_l/β) for the Fissionable Isotopes ^{235}U, ^{232}Th, ^{233}U and ^{238}U

Group	^{235}U		^{232}Th		^{233}U		^{238}U	
	λ_l	β_l/β	λ_l	β_l/β	λ_l	β_l/β	λ_l	β_l/β
1	54.51	0.038	56.03	0.034	55.11	0.086	52.38	0.013
2	21.84	0.213	20.75	0.15	20.74	0.274	21.58	0.137
3	6	0.188	5.74	0.155	5.3	0.227	5	0.162
4	2.23	0.407	2.16	0.446	2.29	0.317	1.93	0.388
5	0.496	0.128	0.571	0.172	0.546	0.073	0.49	0.225
6	0.179	0.026	0.211	0.043	0.221	0.023	0.172	0.075

Table 12: Group Delayed Neutrons Data (β_l/β) for the Fissionable Isotopes ^{239}Pu, ^{240}Pu, ^{241}Pu and ^{242}Pu

Group	^{239}Pu		^{240}Pu		^{241}Pu		^{242}Pu	
	λ_l	β_l/β	λ_l	β_l/β	λ_l	β_l/β	λ_l	β_l/β
1	53.75	0.038	53.56	0.028	54	0.01	53.73234	0.004
2	22.29	0.28	22.14	0.273	23.2	0.229	23.49651	0.195
3	5.19	0.216	5.14	0.192	5.6	0.173	5.2912	0.162
4	2.09	0.328	2.08	0.35	1.97	0.39	2.050731	0.411
5	0.549	0.103	0.511	0.128	0.43	0.182	0.498667	0.218
6	0.216	0.035	0.172	0.029	0.2	0.016	0.189903	0.01

As was the case for the decay heat group source data (refer to Appendix A), the delayed neutron data uses a unique group structure for each fissionable isotope. In order to reduce computational, memory and coding requirements, a common group structure was chosen and new relative yield (β_l/β) values calculated to satisfy the following relationship.

$$\sum_{l=1}^{6} \frac{\beta_{i,l}}{\beta} e^{-\lambda_{i,l} t} = \sum_{k} \gamma_{i,k} e^{-\Lambda_k t} \qquad (\mathbf{5}.6)$$

The group structure was chosen to be the same as that for the isotope ^{235}U (refer to Table 11). The methods used to determine values for $\gamma_{i,k}$ are not discussed here, but rather comparisons between the source and modified delayed neutron decay curves are given in Figure 26 and Figure 27. Note that in order to improve readability, the terms β_l/β and λ_l, as used in paragraph 3.2.3.3, refer to the modified constants $\gamma_{i,k}$ and Λ_k respectively.

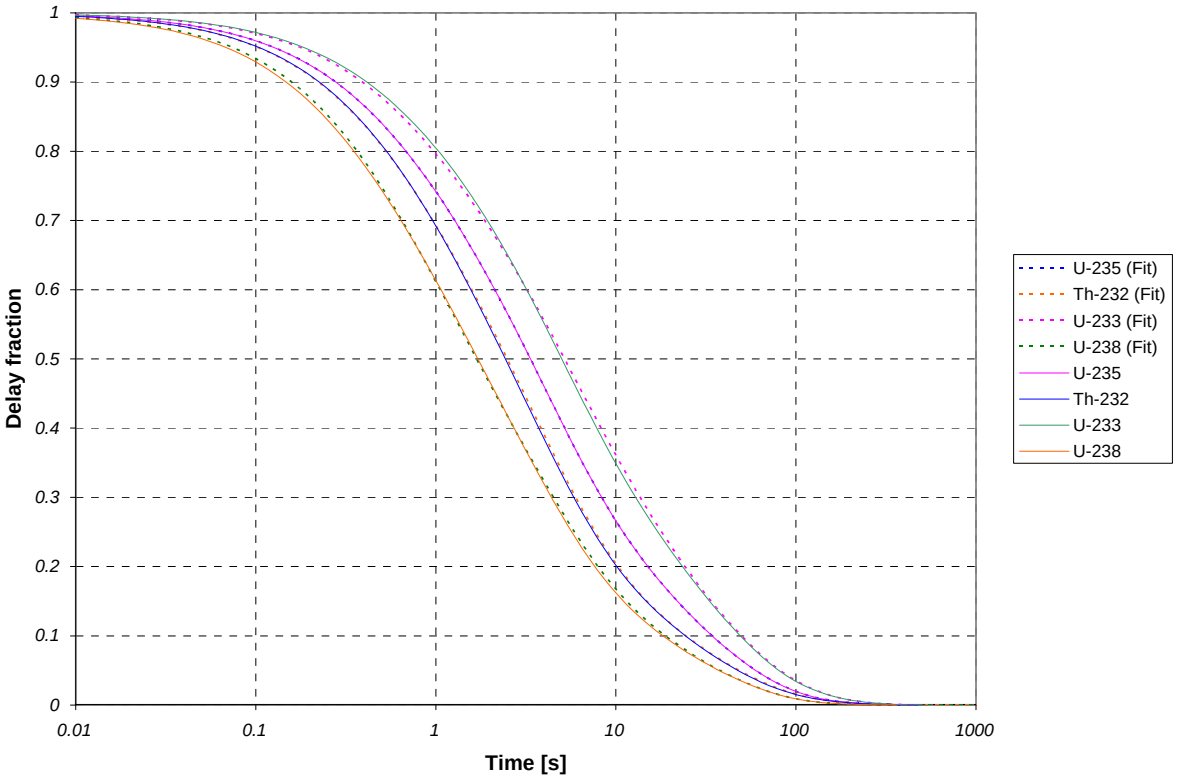

Figure 26: Delayed Neutron Decay Curves for ^{235}U, ^{232}Th, ^{233}U and ^{238}U

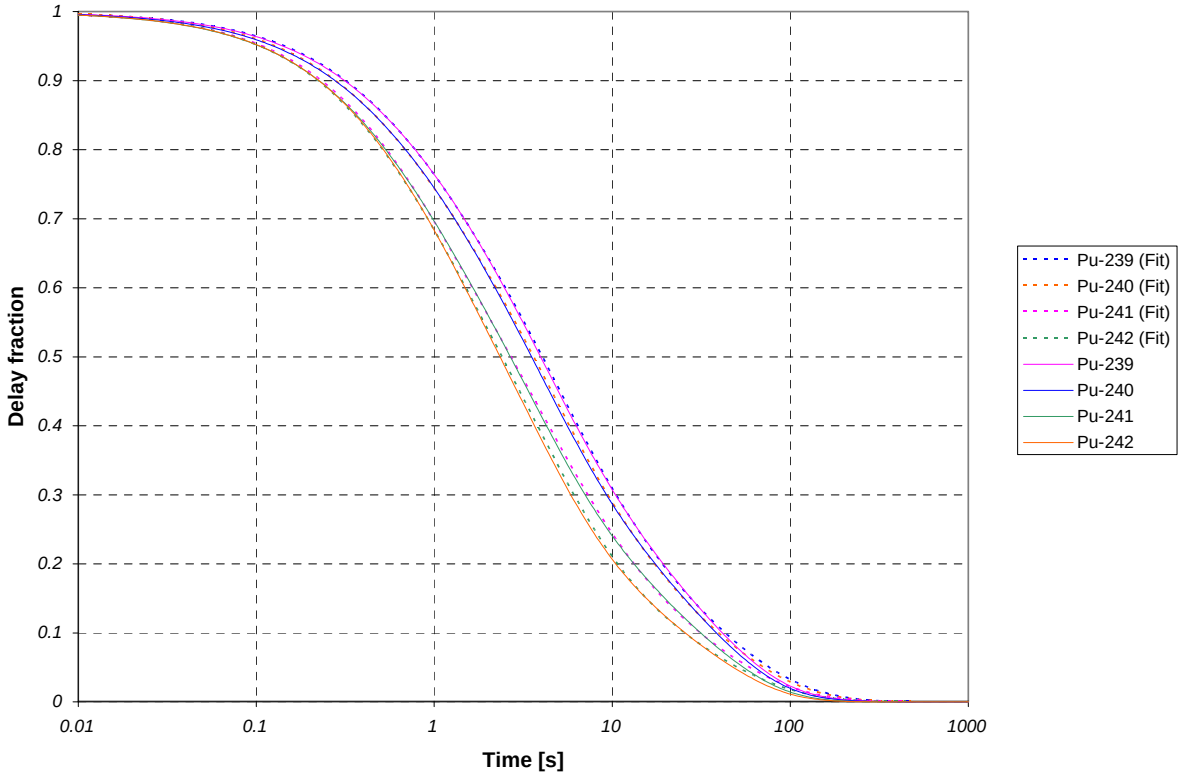

Figure 27: Delayed Neutron Decay Curves for ^{239}Pu, ^{240}Pu, ^{241}Pu and ^{242}Pu

The maximum error introduced by the fitted delayed neutron data to the total production is 0.015% for ^{232}Th. In the absence of prompt production (production by delayed neutrons alone), the maximum error introduced is 1.2%. This error is, however, within the source data uncertainty bounds ([15] and [16]). The fitted delayed neutron data is given in Table 2.

5.4 APPENDIX D: SATURATION FISSION PRODUCT YIELD AND DECAY DATA

The decay constants and fission yields of neutron poison specified in Table 4 and Table 5 are taken from ENDF/B IV [12]. The original data could not be obtained and therefore the more recent ENDF/B VI [14] is compared with the data used in TINTE. A comparison of decay constants for the relevant decay chains is given in Table 13.

Table 13: Comparison of the Decay Constants of Selected Isotopes, ENDF/B VI versus TINTE

Isotope	ENDF/B VI		TINTE	Difference
	$T^{1/2}$ [h]	λ [s^{-1}]	λ [s^{-1}]	[%]
$^{135}Xe_{54}$	9.14	2.107E-05	2.116E-05	0.445
$^{135}I_{53}$	6.57	2.931E-05	2.883E-05	1.651
$^{149}Sm_{62}$	stable	0	1.E-30	n/a
$^{149}Pm_{61}$	53.08	3.627E-06	3.626E-06	0.0378
$^{151}Sm_{62}$	**788916.7**	**2.441E-10**	**5.751E-09**	**95.76**
$^{151}Pm_{61}$	28.4	6.780E-06	6.876E-06	1.402
$^{157}Gd_{64}$	stable	0	1.E-30	n/a
$^{157}Eu_{63}$	15.18	1.268E-05	1.260E-05	0.665

^{149}Sm and ^{157}Gd are both stable isotopes. For numerical reasons (to prevent division-by-zero errors), the decay constants of these isotopes are represented as 1E-30 s rather than 0 s. The error introduced by this approximation is negligible. In general, the decay constants differ by less the 2%, which is acceptable.

For ^{151}Sm (in bold), however, the difference is very large. The decay constant for this isotope is relatively small though. The ratio $\lambda_X / \sigma_X \phi_2$ is in the order of 10%, i.e. the effective decay constant ($\lambda_2 = \lambda_X + \sigma_X \phi_2$, refer to paragraph 3.2.4) is dominated more by the absorption term $\sigma_X \phi_2$ than the decay constant λ_X. According to VSOP [19] steady-state calculation outputs for a typical LEU pebble bed reactor [20], the ^{151}Sm absorption per neutron lost is 10% of the ^{135}Xe value and 30% of the ^{149}Sm value. Therefore, despite the 96% difference in decay constant, the overall effect on calculation results is expected to be small.

In order to validate the fission yield values of Table 5, the more recent ENDF/B VI was considered. Cumulative and independent fission yields for the relevant isotopes are given in Table 14 through Table 17. The effective fission yields for each parent/daughter isotope pair was determined as follows: The parent isotopes (^{135}I, ^{149}Pm, ^{151}Pm and ^{157}Eu) are assumed to be formed directly from fission, therefore the cumulative fission yield values, summed for all isotope states, are used to account for formation by decay of higher level isotopes. The daughter isotopes (^{135}Xe, ^{149}Sm, ^{151}Sm and ^{157}Gd) are treated independently, and therefore the independent fission yield values, summed for all isotope states, are used. The resulting effective fission yields are given in Table 18.

Table 14: Cumulative Fission Yields of Selected Isotopes in the Ground State, from ENDF/B VI[‡‡]

Isotope	γ_{U5}	γ_{Th2}	γ_{U3}	γ_{U4}	γ_{U6}	γ_{U8}	γ_{Pu9}	γ_{Pu0}	γ_{Pu1}	γ_{Pu2}
$^{135}Xe_{54}$	0.065385	0.055285	0.062592	0.055775	0.060797	0.069676	0.076083	0.072317	0.0717	0.074943
$^{135}I_{53}$	0.0628187	0.055183	0.050323	0.049011	0.059748	0.069407	0.065419	0.067316	0.069431	0.073885
$^{149}Sm_{62}$	0.0108163	0.010836	0.007781	0.010358	0.013384	0.016253	0.012166	0.013939	0.014741	0.015984
$^{149}Pm_{61}$	0.0108163	0.010836	0.007781	0.010358	0.013384	0.016253	0.012166	0.013939	0.014741	0.015984
$^{151}Sm_{62}$	0.0041877	0.003636	0.003157	0.003181	0.004149	0.007994	0.007384	0.008547	0.00913	0.010225
$^{151}Pm_{61}$	0.0041877	0.003636	0.003157	0.003181	0.004149	0.007994	0.007384	0.008547	0.00913	0.010225
$^{157}Gd_{64}$	6.151E-05	9.32E-06	6.3E-05	0.000109	0.000234	0.000414	0.000742	0.000994	0.001354	0.001683
$^{157}Eu_{63}$	6.15E-05	9.32E-06	6.3E-05	0.000109	0.000234	0.000414	0.000741	0.000994	0.001354	0.001683

Table 15: Cumulative Fission Yields of Selected Isotopes in the First Excited State, from ENDF/B VI[‡‡]

Isotope	γ_{U5}	γ_{Th2}	γ_{U3}	γ_{U4}	γ_{U6}	γ_{U8}	γ_{Pu9}	γ_{Pu0}	γ_{Pu1}	γ_{Pu2}
$^{135}Xe_{54}$	0.0110156	0.008187	0.01546	0.0122189	0.009559	0.01036	0.0171394	0.013446	0.0118204	0.0116123

Table 16: Independent Fission Yields of Selected Isotopes in the Ground State, from ENDF/B VI[‡‡]

Isotope	γ_{U5}	γ_{Th2}	γ_{U3}	γ_{U4}	γ_{U6}	γ_{U8}	γ_{Pu9}	γ_{Pu0}	γ_{Pu1}	γ_{Pu2}
$^{135}Xe_{54}$	0.0007851	2.653E-05	0.004206	0.001749	0.0002728	0.0001115	0.003141	0.001450	0.000655	0.0003068
$^{135}I_{53}$	0.02927	0.008389	0.03305	0.02783	0.01779	0.01355	0.04287	0.03447	0.03009	0.02165
$^{149}Sm_{62}$	1.709E-12	0	1.25E-10	2.94E-10	2.04E-12	1.57E-14	8.19E-10	3.61E-11	7.18E-13	3.94E-13
$^{149}Pm_{61}$	3.87E-08	4.71E-11	5.36E-07	1.12E-06	4.0E-08	1.18E-09	2.43E-06	2.96E-07	2.29E-08	1.29E-08
$^{151}Sm_{62}$	4.75E-09	1.22E-12	7.E-08	1.16E-07	2.43E-09	7.76E-11	3.85E-07	4.26E-08	2.58E-09	1.65E-09
$^{151}Pm_{61}$	6.42E-06	3.81E-08	2.644E-05	3.719E-05	3.92E-06	4.85E-07	0.0001076	3.106E-05	5.86E-6	4.24E-06

[‡‡] Values for U3, U5, Pu9, Pu0, Pu1 and Pu2 are at 0.023 eV. Values for Th2, U4, U6 and U8 are at 0.5 MeV.

Isotope	γ_{U5}	γ_{Th2}	γ_{U3}	γ_{U4}	γ_{U6}	γ_{U8}	γ_{Pu9}	γ_{Pu0}	γ_{Pu1}	γ_{Pu2}
$^{157}Gd_{64}$	1.48E-09	2.37E-13	1.66E-08	3.51E-08	1.53E-09	8.04E-11	2.9E-07	7.04E-08	4.15E-09	5.58E-09
$^{157}Eu_{63}$	6.35E-07	1.58E-09	2.22E-06	4.44E-06	1.04E-06	1.96E-07	3.46E-05	1.82E-05	4.23E-06	5.1E-06

Table 17: Independent Fission Yields of Selected Isotopes in the First Excited State, from ENDF/B VI[‡‡]

Isotope	γ_{U5}	γ_{Th2}	γ_{U3}	γ_{U4}	γ_{U6}	γ_{U8}	γ_{Pu9}	γ_{Pu0}	γ_{Pu1}	γ_{Pu2}
$^{135}Xe_{54}$	0.0017812	7.55E-05	0.008063	0.005014	0.000776	0.000157	0.007523	0.003551	0.001614	0.000751

Table 18: Effective Fission Yields of Selected Decay Chain Isotopes, from ENDF/B VI

Isotope	γ_{U5}	γ_{Th2}	γ_{U3}	γ_{U4}	γ_{U6}	γ_{U8}	γ_{Pu9}	γ_{Pu0}	γ_{Pu1}	γ_{Pu2}
$^{135}Xe_{54}$	0.002566	0.000102	0.012269	0.006763	0.001049	0.000269	0.01066	0.005	0.00227	0.001057
$^{135}I_{53}$	0.06282	0.05518	0.05032	0.04901	0.05975	0.06941	0.06542	0.06732	0.06943	0.07389
$^{149}Sm_{62}$	1.71E-12	0	1.25E-10	2.94E-10	2.04E-12	1.57E-14	8.19E-10	3.61E-11	7.18E-13	3.94E-13
$^{149}Pm_{61}$	0.01082	0.01084	0.00778	0.01036	0.01338	0.01625	0.01217	0.01394	0.01474	0.01598
$^{151}Sm_{62}$	4.75E-09	1.22E-12	7.0E-08	1.16E-07	2.43E-09	7.76E-11	3.85E-07	4.26E-08	2.58E-09	1.65E-09
$^{151}Pm_{61}$	0.004188	0.003636	0.003157	0.003181	0.004149	0.007994	0.007384	0.008547	0.00913	0.01023
$^{157}Gd_{64}$	1.48E-09	2.37E-13	1.66E-08	3.51E-08	1.53E-09	8.04E-11	2.9E-07	7.04E-08	4.15E-09	5.58E-09
$^{157}Eu_{63}$	6.15E-05	9.32E-06	6.3E-05	0.000109	0.000234	0.000414	0.000741	0.000994	0.001354	0.001683

Table 19: Difference in Fission Yields of Selected Decay Chain Isotopes, ENDF/B VI versus TINTE Values

Isotope	γ_{U5}	γ_{Th2}	γ_{U3}	γ_{U4}	γ_{U6}	γ_{U8}	γ_{Pu9}	γ_{Pu0}	γ_{Pu1}	γ_{Pu2}
$^{135}Xe_{54}$	-6.64E-05	0.0132	0.001131	-0.00426	0.001451	-0.000119	0.000836	0.0065	3.1E-05	0.00124
$^{135}I_{53}$	0.000681	-0.02	-0.00172	0.0145	0.00375	-0.00391	-0.00242	-0.00432	6.87E-05	-0.00439
$^{149}Sm_{62}$	-1.71E-12	0	-1.25E-10	-2.94E-10	-2.04E-12	-1.57E-14	-8.19E-10	-3.61E-11	-7.18E-13	-3.94E-13
$^{149}Pm_{61}$	2.37E-05	3.8E-06	0.00306	0.000482	-0.00254	-0.00541	-0.00133	-0.0031	-0.0039	-0.00514
$^{151}Sm_{62}$	-4.75E-09	-1.22E-12	-7E-08	-1.16E-07	-2.43E-09	-7.76E-11	-3.85E-07	-4.26E-08	-2.58E-09	-1.65E-09
$^{151}Pm_{61}$	8.33E-06	0.00056	0.00104	0.00102	4.71E-05	-0.0038	-0.00319	-0.00435	-0.00493	-0.00603
$^{157}Gd_{64}$	-1.48E-09	-2.37E-13	-1.66E-08	-3.51E-08	-1.53E-09	-8.04E-11	-2.9E-07	-7.04E-08	-4.15E-09	-5.58E-09
$^{157}Eu_{63}$	-1.96E-07	5.2E-05	-1.71E-06	-4.81E-05	-0.000173	-0.000353	-0.00068	-0.00093	-0.00129	-0.00162

Differences between ENDF/B VI values (Table 18) and TINTE values (Table 5) ($\gamma_{TINTE} - \gamma_{ENDF/BVI}$) are given in Table 19. For ^{235}U fuel, the differences are relatively small. For all non-^{235}U fissionable isotopes and all non-^{135}Xe decay chain isotopes, however, the differences are larger. This is because accurate data was previously not available for these values.

For Sm, Pm, Gd and Eu isotopes, values were only available for ^{235}U fuel. In these cases, the values for the other fissionable isotopes were assumed equal to those for ^{235}U. Similarly, data for the ^{135}Xe and ^{135}I was not available for the fissionable isotopes ^{234}U, ^{236}U, ^{240}Pu and ^{242}Pu. These were therefore assumed equal to the values for ^{235}U, ^{235}U, ^{239}Pu and ^{241}Pu respectively.

An estimation of the approximate error in neutron poison concentration, introduced by these assumptions and differences, may be found for the equilibrium condition as follows (refer to Equation (**3**.91)).

$$\varepsilon_{X_{eq}} = \frac{(\gamma_X + \gamma_I)_{TINTE}}{(\gamma_X + \gamma_I)_{ENDF/B}} - 1$$

Table 20 shows the estimated error in equilibrium neutron poison concentration (ENDF/B VI versus TINTE values) calculated using the above equation.

Table 20: Estimated Error in Neutron Poison Concentrations

Isotope	ε_{U5} [%]	ε_{Th2} [%]	ε_{U3} [%]	ε_{U4} [%]	ε_{U6} [%]	ε_{U8} [%]	ε_{Pu9} [%]	ε_{Pu0} [%]	ε_{Pu1} [%]	ε_{Pu2} [%]
^{135}Xe$_{54}$	0.94	-12.27	-0.95	18.33	8.56	-5.78	-2.08	3.02	0.14	-4.19
^{149}Sm$_{62}$	0.22	0.04	39.31	4.65	-19.01	-33.30	-10.90	-22.23	-26.46	-32.18
^{151}Sm$_{62}$	0.20	15.39	32.90	31.90	1.14	-47.51	-43.18	-50.91	-54.04	-58.96
^{157}Gd$_{64}$	-0.32	557.74	-2.74	-43.96	-73.82	-85.18	-91.73	-93.83	-95.47	-96.36

The same argument as was previously used in Appendix B is now applied. In a typical pebble-bed-type thermal reactor, operating on LEU fuel, more than 99% of the fission reactions take place in the isotopes ^{235}U, ^{239}Pu and ^{241}Pu, in the approximate ratios 6:3:1 (using data from [20]). Using this assumption, the effective error for each neutron poison is estimated at 0.01%, 6%, 18% and 36% for the isotopes ^{135}Xe, ^{149}Sm, ^{151}Sm and ^{157}Gd respectively.

Additionally, taking into account that the ratio of absorption of these four elements is approximately 140:40:20:1 (using data from [20]), a total effective error may be estimated at 3%.

6. REFERENCES

The following documents are referred to in this document.

	Document Title	Preparer/Author	Document Number	Revision or Date of Issue
[1]	Legacy and Software Under Development Analysis Software V&V Plans	J A Odendaal	PBMR PS0080	B
[2]	Legacy-Based Analysis Software Products, A-Posteriori V&V and Reverse Engineering Documentation Plan	J A Odendaal	PBMR 027188	1
[3]	The Two-Dimensional Reactor Dynamics Programme TINTE. Part 1: Basic Principles & Methods of Solution	H Gerwin	Jül-2167: TINTE Part: 1	November, 1987
[4]	The Two-Dimensional Reactor Dynamics Programme TINTE. Part 3: Programme Architecture and User's Manual	H Gerwin, W Scherer	TINTE: Part 3	June, 2001
[5]	Verification of the Mathematical Models for the Neutron Flux of the Code TINTE	P Lourens	PBMR 013621	B
[6]	TINTE Thermal-hydraulics Calculation Theory Report	O Ubbink	PBMR 053437	A
[7]	Nuclear Reactor Physics	W M Stacey	ISBN 978-3-527-40679-1	2007
[8]	Treatment of the Upper Cavity in a Pebble-Bed High-temperature Gas-cooled Reactor by Diffusion Theory	H Gerwin, W Scherer	Nucl. Sci. Eng. 97	1987
[9]	Determination of Equivalent Cross Sections for Representation of Control Rod Regions in Diffusion Calculations	W Scherer, H J Neef	Jül -1311	1974
[10]	A Leakage Iterative Method for Solving the Three Dimensional Diffusion Equation	Y Naito, M Mackave, K Shibuya	Nucl. Sci. Eng., 58	1975
[11]	Finite Difference Method for Solving the Spatio-Temporal Diffusion Equation in the Two-Group Approximation	R Monterosso, E Vincenti	EUR 596.e	1964
[12]	ENDF/B IV, described in ENDF-102 Data Formats and Procedures for the Evaluated Nuclear Data File, ENDF	D Garber, C Dunford, S Pearlstein	BNL-NCS-50496	1975
[13]	Introductory Nuclear Reactor Dynamics, Chapter 2.2	K O Ott, R J Neuhold	American Nuclear Society, ISBN 0-89448-029-4	1985

	Document Title	Preparer/Author	Document Number	Revision or Date of Issue
[14]	Cross Section Evaluation Working Group, ENDF/B-VI Summary Documentation	Edited by P F Rose	BNL-NCS-17541 (ENDF-201)	1996
[15]	Delayed Neutron Data – Review and Evaluation	S A Cox	ANL/NDM-5	April, 1974
[16]	Delayed-Neutron Yields in Nuclear Fission	R J Tuttle	INDC(NDS)-107/G+Special	March, 1979
[17]	Delayed Neutrons from Fission—A Compilation and Evaluation of Experimental Data	L Tomlinson	AERE-R.6993	February, 1972
[18]	Brookhaven National Lab Report BNL-325	S F Mughabghab, D I Garber	BNL-325	vol. 1, 3rd ed., 1973
[19]	VSOP 99	-H.J.Rütten et al.	JÜL-3820	October 2000 (Update July 2004)
[20]	Core Neutronic Analysis: SAS Modelling in VSOP99/3 for TINTE Use	S Sen	PBMR T000232	1
[21]	Berechnung der Nachzerfallsleistung der Kernbrennstoffe von Hochtemperaturreaktoren mit kugelförmigen Brennelementen	Deutsches Institut für Normung (DIN)	DIN 25 485	May, 1990
[22]	Fission Energy Release for 16 Fissioning Nuclides	Stanford University, Dept. of Mechanical Engineering	NP-1771	March, 1981
[23]	Die Behandlung der Nachzerfallswärme im Reaktordynamikprogramm TINTE	H Gerwin, W Scherer	ISSN 0944-2952	July, 1993
[24]	CRC Handbook of Chemistry and Physics, CRC Press Inc., Boca Raton, Florida, USA.	n/a	PBMR-10304	87th Edition, 2006
[25]	Product Specification: PBMR Fuel Spheres (Type A)	K T Brown	PB-FTP-0001	D
[26]	PBMR Fuel Kernel Model for the Prediction of Accurate Temperature Profiles, Proceedings of the 16th International Conference on Nuclear Engineering ICONE16	OUbbink, P du Toit, P Lourens, W Joubert	ICONE16-48759	May 11-15, 2008
[27]	TINTE Transient Results for the OECD 400 MW PBMR Benchmark, Proceedings of ICAPP '08	G Strydom	ICAP 2008 paper 8180 Bx121-A	2008

Document Title		Preparer/Author	Document Number	Revision or Date of Issue
[28]	A Mathematical Model and FORTRAN	P Lourens	PBMR T000103	C

Jül-4317
Januar 2010
ISSN 0944-2952